Evaluation of Cement-Modified Soil (CMS) with Microcracking and Its Effects on Flexible Pavement Performance

By

George A. Tannoury

M.Sc., University of Nevada, Reno, Nevada, USA, 2007

M.Sc., University of Balamand, North Lebanon, Lebanon, 2001

B.Sc., University of Balamand, North Lebanon, Lebanon, 2000

Submitted to graduate degree program in Civil, Environmental, and Architectural Engineering and the Graduate Faculty of the University of Kansas in partial fulfillment of the requirements for the degree of Doctor of Philosophy

_____

Chairperson: Dr. Jie Han, Professor

_____

Dr. Masoud Darabi, Assistant Professor

_____

Dr. Robert L. Parsons, Professor

_____

Dr. Steven D. Schrock, Professor

_____

Dr. Chi Zhang, Assistant Professor

Date Defended: December 3rd, 2019

The Dissertation Committee for George A. Tannoury certifies that this is the approved version of the following dissertation:

Evaluation of Cement-Modified Soil (CMS) with Microcracking and Its Effects on Flexible Pavement Performance

_____

Chairperson: Dr. Jie Han, Professor

Date Approved: December 3rd, 2019

ABSTRACT

Cement modification of subgrade has been widely practiced for the past few decades. Recently, cement has become a more economical binder to modify in-situ subgrade soil since other binders, such as fly ash, have become less available and therefore their prices have increased significantly. In addition, a much higher percentage of fly ash needs be used, when compared with cement to achieve the same subgrade strength and stiffness. In general, cement-modified subgrade is prone to develop shrinkage cracking, which can eventually reflect through asphalt pavement layers to the surface after construction. For some subgrade soils, a high cement content is needed to meet the unconfined compressive strength requirement without jeopardizing durability. A higher cement content will result in higher shrinkage cracking potential. To overcome this problem, a microcracking technology has been developed and adopted in the field. This technology involves re-compaction of cement-modified soil (CMS) with a roller, 24 to 48 hours after initial compaction, to induce microcracks in the CMS and minimize the potential for large shrinkage cracks. Microcracking of CMS is not expected to significantly reduce the strength and stiffness of CMS, but it is expected to increase its hydraulic conductivity and reduce the potential for large shrinkage cracks. Unfortunately, the procedure to simulate microcracking of CMS in the laboratory and to evaluate its effect on properties of CMS has not been established yet.

This dissertation documents the development of such a procedure and discusses the effect of microcracking on the properties (strength and modulus) of CMS specimens. The developed procedure utilized unconfined compression (UC) tests to generate micro-cracks in specimens. To generate micro-cracks, the loading stress level was found to be equal to the unconfined

compressive strength of the CMS specimen. The laboratory results showed that microcracking increased the hydraulic conductivity of the specimen and reduced its electrical resistivity when the specimen was saturated.

To evaluate the effects of microcracking on the field performance of CMS, field and laboratory tests, including Electrical Resistivity (ER) tests, Light Weight Deflectometer (LWD) tests, Falling Weight Deflectometer (FWD) tests, and Resilient Modulus (M_r) tests, were conducted on the CMS at two different locations in the State of Kansas, USA. The ER results from the field did not show a clear correlation between the ER value and the microcracking process because the ER results fluctuated within the device accuracy range. The (LWD) tests conducted in the field showed that adding cement increased the subgrade modulus. However, after applying three passes of roller compaction to generate the microcracks in the CMS in the field, the subgrade modulus dropped to approximately 40% of its original value on average. The back-calculation analyses of the FWD test data from both sites showed that the actual resilient moduli of the microcracked CMS layers in the field were significantly higher than the laboratory resilient moduli of the microcracked and uncracked reconstituted specimens. Also, the laboratory resilient moduli of four cored specimens from one of the sites were approximately 25 to 50 percent higher than those of reconstituted specimens from the same site. However, the laboratory resilient modulus test results showed that the microcracked specimens reconstituted from the soils obtained from the field had slightly higher M_r values than the uncracked specimens.

In addition, the performance of an asphalt concrete pavement over the CMS with microcracking was evaluated based on a mechanistic empirical approch. The KENLAYER Computer Program was used to predict the pavement responses under traffic loading. The hot mix asphalt (HMA) and the subgrade were modeled as linearly elastic materials and their stiffness

values used in KENLAYER were backcalculated from FWD testing using the ELMOD V.6 software. However, the CMS was either modeled as a non-linearly elastic material with its properties determined from the laboratory resilient modulus tests or as linearly elastic material with the properties backcalculated from the FWD tests. Furthermore, the typical pavement structural distresses, such as permanent deformation (rutting) and fatigue cracking, and the remaining service life were evaluated for the actual pavement thicknesses used in the field.

ACKNOWLEDGMENTS

I would like to begin by thanking my advisor and mentor, Professor Jie Han, for his help, personal guidance, patience and support in my quest to complete this research and in my journey as a Ph.D. student. I am thankful to him for the dedication and effort in reviewing the materials contained in this dissertation. Without Prof. Jie Han help and active involvement, this work would not have been successful. It has been a great pleasure and privilege to be one of Prof. Han's students.

I am also very grateful to my Ph.D. committee members, Dr. Masoud Darabi, Dr. Robert L. Parsons, Dr. Steven D. Schrock, and Dr. Chi Zhang for their guidance, help and valuable comments in improving this dissertation.

I would like to thank Dr. Mahdi Al-Naddaf for his help and support in conducting the experimental work of this research.

I am truly thankful to the Kansas Department of Transportation (KDOT) and Terracon for their participation in funding this study. Special thanks goes to Mr. Luke Metheny and Mr. Isaac Ferguson with KDOT for their support in facilitating the field work and my supervisors at Terracon, Mr. Matt Catlin and Mr. Scott Randle, for allocating the funding of this researsch.

My sincere thanks also go to Dynatest and Dr. Gabriel Bazi, for providing us the ELMOD V.6 software used in analyzing the FWD data.

Finally, my special thanks for my parents, my wife Dr. Diala Tannoury and my three kids Anthony, Carelle, and Kyle for their patience with me during the completion of this work. They sacrificed a lot during my time as a Ph.D. student and made my Ph.D. study possible.

TABLE OF CONTENTS

LIST OF TABLES

LIST OF FIGURES

CHAPTER 1 INTRODUCTION

Performance of pavement structures highly depends on the quality of aggregate materials used in the construction and the competency of subgrade support. The aggregate used in roadway construction projects located in the western half of the State of Kansas, is typically imported from quarries located in southeast Kansas or from the State of Oklahoma thus increasing construction cost. Chemical modification/stabilization of subgrade has been used for several decades to improve its inferior engineering properties and provide a stable working platform during construction. The chemical modification/stabilization of the subgrade is relied heavily on the use of lime, fly ash, and cement. Cement modification of subgrade was widely practiced in the 40s to 50s of the 20th century. In the last few decades, fly ash, a bi-product of energy generation from coal-fired power stations, has dominated the chemical stabilization industry and was considered as the most cost-effective stabilizer in many states across the country. But more recently, the high demands on fly ash coupled with the increase of its prices allowed cement to revive its old popularity in the subgrade stabilization industry. Furthermore, current trends suggest fly ash supplies may continue to decrease while its price increases.

In several states, cement has become a more economical binder to modify in-situ subgrade soil since less percentages of cement need to be used to achieve the same subgrade strength and stiffness that fly ash could develop on a particular soil. Soil cement comprises native soils with or without aggregate mixed with measured amounts of Portland cement and water that harden after proper compaction and curing to form a strong, durable, frost resistant paving material (Halsted et al. 2006). Soil-cement can be mixed in a central plant using local or borrow material or can be

mixed in place using on-site materials. The later technique is more cost effective in large pavement projects. Cement modified soil can be used under rigid or flexible pavement.

The main advantages of soil-cement base are providing a stiffer and stronger base than an unbound granular base; delaying the onset of surface distresses related to fatigue cracking and rutting and continued strength gain as the soil-cement material ages.

In general, cement-modified fine-grained soils requires a relatively higher cement content to achieve the required durability and therefore, are prone to develop shrinkage cracking, that can eventually reflect through asphalt pavement layers to the surface after construction. When CMS is used under rigid pavement, the shrinkage cracking will not have any significant impact on the pavement performance as these cracks could not reflect through the rigid concrete surfacing. However, when used under flexible pavement, these reflective cracks will serve as an easy pathway for surface water to infiltrate into the cohesive subgrade that will exhibit a significant drop in its strength and stiffness and will result in premature failures of the pavement. Research has shown that shrinkage cracking of soil-cement first decreases with cement content, then reach a minimum amount, and thereafter increase with the cement content. Generally, the optimum cement content resulting in the least amount of shrinkage is lower than the cement content required to achieve durable soil-cement. Also, for some subgrade soils, a high cement content is needed to meet the unconfined compressive strength and stiffness requirement without jeopardizing the long-term durability. The required high cement content will result in higher shrinkage cracking potential. To overcome this problem, a microcracking technology has been developed and adopted in the field. This technology involves re-compaction of cement-modified soil (CMS) with a roller, 24 to 72 hours after initial compaction, to induce microcracks in the CMS and minimize the potential for large shrinkage cracks. Microcracking of CMS is not expected to significantly reduce the strength

and stiffness of CMS, but it is expected to increase its hydraulic conductivity and reduce the potential for large shrinkage cracks. Unfortunately, the procedure to simulate microcracking of CMS in the laboratory and to evaluate its effect on the properties of CMS has not been established yet. This report documents the development of such a procedure and discusses the effect of microcracking on the properties (mainly strength and modulus) of CMS specimens.

The overall objective of this study was to evaluate laboratory and field performance of CMS after microcracking and its benefits for pavement applications. Although the previous research confirmed the applicability and effectiveness of this construction method in the field, no literature was found describing a procedure or method to simulate the microcracking process in the laboratory. This study proposes a laboratory method that can be used to simulate the microcracking process on CMS in the field using Unconfined Compression (UC) tests. The UC specimens were used to evaluate the properties of CMS with and without microcracking, including their strength and stiffness.

More details concerning CMS and its observed performance are described in the following chapters. Chapter 2 consists of a literature review describing the composition and mechanisms of CMS and the research on its use for soil stabilization including microcracking. Chapter 3 describes the materials and laboratory tests adopted in this study. Chapters 4 and 5 discuss the laboratory results and the field work, respectively. Chapter 6 discusses the evaluation of flexible pavements on CMS with microcracking using a mechanistic empirical approach including environmental effects on the pavement system. In this evaluation, the pavement responses were determined for several scenarios for fatigue and rutting analyses. Chapter 7 provides the conclusions and recommendations from this study.

CHAPTER 2 LITERATURE REVIEW

2.1 INTRODUCTION

This chapter presents a brief description of the additives that can be used to modify/stabilize subgrade soil and their chemical reactions with moist soil, the use of cement for soil stabilization, the causes for shrinkage cracking of Cement-Modified Soil (CMS), and the background of the microcracking technology. Also, it includes a brief review on pavement design and evaluation, the numerical methods for determining the pavement responses (i.e. stresses, strains and deflections) under traffic loading, and the generalized constitutive models for soil resilient modulus.

2.2 STABILIZATION ADDITIVES

In-place stabilization is an economically feasible solution that could significantly reduce the construction cost, reduce the maintenance cost throughout the life of the pavement, and extend the pavement life. For the projects where the on-site soils have strength deficiencies or have problematic behavior (i.e. shrink/swell), the design will typically require high-quality materials that are often expensive or not readily available near the project. Costs associated with hauling suitable materials to the site will result in a significant increase in total construction cost. In most of the time, to maintain a long-lasting pavement for these projects, where the on-site native soils may not meet the specification of the project, a stabilized subgrade soil is often essential. The stabilization can help improve the engineering properties of these inferior soils. However, the short- and long-term behaviors of these stabilized materials differ substantially depending on the

type and quantity of the stabilizing agent, the pavement structure, and the environmental conditions during and after construction.

The strength of a soil depends on its internal friction and cohesion. The internal friction angle of a soil is related to its mineralogy, gradation, particle angularity, and degree of compaction. Soil cohesion results from the adherence of particles due to surface tension, physical-chemical forces, and cementation between them. The hygroscopic water surrounding the soil particles is important for soil compaction to reach an optimum condition and a maximum density.

Typically, clay materials can behave like solid, semisolid, plastic, or liquid, depending on its moisture content (see Figure 2-1). The cohesive properties of soil are dependent on the amount and nature of clay particles. The ASTM D4318 Standard Test Method is used to determine Liquid Limit, Plastic Limit, and Plasticity Index of soils. The plasticity index (PI) is the difference between the liquid limit and the plastic limit of the soil. A greater PI value for a soil is an indication that there is a larger proportion of expansive clay (e.g. montmorillonite) and a substantial potential of volume changes during wetting and drying.

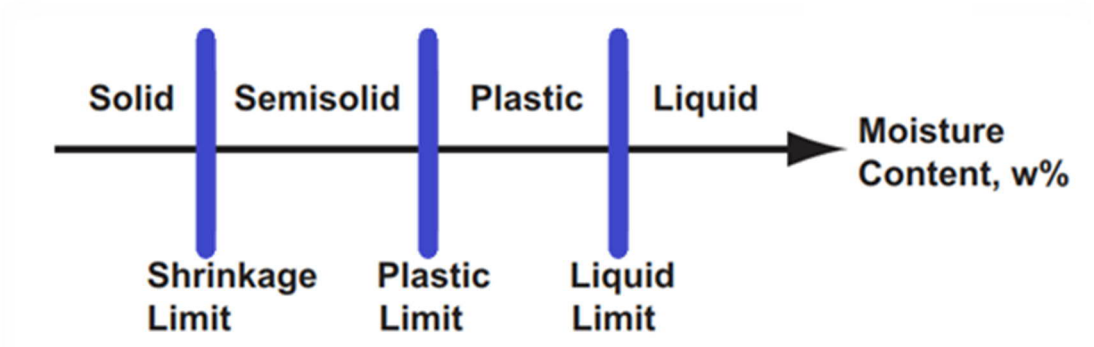

Figure 2-1 Physical state versus moisture contents of clay materials.

Chemical additive may be used to improve soil behavior, e.g., fill or partially fill the voids between soil particles thus reducing the hydraulic conductivity of the soil. The reduction of the

voids may also affect volumetric change behavior for the soil from being contractive to dilative. The main function of a chemical additive is to bond soil particles together, promote cohesive shear strength, increase the difficulty of particle movement under loads, and improve the durability of the soil. The stabilizing agent can affect the soil fabric typically by flocculation upon mixing and cementation over longer periods (NCHRP 2004).

Lime, fly ash, cement kiln dust (CKD), and Portland cement are the most known types of chemicals used in subgrade stabilization. The availability of these chemicals varies from one area to another. Selecting a stabilizer or additive is based on the type of soil that needs to be stabilized, the reason behind the utilization of the stabilized layer, the desired enhancement of the soil properties, the stabilized soil layer strength and durability requirement, and the condition of the environment and overall cost (US Army Engineer School 1992).

Lime is made from calcium carbonate ($CaCO_3$) found in limestone, chalk or sea shells. There are two common types of lime: (1) quicklime (i.e., calcium oxide (CaO)) and (2) hydrated lime or slaked lime (i.e., chemically represented as calcium hydroxide $Ca(OH)_2$). Lime is obtained by heating the raw material to a temperature between 1,470 ^oF and 2,000 ^oF. When heated to these temperatures, the chalk breaks down by giving off carbon dioxide (CO_2) and leaving calcium oxide (CaO) that is known as quicklime. When exposed to water, the quicklime (CaO) chemically reacts with the H_2O molecules and transforms to hydrated lime $Ca(OH)_2$. This reaction is exothermic. The hydrated lime can react again when exposed to the atmosphere by absorbing carbon dioxide (CO_2) to become once again ($CaCO_3$).

Fly ash is a chemical byproduct of the coal fire in power plants. The fly ash is considered a pozzolanic material and contains substances, such as SiO_2, TiO_2, Al_2O_3, Fe_2O_3, MnO, MgO, CaO, Na_2O, K_2O, P_2O_5, SO_3, and organic carbons (Das 1990). The classification of fly ash is based

on the chemical composition and Class C and Class F are the two types of fly ash used in construction. Class C contains a significant quantity of free lime and can produce pozzolanic and cementitious reactions with water. A high content of calcium oxide results in lighter color fly ash, while a high content of organics results in darker color fly ash. Class F fly ash is less commonly used fly ash due to its lack of self-cementitious properties and its requirement for an activator to react. Fly ash can improve engineering properties of soil. However, the properties of fly ash vary among production plants and depend on the chemical compound of the coal and combustion technology used at each plant (Muhunthan and Sariosseiri 2008).

The CKD is a byproduct of the Portland cement manufacturing process. The dust is a particulate mixture of partially calcined and unreacted raw feed, clinker dust and ash, enriched with alkali sulfates, halides, and other volatiles. Several factors influence the chemical and physical properties of CKD. Because plant operations differ considerably with respect to raw feed, type of operation, dust collection facility, and type of fuel used, the use of the terms for typical or average CKD when comparing different plants can be misleading. CKD is not only cost effective, but also has several desired properties and therefore has become, over the years, a popular stabilization agent.

2.3 CEMENT IN SOIL STABILIZATION

The main purpose of using soil stabilizer(s) is to provide sufficient amount of calcium ions (Ca^{2+}) so that the monovalent cations, like sodium Na^{+} (typically available on the surfaces of clay particles), are exchanged to lower the plasticity and improve the workability of the soil. Portland cement can supply this necessary ingredient and, when used properly, can effectively modify the

properties of clayey soils/aggregates. The four basic reactions occurring in cement stabilization are cation exchange, particle restructuring, cementitious hydration, and pozzolanic reaction.

2.3.1 **Cation Exchange**

When lime or cement is mixed with soil, it traps moisture and allows for a process of ionization and production of calcium cations to take place. These cations exchange with the clay lattice to substitute the monovalent ions, like sodium Na+ with calcium ions (Ca2+). The method for chemical stabilizer(s) used to exchange ions is the same as applied by calcium cation with clay structures, specifically with the sodium and potassium of the structure. A key requirement for attaining the benefits of this type of stabilization is to have sufficient mixing. The clay structure is broken down and excess water is released due to the strong ionization energy of calcium that bonds together the clay particles within hours after the clay is mixed with cement.

2.3.2 **Particle Restructuring**

This phenomenon involves the change of the texture of the clay material from a plastic to a more friable material. It is also known as the flocculation and agglomeration of the clay particles that result in an increase of the internal friction angle of the clay. The restructuring of the clay occurs within several hours after the clay is mixed with cement.

2.3.3 **Cementitious Hydration**

This phenomenon involves a series of chemical reactions which occur with the introduction of water to calcium and silica present in cement. This reaction will result in the formation of calcium-silicate-hydrate (C-S-H), calcium aluminum hydrate (C-A-H), and excess calcium hydroxide

$Ca(OH)_2$. The C-S-H and C-A-H are what bond the clay particles together to form a solid matrix. This process starts after one day to one month after mixing.

2.3.4 **Pozzolanic Reaction**

Subsequently to the hydration reaction, a slower pozzolanic reaction involves the excess calcium hydroxide $Ca(OH)_2$ from the hydration reaction combined with water and silica or alumina dissolved from the clay particles to form additional C-S-H or C-A-H, respectively. This reaction occurs over months and years and can further strengthen the soil-cement structure.

2.4 SHRINKAGE CRACKING OF CEMENT-MODIFIED SOIL

Cement is commonly used in practice to modify/improve engineering properties of inferior soils. Cement-modified soil (CMS) often has a shrinkage potential that can significantly affect the performance of hot mix asphalt (HMA) pavements, especially when it is placed directly underneath HMA layers. Shrinkage that is associated with cement-modified soil can be divided into two categories: autogenous shrinkage (resulting from hydration of cement) and drying shrinkage (resulting from loss of moisture). George (1968) and Bofinger et al. (1978) studied the shrinkage cracking phenomenon extensively and concluded that drying is the major cause for shrinkage. The degree of shrinkage cracking depends on several influence factors: tensile strength of the modified soil (George, 1968; Bofinger et al. 1978), restraint by friction between the modified soil layer and its underlying layer (Bofinger, 1971; George, 1973), creep characteristics of the modified soil (George, 1968; Bofinger et al. 1978), temperature (Bofinger, 1971; George, 1973), amount and type of clay in the modified soil (George, 1968), and moisture content and degree of compaction (Bofinger et al. 1978).

In general, the loss of moisture in the soil-cement mixture is the primary reason for shrinkage that eventually will crack the stabilized layer. Another factor that could also lead to shrinkage of chemically-stabilized layers is the change in temperature. A study comparing the time rate of shrinkage of Kaolinite soil-cement and Montmorillonite soil-cement showed that Kaolinite soil-cement shrank faster due to the large particle size of the kaolin clay, implying that most of the soil water is not absorbed to the surface and can be evaporated. Also, complete hydration of cement would require over 40 percent of water by weight. The same study showed that the drying effect of cement on specimens coated with wax will result in some shrinkage without loss of moisture. This study proves that hydration of cement would steal the moisture of the soil matrix.

Past studies have well documented the factors that cause shrinkage in CMS; however, recent efforts have focused on understanding design and construction practices that can minimize the shrinkage cracking problem. Common techniques employed by most DOTs to reduce the shrinkage and reflective cracking problems on soil-cement pavements include a lower cement content, thicker base, aggregate base interlayer design, and an asphalt surface treatment design. Lowering the cement content would affect the durability and increasing the thickness of the base will create more challenges achieving the compaction for the bottom part of the base.; whereas, incorporating the aggregate base interlayer or the asphalt surface treatment would increase the construction cost tremendously.

George (2001) conducted a soil stabilization field trial in Mississippi and concluded that pre-cracking of a stabilized base by roller compaction at 24 hours after placement minimized its shrinkage cracking. The Portland Cement Association (PCA, 2003) recommends 7-day unconfined compressive strengths of CMS should be within the range of 300-400 psi in the design

phase. During construction, PCA (2003) recommends compaction of CMS at or slightly below its optimum moisture content with moist curing until a moisture barrier is placed.

2.5 BACKGROUND OF MICROCRACKING TECHNOLOGY

Microcracking can be defined as a special reflective-cracking mitigation technique used during the construction of an asphalt pavement with soil-cement subgrade. The main purpose of the micro-cracking is to produce a fine network of hairline cracks in the soil-cement subgrade by applying several passes of heavy vibratory roller compaction (usually same roller capacity used during construction) shortly after the soil-cement subgrade construction. Although most early methods for reducing shrinkage cracking in CMS focused on controlling desiccation using moist-curing or asphalt-curing membranes, more recent techniques explored the use of stress relief layers, such as chip seals, geosynthetics, or thin unbound granular base layers, to reduce reflective cracking. These techniques can reduce the likelihood of reflective-cracking but, require additional steps in the construction process that will increase construction cost. An innovative concept originated in Austria to use a vibratory smooth drum roller to create a microcracked CMS layer during the early curing stage (Litzka and Haslehner, 1995). The study reported that this microcracking process prevented the development of large stress cracks in the asphalt overlay (Litzka and Haslehner, 1995). According to Litzka and Haslehner (1995), microcracking is typically performed by three passes of a roller 24 to 48 hours after compaction (Sebesta, 2005). Brandl (1999) reported that the microcracking technique was most suitable among the available options for minimizing cracking on the Austrian–Hungarian Highway. Figure 2-2 shows a typical cement modified soil surface after microcracking.

Figure 2-2 Typical cement modified soil surface after microcracking.

The objective of microcracking is to induce hundreds of tiny cracks to accommodate the need for shrinkage without significantly impacting the final pavement stiffness (Zhong, 2018). Figure 2-3 illustrate two pavement sections comprised of soil-cement subgrade with and without microcracking. These induced cracks will substitute the natural large individual cracks that have the potential to reflect up into flexible surface layers and influence the structural performance. After the initial successful microcracking work in Austria, this construction technique was tried in Texas as early as 2000 to evaluate this microcracking concept. Scullion (2002) described these efforts, including the test sites on residential streets, and presented a specification for the microcracking process in the field. This study showed favorable results using the microcracking procedure. While the microcracking treatment applied on some soil-cement sections showed apparent effectiveness that was demonstrated using field deflection testing and comparison of the

back calculated in-situ moduli with the design moduli, other microcracked soil-cement sites did not perform as predicted and did exhibit some cracking. The cracking developed in microcracked sections is likely related to the type of soil, the cement content, the lack of means to control the degree of microcracking in the field, the mixing temperature, and the age after mixing at which the microcracking is applied.

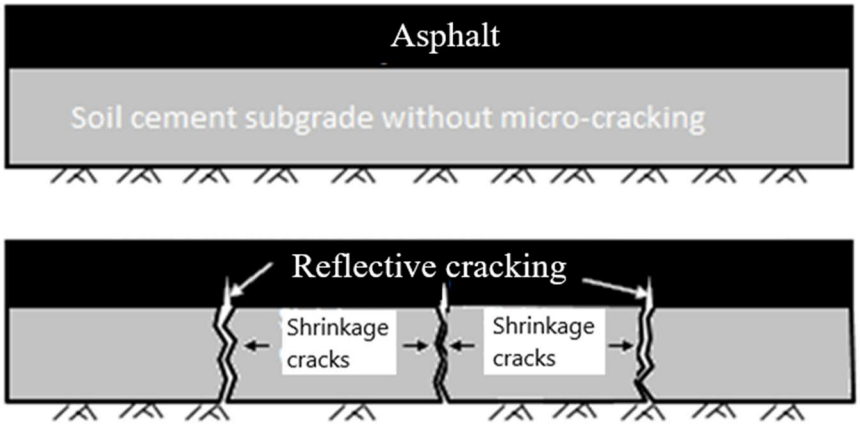

(a)

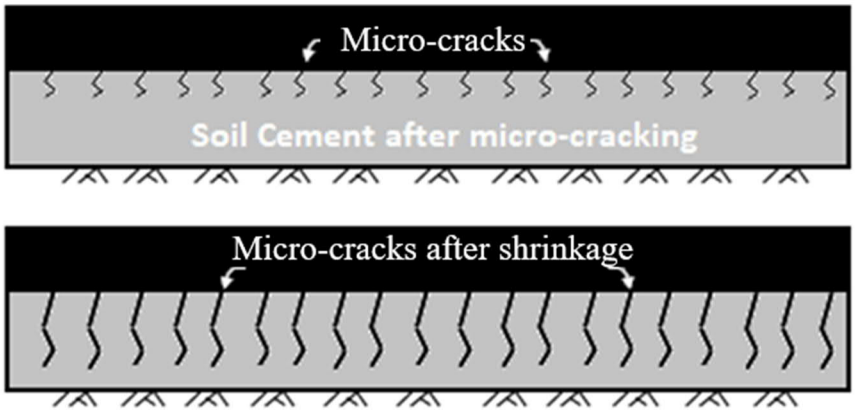

(b)

Figure 2-3 Typical asphalt pavement section with soil-cement: (a) without microcracking and with reflective-cracking and (b) with microcracking and without reflective-cracking.

Although the previous research confirmed the applicability of this construction method in the field, no literature was found describing a procedure or method to simulate the microcracking process in the laboratory. This research proposes a laboratory method that can be used to simulate the microcracking process on CMS in the field using Unconfined Compression (UC) specimens. The UC specimens were used to evaluate the properties of CMS with and without microcracking, including their strength and stiffness.

2.6 PAVEMENT DESIGN AND EVALUATION

Over the years, the flexible pavement design methods have evolved from being purely empirical (i.e., based on soil index testing, such as Casagrande soil classification), statistically empirical to more rational mechanistic-empirical approaches that involve material strengths and other environmental factors relevant to the pavement performance (Loulizi et al. 2001). In 1929 the California Highway Department used a strength test to relate the thickness of the pavement to the strength of the subgrade determined from a measure of material strength known as the California Bearing Ratio (CBR) (Huang, 2004). The statistically empirical design method was developed after many field traffic tests in 1950s. For the statistically empirical pavement design method, the performance of a pavement is predicted and designed based on the terminal serviceability index while subjected to controlled or normal traffic loads (O'Flaherty, 2002). The most famous empirical design method and the mechanistic-empirical design method are discussed briefly in the following sections.

2.6.1 **1993 AASHTO Guide for Design of Pavement Structures 1993**

This guide is the extension and revision of the 1972 and 1986 AASHTO guides, which were derived from the AASHO road tests in Illinois, USA from 1958 to 1930 (Highway and Officials, AASHTO, 1993). This design is based on the following aspects:

- Performance criteria (i.e., initial Pavement Serviceability Index (PSI) and terminal PSI), which are empirical measures of the initial and terminal pavement conditions.
- Traffic: applied axle-loads of all load configurations are converted to Equivalent Single Axle Loads (ESALs)
- Material properties for structural design: resilient modulus
- Reliability: account for uncertainties in predicting traffic loads and depend on the functional classification of a road (i.e., urban, rural, etc.)
- Layer coefficients a_i: represent the structural capacity of a pavement layer (estimated from a chart based on HMA modulus, correlated from CBR, R-value or the resilient modulus for granular material, and estimated from unconfined compressive strength for soil cement).

2.6.2 **Equivalent Single Axle Load (ESAL)**

ESAL is a concept developed from the data collected at the American Association of State Highway Officials (AASHO) Road Test to establish a damage relationship considering the effects of axles carrying different loads. The reference axle load is an 18,000-lb single axle with dual tires. The total equivalent single axle load (ESAL) is given by Equation 2-1.

$$ESAL = \sum_{i=1}^{m} n_i \times F_i \qquad \text{(Equation 2-1)}$$

where m = the number of axle groups,

i = the axle load group,

F_i = the Equivalent Axle Load Factor (EALF) for i^{th} axle load group, and

n_i = the number of passes for the i^{th} axle load group

The EALF is given by:

$$\text{EALF} = \frac{\text{Number of 18 kip ESALs causing a given loss in serviceability}}{\text{Number of x kip axle causing the same serviceability loss}}$$

The EALF is determined from the failure criteria that control fatigue and permanent deformations. The failure criterion to control fatigue cracking related to the AC layer as recommended by the Asphalt Institute (AI, 1982) is shown in Equation 2-2.

$$N_f = f_1(\varepsilon_t)^{-f_2}(E)^{-f_3} \qquad \text{(Equation 2-2)}$$

where N_f = the allowable number of load repetitions;

E= dynamic modulus of the asphalt mixture; and

f_1, f_2, and f_3= calibration constants for the asphalt mixture.

Based on the theoretical analysis of EALF by the layered theory, it is possible to assume that the tensile strains are directly proportional to the axle load (Deacon 1969). This relationship is based on an assumed f_2 of 4 and is depicted in Equation 2-3.

$$EALF_i = \left(\frac{Load_{18}}{Load_i}\right)^4 = \left(\frac{\varepsilon_i}{\varepsilon_{18}}\right)^4 \quad \text{(Equation 2-3)}$$

The failure criterion to control permanent deformation of subgrade as recommended by the Asphalt Institute (AI, 1982) is shown in Equation 2-4 and Equation 2-5.

$$N_d = f_4\ (\varepsilon_c)^{-f_5} \quad \text{(Equation 2-4)}$$

where N_d= the allowable number of load repetitions to control permanent deformation,

ε_c= the compressive strength at the surface of the subgrade, and

f_4 and f_5 = calibration constants.

$$EALF_i = \frac{N_{d18}}{N_{di}} = \left(\frac{\varepsilon_{ci}}{\varepsilon_{c18}}\right)^{f_5} \quad \text{(Equation 2-5)}$$

2.6.3 AASHTO Mechanistic-Empirical Pavement Design Guide (MEPDG)

The mechanistic-empirical design method (NCHRP, 2004) is based on the mechanics of pavement layers that relate an input, such as a wheel load, to a pavement response, such as stress and strain, which are empirically related to pavement distresses. The mechanistic-empirical flexible pavement design method relies on fundamental models of vehicular loading, material properties, and structural responses to loading and environment interaction. In this method, the influence of stresses, strains, and deflections due to the accumulated traffic loads and environmental conditions on the deterioration of the pavement structure is considered. Most of the analytical pavement design methods use a linearly elastic theory to determine stresses, strains, and deflections (Tutumluer, 2007). This theory is based on linearly elastic, homogeneous, and isotropic materials

and requires only the modulus of elasticity and Poisson's ratio for each pavement layer. Although this theory simplifies the analysis, most materials used in roadway construction do not behave linearly, in particular, for unbound granular base and subgrade layers. In addition to the pavement response determination, the pavement design requires a prediction of the performance of the pavement structure. Therefore, performance prediction models are needed to relate the type of deterioration, such as rutting and fatigue cracking, to the number of load repetitions to failure (O'Flaherty, 2002). These models often require carful calibration. The Mechanistic Empirical Pavement Design Guide (MEPDG) (NCHRP, 2004), uses a multilayer elastic theory where the pavement layers are treated as linearly elastic materials and a finite element code is used when the nonlinearity of unbound layers is considered.

Flexible pavements are expected to withstand the combined effects of traffic loading and environments for a predetermined period (called design life). The performance of a pavement as well as the pavement condition change with time and traffic. The mechanistic-empirical design process entails the incorporation of both the climate variations and the traffic data into the determination of the pavement responses (e.g., the tensile strain at the bottom of the asphalt layer and the compressive strain on top of the subgrade). The calculated pavement responses are used in the damage models to accumulate the damage with time, which is empirically related to the pavement distress, and predicts the remaining pavement life.

2.6.4 **Pavement Evaluation**

Flexible pavement performance can be correlated with the pavement surface deflections, which can be measured by non-destructive test methods. The nondestructive test equipment and methods for determining the surface deflections can be divided into three categories: the steady-state

deflection method (Dynaflect and Road Rater), the static deflection method (Benkelman Beam), and the impact load deflection method (Falling Weight Deflectometer). Among these methods, the FWD test is the widely used nondestructive dynamic test for evaluation of the quality and performance of pavement structures. Maintenance strategies in many countries all over the world are based on the results of this test (Al-Khoury et al. 2000).

CHAPTER 3 MATERIAL CHARACTERIZATION

3.1 INTRODUCTION

In this study, laboratory test procedures were used to examine the native and cement-modified soils for subgrade stabilization in two project sites in Kansas. Before the development of the procedure to generate microcracking of CMS specimens in the laboratory, several test methods were adopted in the laboratory to characterize the properties of native soil and CMS and are discussed in this chapter

3.2 MATERIALS

3.2.1 Soil Selection

Two different soils from on-going pavement reconstruction projects located in Marion County and Sedgwick County were selected and evaluated in this research. These soils were classified as clayey sand with gravel (SC) and fat clay with sand (CH), respectively, according to the Unified Soil Classification System (USCS) described in ASTM D2487. The Marion County soil (bulk) was collected from a project located along 330th Street, between K-15 and the Marion-McPherson County Line, west of Tampa, Kansas. This site will be later referred to as 330th MN. The 330th MN existing roadway was previously paved with a two-inch thick Hot Mix Asphalt (HMA) layer that exhibited severe distresses (longitudinal, transverse, and fatigue cracking). The bulk soil was excavated at depths of approximately one foot along a one-mile road segment of the eight-mile roadway that was planned to be built on a one-foot thick soil-cement subgrade overlaid by a three-inch thick HMA layer. In addition, the bulk soil specimen from depths of approximately one to

three feet below the existing grades were obtained by Terracon, on May 8, 2017, prior to initiation of construction activities for this project.

The Sedgwick County bulk soil was retrieved from a project located East 87th Street South, between S. 95th Street and Greenwich Road, about four miles southeast of Derby, Kansas. This site will be later referred as 87th SG. The existing roadway was previously surfaced with a layer of river sand and gravel of approximately six inches thick. The soil specimens were collected from the existing roadway surface down to a depth of approximately ten inches along the proposed project alignment. The pavement section for this project comprised of ten inches of CMS overlaid by a two-inch thick HMA layer. Also, bulk subgrade soil specimens from depths of approximately one to three feet below the existing grades were sampled by Terracon, on May 10, 2018, prior to starting construction activities for this project. Figure 3-1 shows the locations of these two sites on the Google Map.

The 330th MN and 87th SG pavement reconstruction projects depicted in Figure 3-1 are low volume, two-lane roadways with total traffic of 548,687 Equivalent Single Axle Load (EASLs) and 82,000 ESALs, over the proposed design lives of 20 years and 8 years, respectively.

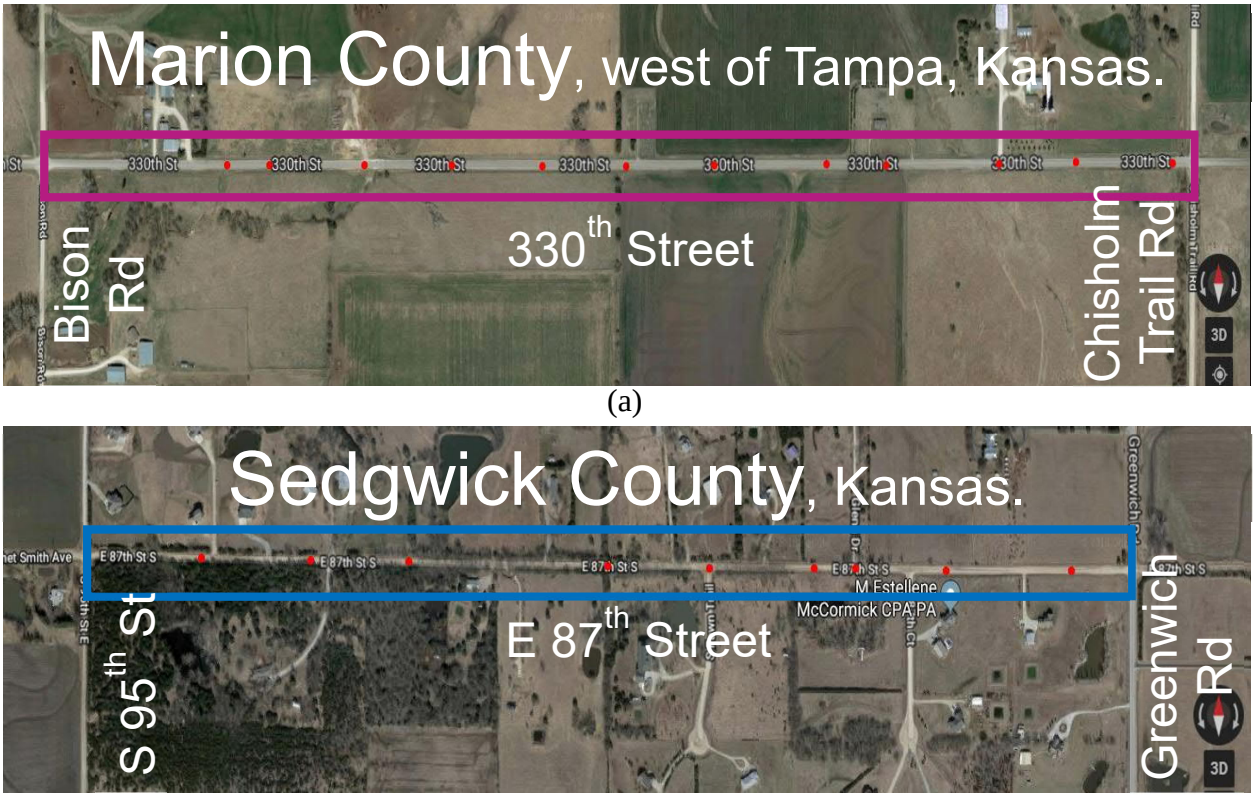

Figure 3-1 Google map for the collected soil locations of: (a) clayey sand with gravel (SC) and (b) fat clay with sand (CH).

3.2.2 **Additives**

The additive of interest for this study is Portland cement (hydraulic cement) Type I/II that was selected to modify the native soil and improve its properties. The chemical properties of this additive are presented in Figure A-1 and Figure A-2 Appendix A.

3.3 LABORATORY TESTING

3.3.1 **Specimen Preparation**

The bulk soil specimens collected from these projects at depths of approximately zero to one foot below the existing pavement subgrade along the 330th MN site and depths of approximately zero to ten inches below the granular surface along 87th SG site were first mixed thoroughly, and a

portion of the mixed soil was dried for 24 hours at 60 °C in a large oven. To determine the Atterberg limits of each soil, the dry soil was washed through a No. 40 (0.425 mm) sieve using water in accordance with ASTM D4318. The portion of the soil that passed the No. 40 sieve was dried again for 24 hours at 60 °C and then crushed using a mortar and pestle. The compaction characteristics of these soils were determined to prepare reconstituted soil specimens mixed with cement. To evaluate the unconfined compressive strengths of the reconstituted specimens mixed with cement at different cement contents, the dry soil was crushed, pulverized, and passed through the ¾-in (19 mm) sieve.

3.3.2 **Soil Classification**

The grain size distribution, the Atterberg limits, the standard Proctor compaction curves, and the laboratory California Bearing Ratios (CBR) were determined for these two soils. Sieve analyses were performed using a wet sieve method in accordance with ASTM D442 to obtain the grain size distribution of the native soil. Two specimens for each material source (approximately 2.9 lb) 1300 g) of oven-dried soil each) were washed through a No. 200 sieve (0.075 mm). The portions of the soils retained on and passing the sieve were dried and weighed. Based on the percent of soil passing the No. 200 (0.075 mm) sieve, the 330th MN soil within a depth of approximately 12 inches from the subgrade surface was classified as a coarse-grained soil. On the other hand, the 87th SG soil was classified as a fine-grained soil. Figure 3-2 (a) and (b) present the grain size distribution curves of the 330th MN and 87th SG soils, respectively.

The liquid limits, plastic limits, and plasticity indices of the native soils were determined according to ASTM D4318. The liquid limits were determined using the multipoint liquid limit method (Method A) described in ASTM D4318. Based on the Atterberg limits, the soils from 330th

MN were classified as a Clayey Sand with gravel (SC) and lean clay (CL) of the fine portion according to the Unified Soil Classification System (USCS) described in ASTM D2487. On the other hand, the soil from 87th SG was classified as Fat Clay with sand (CH) according to the Unified Soil Classification System (USCS) described in ASTM D2487. Table 3-1 presents the Atterberg limits of the soils from both projects.

Table 3-1 Atterberg limits of Soils from 330th MN and 87th SG soil.

Project Location	**330th MN**	**87th SG**
USCS Classifications	**SC soil**	**CH soil**
Liquid limit (LL)	30	50
Plastic limit (PL)	15	21
Plastic index (PI)	15	29

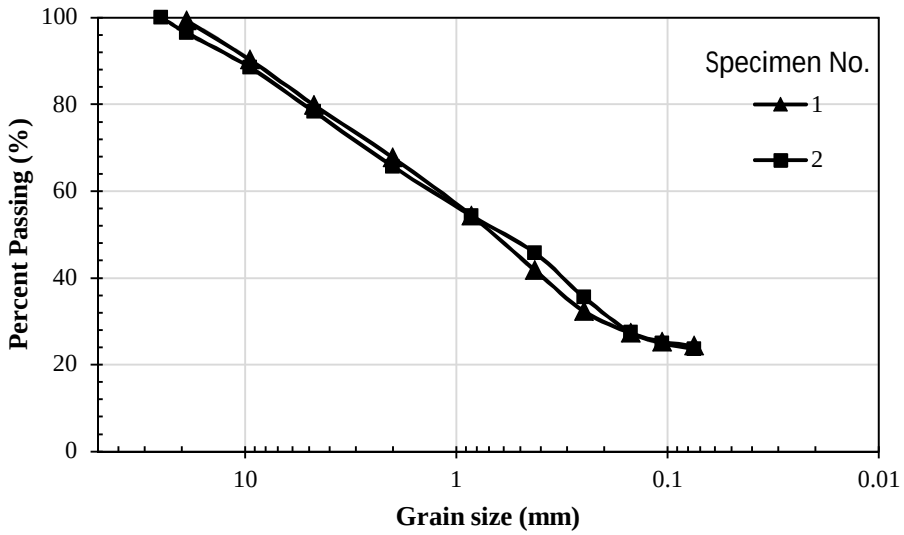

(a)

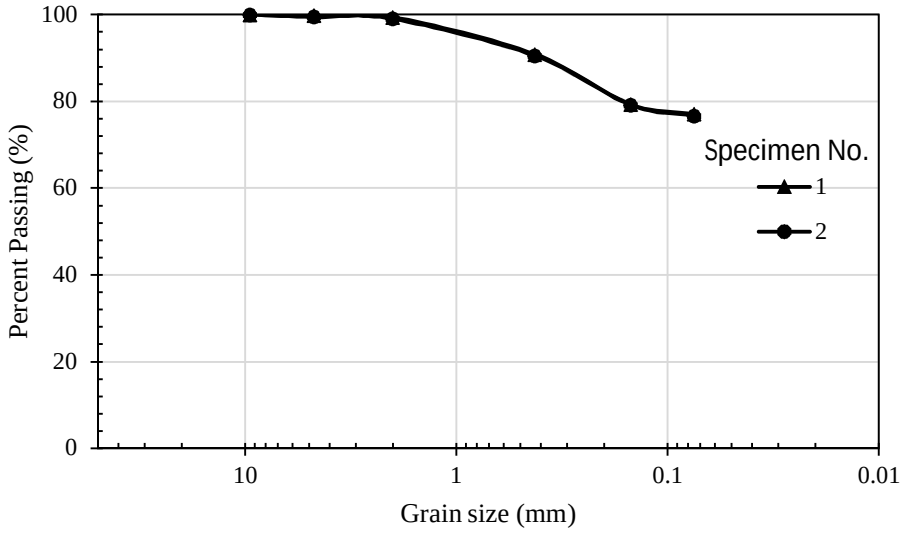

(b)

Figure 3-2 Grain size distribution curves of the native soils from: (a) 330th MN and (b) 87th SG (1 inch = 25 mm).

3.3.3 **Soil Compaction Characteristics**

The native soils were tested to determine their optimum moisture contents and maximum dry densities using the standard Proctor compaction method described in ASTM D698. Method C was utilized to determine the moisture content-maximum dry density curves presented in Figure 3-3 (a) and Figure 3-4 (a). After the compaction tests, the same specimens were tested for their California Bearing Ratios (CBR) following the procedure described in ASTM D1883. Figure 3-3(b) and Figure 3-4 (b) present the effect of the moisture content on the California Bearing Ratio, indicating the susceptibility of the subgrade strength to moisture content. For each project, two specimens were compacted with two different methods (hand and mechanical compaction) and then tested for the maximum dry unit weight and CBR. Since the mechanical compaction generates more uniform distribution of compaction energy than hand compaction, a lower optimum moisture content and a higher maximum dry density were obtained for soil specimens using mechanical compaction. However, the curves generated by hand compaction were used in this research since subsequent work was mostly performed by hand. The optimum moisture content, the maximum dry density, and the CBR at the optimum moisture content for each native soil are presented in Table 3-2.

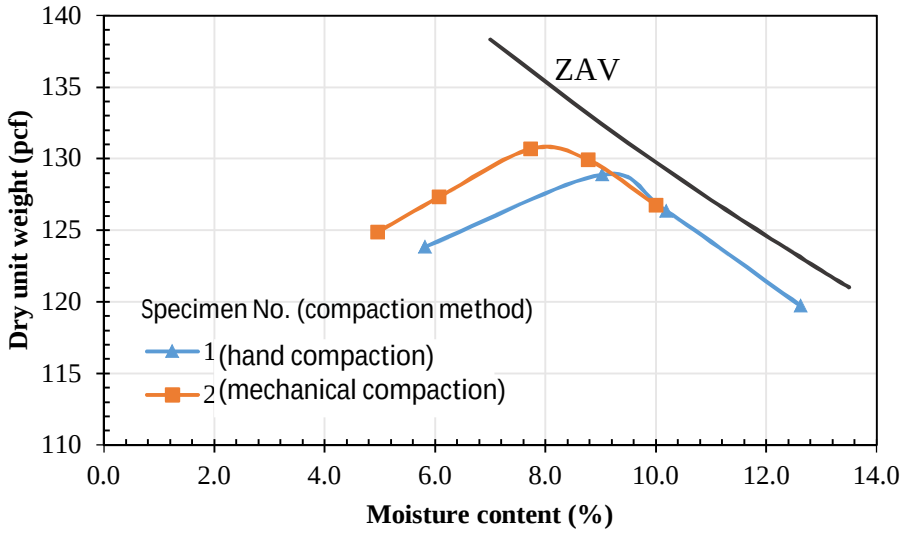

(a)

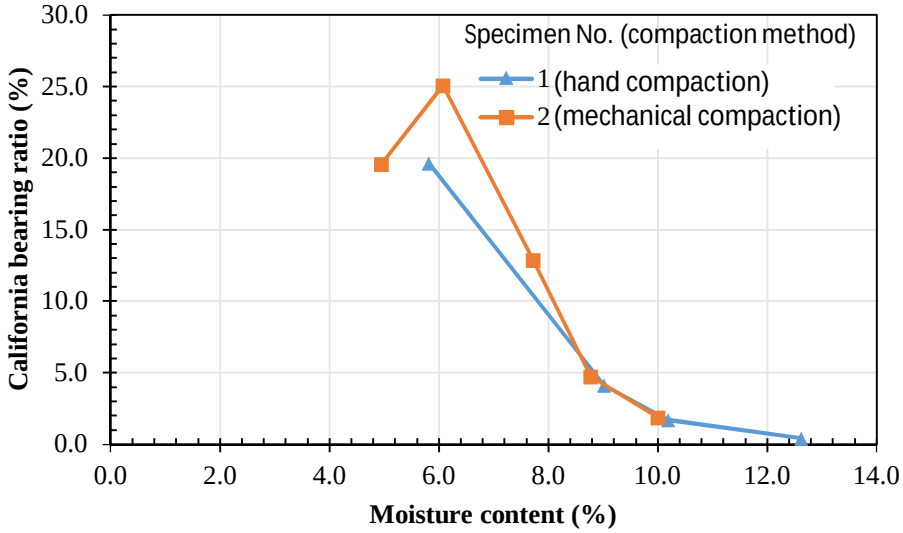

(b)

Figure 3-3 Compaction characteristics of the native soil from 330th MN: (a) compaction curves and (b) effect of moisture content on CBR (ZAV = zero air void).

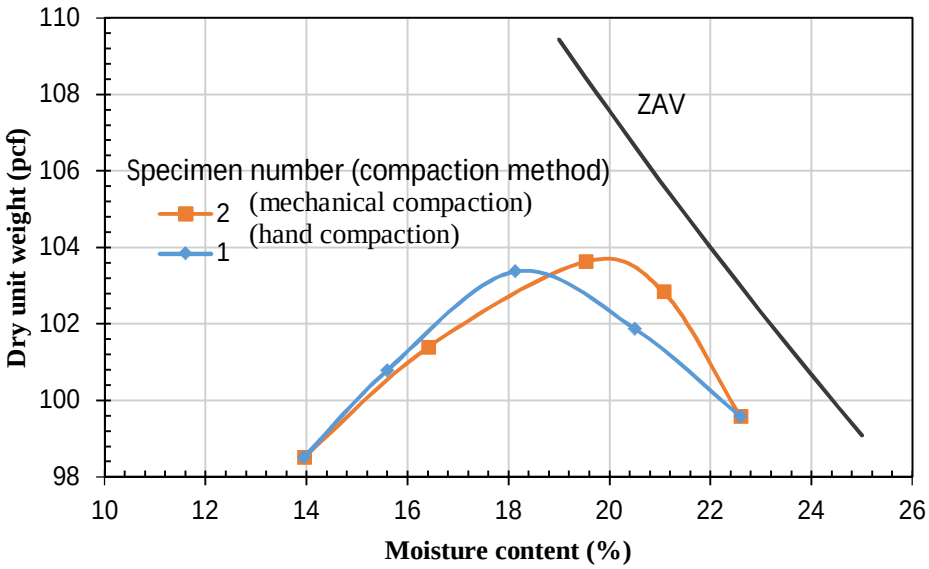

(a)

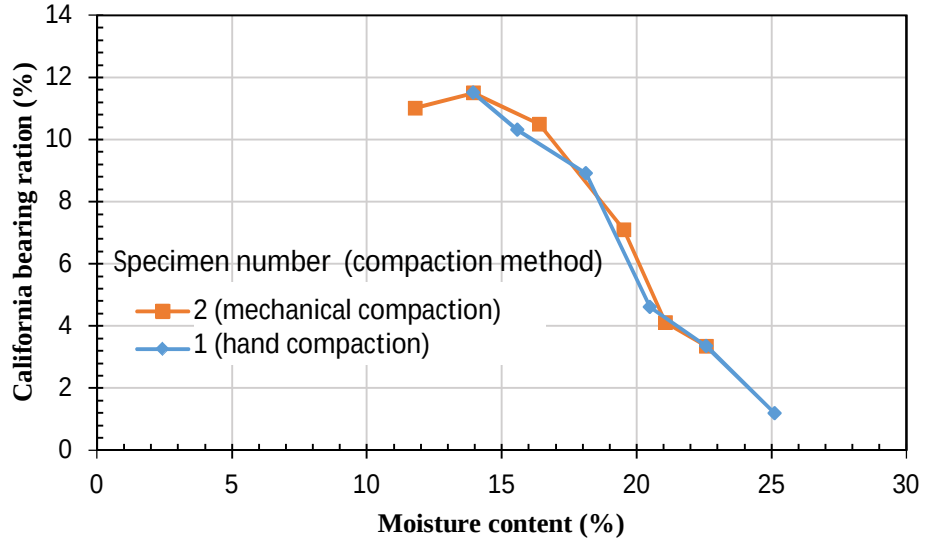

(b)

Figure 3-4 Compaction characteristics of the native soil from 87th SG: (a) compaction curves and (b) effect of moisture content on CBR.

Table 3-2 Compaction Characteristics of Soils from 330th MN and 87th SG soil.

Project Location	**330th MN**	**87th SG**
USCS Classifications	**SC soil**	**CH soil**
Optimum moisture content, w_{opt} (%)	9.2	19.0
Maximum dry unit weigh, γ_d (pcf)	129	103
California Bearing Ratio (CBR) at w_{opt} (%)	4.0	7.6

3.3.4 **Unconfined Compressive Strength**

The specimen preparation procedure consisted of adding a specific percentage of the Portland cement to the native soil and then mixing them by hand. The amount of Portland cement was calculated as a percentage by dry weight of the soil. Specimens were prepared for unconfined compressive strength (UC) testing in accordance with ASTM D1632 and tested for unconfined compressive strengths following ASTM D1633. The specimens were prepared with different cement contents and at the optimum moisture content or +2% of the optimum moisture content as determined for the native soil from each county. Unconfined compressive strength tests were performed on both un-cracked and microcracked specimens after various curing periods. The curing process took place in a moisture room at approximately 100% relative humidity and 73.4 ±3.6 ^{o}F (23 ± 2 ^{o}C) room temperature. The UC test results are presented in Chapter 4.

3.3.5 **Wet-Dry Cycles**

Wet-dry cycle tests were performed according to ASTM D559. Two identical un-cracked specimens and one microcracked specimen of the 330th MN CMS were prepared at the desired cement content and the optimum moisture content following the UC specimen preparation procedure. The specimens were cured for 7 days in a moisture room and subjected to wet-dry cycles. Each wet-dry cycle consisted of submerging three CMS specimens in water for 5 hours

and then placing them in a 160 °F (71°C) oven for 42 hours. After completing each cycle, one un-cracked specimen was brushed and weighed to determine the mass loss of soil. The other specimens were measured for volumetric change and weighed to determine any change in moisture content. The test continued until 12 wet-dry cycles were completed or until the specimen failed. The wet-dry cycle test results are presented in Chapter 4.

3.3.6 **Hydraulic and Electrical Conductivity**

Hydraulic conductivity tests were performed according to ASTM D5084. Both un-cracked and microcracked specimens of the 330th MN CMS were prepared at the desired cement content and the optimum moisture content following the UC specimen preparation procedure. The specimens were cured for 7 days in a moisture room and then subjected to saturation in a permeability test chamber before testing for hydraulic conductivity. On average, the saturation stage took approximately eight days in order to reach saturation. After completing the saturation, both un-cracked and microcracked specimens were tested for hydraulic conductivity at three different confining pressures. Before and after the saturation stage of each specimen, the specimen electrical conductivity was measured using the Portable Field/Laboratory Spectral Induced Polarization (SIP) Unit (PSIP) as shown in Figure 3-5. The PSIP is a high-performance multi-channel geophysical instrument optimized for laboratory and in-situ near surface SIP, conventional resistivity, time-domain induced polarization and self-potential measurements. The hydraulic and electrical conductivity test results are presented in Chapter 4.

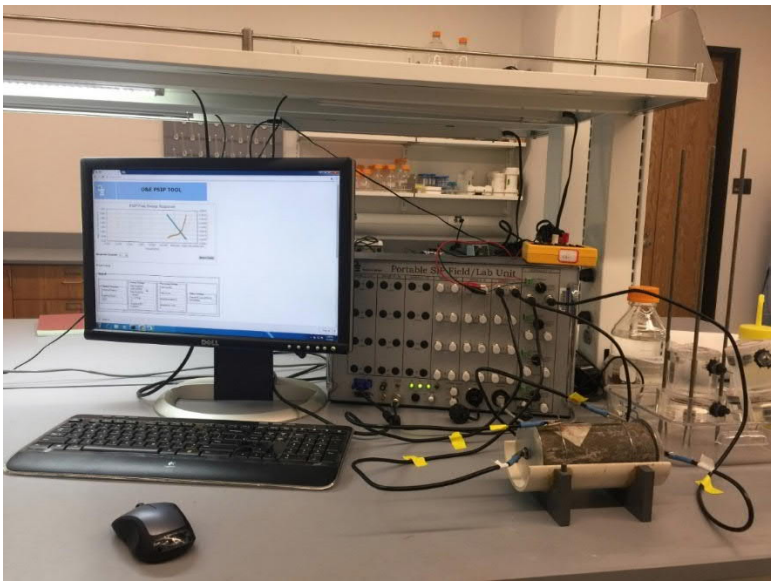

Figure 3-5 Electrical conductivity test setup of the CMS specimen connected to the PSIP unit.

3.3.7 **Resilient Modulus Testing**

Resilient modulus (M_r) is a key parameter in the design of flexible pavements. It is a fundamental material property for characterizing bounded and unbound pavement materials. The resilient modulus (M_r) is defined as the stress dependent ratio of the applied axial stress over the recovered axial strain (i.e., resilient strain) in a cyclic load triaxial test as shown in Equation 3-1.

$$M_R = \frac{\sigma_d}{\epsilon_r} \qquad \text{(Equation 3-1)}$$

where σ_d= the deviator stress, and

ϵ_r= the recoverable axial strain.

This property for a subgrade or base material is necessary for numerical models used in pavement design (Ullidtz, 1987; O'Flaherty, 2002). The resilient modulus for an individual soil can significantly vary with its density, moisture content, gradation, plasticity index, and stress level

(Vanapalli et al. 1999). Figure 3-6 shows the typical triaxial chamber with external LVDTs and a load cell. A typical repeated load triaxial test result is depicted in Figure 3-7.

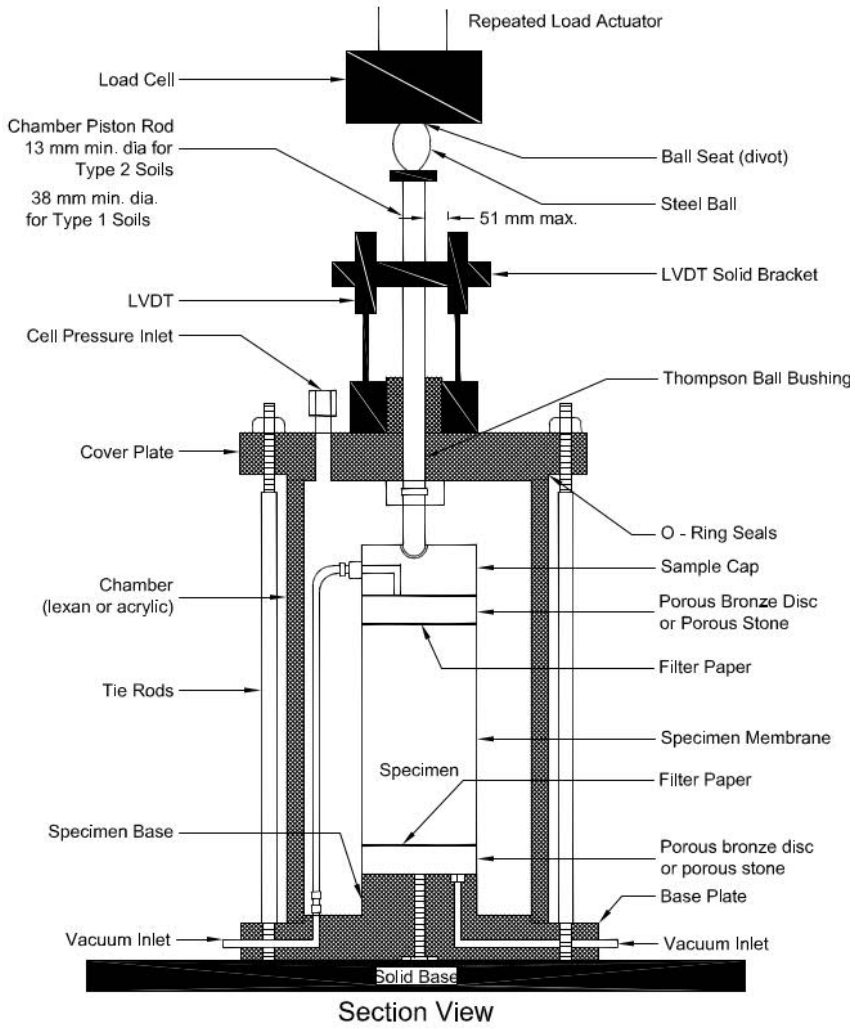

Figure 3-6 Typical triaxial chamber with external LVDTs and load cell (FHWA, 2007).

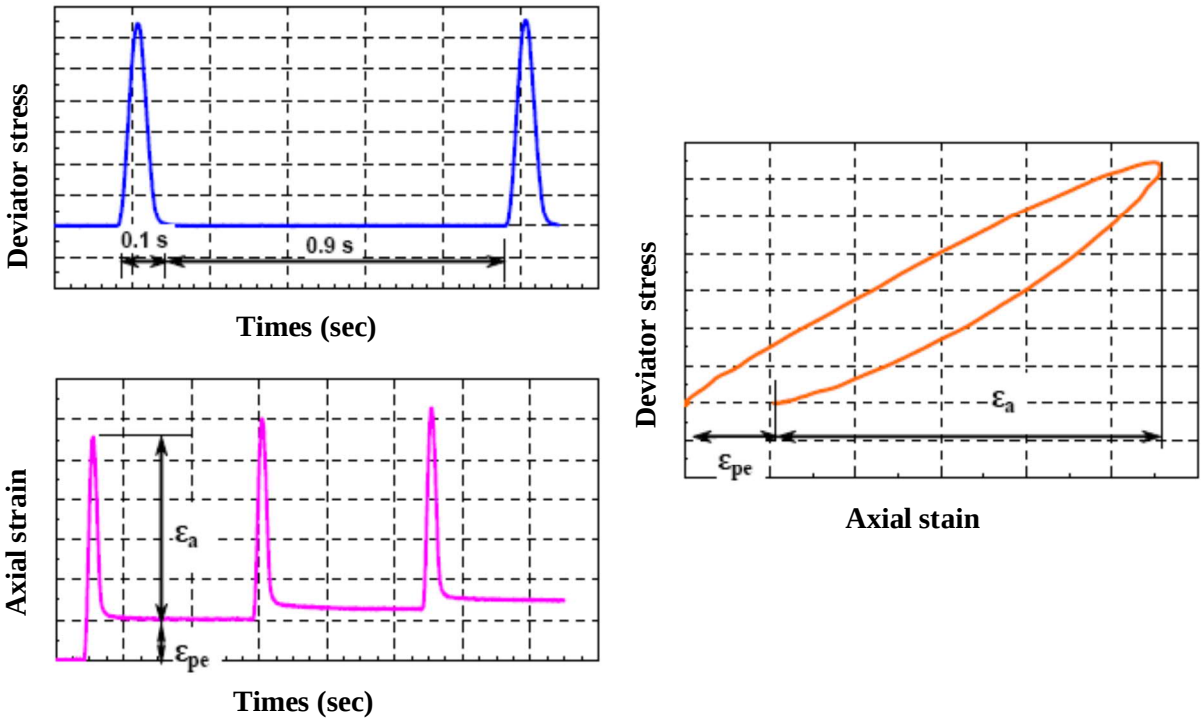

Figure 3-7 Typical results from a repeated load triaxial test (Hanifa et al. 2015).

The resilient modulus test using the cyclic triaxial test equipment is designed to simulate traffic wheel loading on a soil by applying a sequence of repeated or cyclic loading on the specimen. In this research, the standard test method (AASHTO Designation T 307-13) for determining the resilient modulus of soils and aggregate materials –was employed. The stress levels were selected to represent the overburden pressures of specimens in the subgrade. The axial deviatoric stress includes a cyclic stress (an applied deviatoric stress) and a constant stress (typically a seating stress on the soil specimen). It should be noted that the constant stress typically equals 10% of the overall maximum axial stress.

The specimens were first conditioned by applying 500 load cycles to remove most irregularities on the top and bottom surfaces of the test specimen and to suppress most of the initial stage of permanent deformation. The conditioning of the specimens was followed by 15 testing

sequences, as described in Table 3-3, at different levels of cyclic deviatoric stress and confining pressure, such that the resilient moduli are determined at varying normal and shear stress levels. For each load sequence, the resilient modulus values are calculated for the last five cycles and their values are subsequently averaged. The cyclic loading consists of repeated cycles of a haversine shaped load pulse. These load pulses have a 0.1-second load duration and a 0.9-second rest period. The calculated resilient modulus is to characterize the stiffness of pavement materials under repeated loading at different stress levels (both confining pressure and deviatoric stress).

The resilient modulus tests were conducted on the cement-modified soil specimens collected from the field after microcracking using the coring technique. Also, the resilient modulus tests were conducted on un-cracked and microcracked specimens that were prepared in the laboratory by mixing cement at the desired cement contents with the soils collected from 330th MN and 87th SG sites.

Several mathematical models have been proposed by researchers to characterize the resilient moduli of aggregate and cohesive soil. These models relate the resilient modulus to one independent variable: deviator stress, σ_d, confining stress σ_3, or bulk stress, θ ($=\sigma_1 + \sigma_2 + \sigma_3$); or to two independent variables: (σ_d, θ), (σ_d, σ_3) or θ to octahedral stress (τ_{oct}). The details of these models will be presented in Section 5.5 of Chapter 5.

Table 3-3 Testing sequence for CMS specimens.

Sequence No.	Confining Pressure, σ_3		Max. Axial Stress, σ_{max}		Cyclic Stress, σ_{cyclic}		Constant Stress, 0.1 σ_{max}		No. of Load Applications
	kPa	psi	kPa	psi	kPa	psi	kPa	psi	
0	41.4	6.0	27.6	4	24.8	3.6	2.8	0.4	500-1000
1	41.4	6.0	13.8	2	12.4	1.8	1.4	0.2	100
2	41.4	6.0	27.6	4	24.8	3.6	2.8	0.4	100
3	41.4	6.0	41.4	6	37.3	5.4	4.1	0.6	100
4	41.4	6.0	55.2	8	49.7	7.2	5.5	0.8	100
5	41.4	6.0	68.9	10	62.0	9.0	6.9	1.0	100
6	27.6	4.0	13.8	2	12.4	1.8	1.4	0.2	100
7	27.6	4.0	27.6	4	24.8	3.6	2.8	0.4	100
8	27.6	4.0	41.4	6	37.3	5.4	4.1	0.6	100
9	27.6	4.0	55.2	8	49.7	7.2	5.5	0.8	100
10	27.6	4.0	68.9	10	62.0	9.0	6.9	1.0	100
11	13.8	2.0	13.8	2	12.4	1.8	1.4	0.2	100
12	13.8	2.0	27.6	4	24.8	3.6	2.8	0.4	100
13	13.8	2.0	41.4	6	37.3	5.4	4.1	0.6	100
14	13.8	2.0	55.2	8	49.7	7.2	5.5	0.8	100
15	13.8	2.0	68.9	10	62.0	9.0	6.9	1.0	100

CHAPTER 4 MICROCRACKING SIMULATION IN LABORATORY

4.1 CEMENT MODIFIED SOIL

4.1.1 330th MN Site Soil

Portland cement (hydraulic cement) Type I/II was selected to modify the native soil and improve its engineering properties. To design the soil-cement mix, a strength criterion based on unconfined compressive (UC) strength of soil-cement specimens cured for 7 days in the moisture room was adopted. Since this study involved field and laboratory evaluations of the cement modified soil and the actual CMS mixture was designed and constructed in the field to achieve a 7 days UC strength of 300 psi. Therefore, the selected 7-day UC strength in this study for 330th MN was 300 psi. To find the appropriate cement content, the soil was mixed with cement at three different cement contents, 3.5%, 5.0%, and 6.5%. For each cement content, five specimens were prepared in accordance with ASTM D1632 and tested for their unconfined compressive strengths following ASTM D1633. Soil and cement were mixed at ±0.5% of the optimum moisture content as determined for the native soil. The soil-cement mix was placed and compacted in a mold, cured in the mold in a temperature-controlled moist-curing room for 12 to 18 hours, and then removed from the mold using a UC specimen extruder. The specimen was returned to the moisture room for continuous curing and protected from dripping water.

After seven days of the moist curing period, unconfined compression tests were performed on CMS specimens in the moist condition directly after their removal from the moisture room. Table 4-1 summarizes the unconfined compressive strengths for all specimens of the three mixes with the cement contents of 3.5%, 5.0%, and 6.5%. Figure 4-1 shows the effect of the cement content on the UC strength of CMS. At the target UC strength, the cement content was determined

as 5.0%. The 5.0% cement content was used in the following laboratory evaluation performed for this project and represented the cement content used in the field for the construction of this project. The stress-strain curves of the CMS specimens after seven-day curing are presented in Appendix B Figure B-1 .

Table 4-1 Unconfined compressive strength of CMS after cured for seven days for 330th MN soil.

Mix No.	Specimen No.	Cement content (%)	Compressive strength (psi)	Average strength (psi)
1	1	3.5	205	206
	2		212	
	3		262	
	4		208	
	5		144	
2	1	5.0	290	305
	2		306	
	3		349	
	4		337	
	5		242	
3	1	6.5	433	417
	2		394	
	3		397	
	4		443	
	5		420	

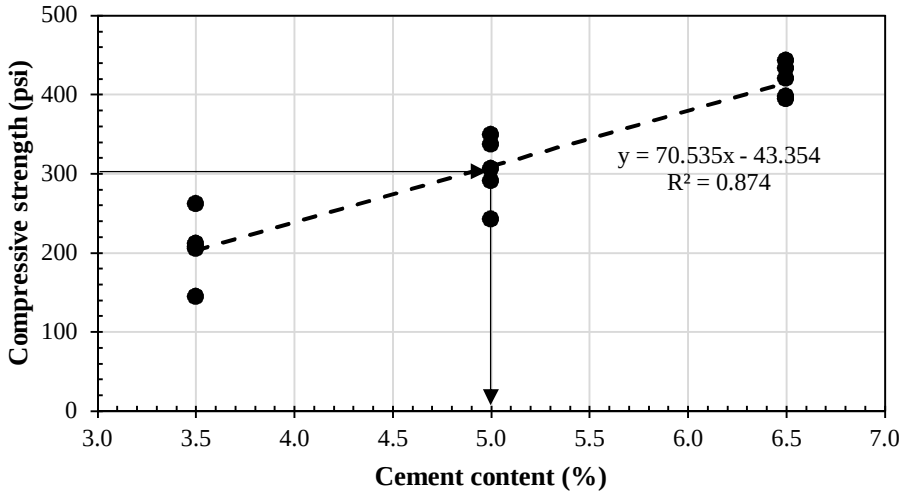

Figure 4-1 Unconfined compressive strength of CMS versus cement content after cured for seven days for the 330th MN soil.

4.1.2 **87th SG Soil**

Similar to the procedure followed for the 330th MN site, Portland cement Type I/II was used to modify the native soil from 87th SG site. In this project, a strength criterion based on the unconfined compressive (UC) strength of 210 psi for soil-cement specimens cured for 7 days in the moisture room was considered for the design of the soil-cement mix. This 7-day UC strength was selected to simulate the field condition based on the project requirement. To find the appropriate cement content, the native soil was mixed with cement at three different cement contents, 4.0%, 5.5%, and 7.0%. For each cement content, three specimens were prepared in accordance with ASTM D1632 and tested for their unconfined compressive strengths following ASTM D1633. Soil and cement were mixed at +2.0% of the optimum moisture content as determined for the native soil. The soil-cement mix was placed and compacted in a mold, cured in the mold in a temperature-controlled moisture room for 12 to 18 hours, and then removed from the mold using a UC specimen extruder. The specimen was returned to the moisture room for continuous curing and protected from

dripping water. After seven days of the moist curing period, unconfined compression tests were performed on CMS specimens in the moist condition directly after their removal from the moisture room. Table 4-2 provides the unconfined compression test results of the three mixes from Sedgwick County with the cement contents of 4.0%, 5.5%, and 7.0%. Figure 4-2 shows the effect of the cement content on the UC strength of CMS. As expected, the unconfined compressive strength of CMS increases as the cement content increases. At the target UC strength, the cement content was determined as 5.5%. This cement content was used in the following laboratory evaluation and represents the cement content used in the field for the construction of the project. Figure B-2 in Appendix B presents the original stress-strain curves of the CMS specimens after seven-day curing for 87th SG soil.

Table 4-2 Unconfined compressive strength of CMS after cured for seven days for 87th SG soil.

Mix No.	Specimen No.	Cement content (%)	Compressive strength (psi)	Average strength (psi)
1	1	4.0	138	133
	2		132	
	3		130	
2	1	5.5	194	202
	2		200	
	3		211	
3	1	7	291	301
	2		298	
	3		315	

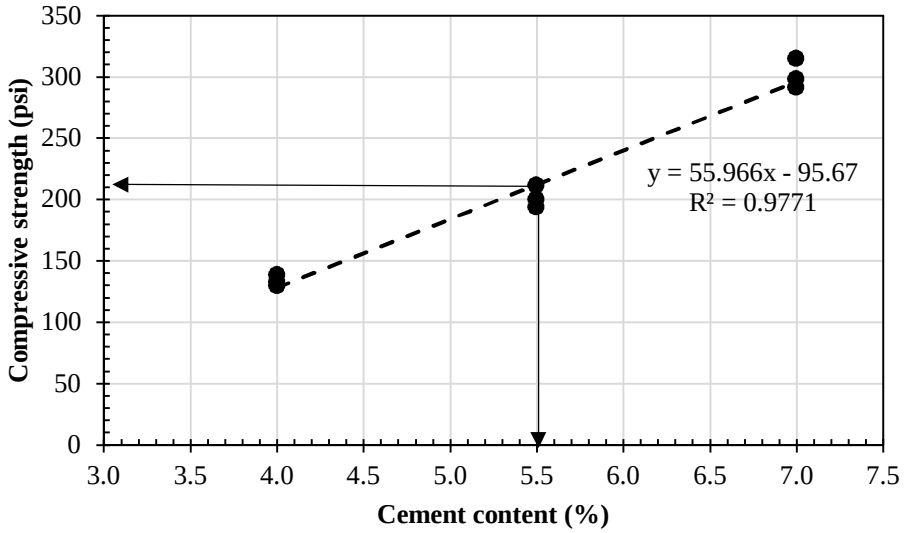

Figure 4-2 Unconfined compressive strength of CMS versus cement content after cured for seven days for the 87th SG soil.

4.2 MICROCRACKING

4.2.1 **330th MN Soil**

The simulation of the microcracking process in the laboratory was intended to replicate the procedure adopted in the field during construction. As mentioned earlier, micro-cracks in a CMS layer are induced in the field by re-compacting the CMS layer with a roller after the initial compaction and a partial curing time of 24 to 48 hours. In other words, the microcracks are generated by preloading the CMS surface of the treated layer and inducing a network of fine cracks. This process will prevent the formation of major and wide shrinkage cracks that typically develop in soils mixed with cement. In practice, unconfined compression tests are conducted in the laboratory to determine the cement content for a CMS mix. In this research, microcracking of the specimens prepared in the laboratory was simulated using the unconfined compression testing machine. The specimens were subjected to axial loading until yielding was identified.

Before development and verification of the microcracking process, the UC strength of CMS specimens was determined after being moist-cured for a period of 48 hours. Six UC specimens of CMS at the desired cement content of 5.0% were prepared and tested after 48-hour moist curing. Table 4-3 provides the UC test results of the specimens using the soil from 330th MN site. The average UC strength of CMS after 48-hour curing was 228 psi, or 75% of the 7-day strength. Figure 4-3 presents the stress-strain curves of the UC tests of the CMS specimens mixed at 5.0% cement content with the 330th MN soil after 48-hour curing. This figure shows that the CMS material had a brittle behavior (i.e., the stress sharply dropped after the peak).

Table 4-3 Unconfined compressive strength of CMS with 5.0 % cement content after 48-hour curing for the 330th MN soil.

Specimen No.	**Compressive strength (psi)**	**Average strength (psi)**
1	234	228
2	197	
3	226	
4	238	
5	233	
6	240	

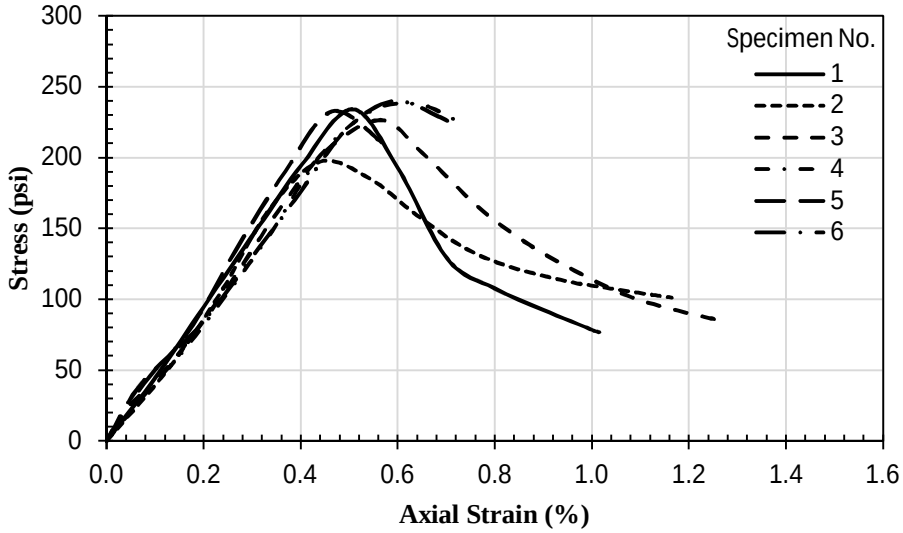

Figure 4-3 Stress-strain curves of CMS with 5.0 % cement after 48-hour curing for the 330th MN soil.

To simulate the microcracking process in the laboratory by preloading the CMS specimen after a short curing period, three trials were made. In these trials, three stress levels of preloading were applied to the UC specimens after the 48-hour curing period: approximately 50%, 70%, and 90% of the ultimate UC strength of the specimens. Figure 4-4 (a) depicts the stress-strain curves of the UC specimens during preloading. For each preloading level, three CMS specimens were prepared and loaded. After the preloading stage, no sign of any cracks was observed on the UC specimens for all preloading levels. This phenomenon was also confirmed when the preloaded specimens were tested to failure after 2-hour waiting time, showing no strength reduction. In fact, the UC strengths of the preloaded specimens were slightly higher than those cured for 48 hours. Figure 4-4 (b) shows the stress-strain curves of the UC specimens after preloading. Table 4-4 summarizes the results of the UC tests for all preloading levels.

The specimens of Trial 3 were preloaded to 90% of the ultimate UC strength and then tested for the UC strength after a 2-hour waiting period. These failed or microcracked specimens

from Trial 3 were loaded again in the UC tests, which showed strength and modulus (E_{50}) reductions by approximately 50% and 42%, respectively, as shown in Figure 4-5 and Table 4-5. The secant modulus, E_{50}, was calculated as the slope of the secant line connecting from the origin to the point on the stress-strain curve corresponding to 50% the UC strength. These reductions are also found in the field after microcracking of CMS layers. Therefore, the procedure of loading the UC specimen to failure and stopping loading soon after reaching the peak strength would create a similar behavior of a microcracked CMS layer in the field.

Table 4-4 The UC test results for the CMS specimens with 5.0 % cement during and after preloading.

Trial No.	**Specimen No.**	**Preloading level**	**Preloading stress (psi)**	**Average preloading (psi)**	**Compressive strength (psi)**	**Average strength (psi)**
Specimen age		**48 hours**			**50 hours**	
Trial 1	1	50%	110	112	211	240
	2		113		251	
	3		112		258	
Trial 2	4	70%	155	155	232	240
	5		155		234	
	6		154		255	
Trial 3	7	90%	210	210	279	231
	8		208		192	
	9		211		222	

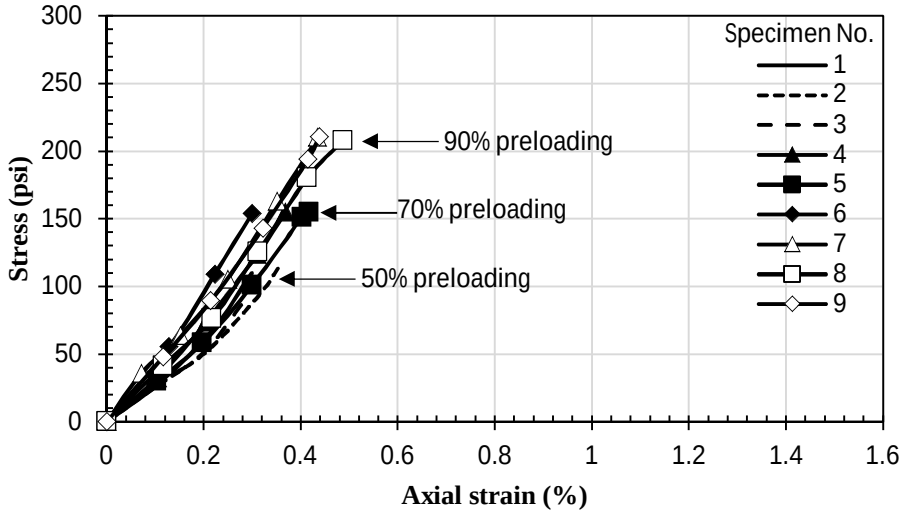

(a)

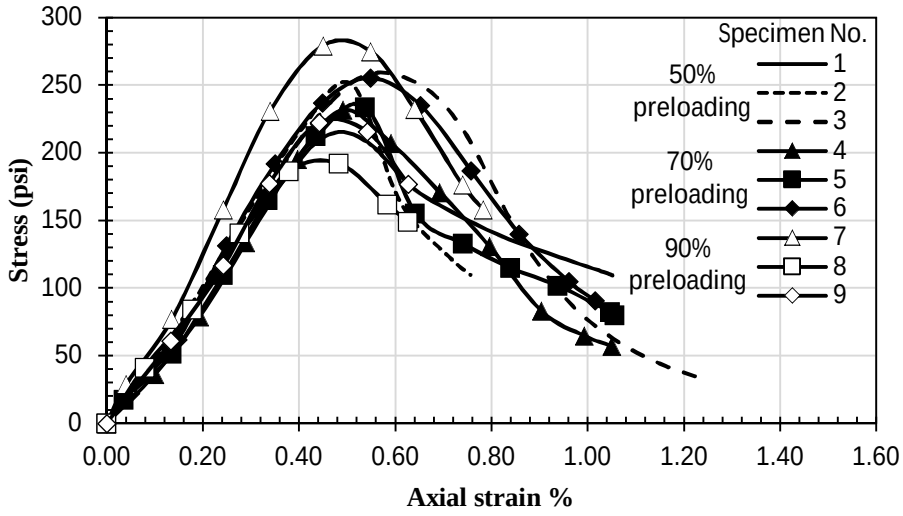

(b)

Figure 4-4 Stress-strain curves of CMS with 5.0% cement after 48-hour curing for the 330th MN: (a) loaded to the preloading stress level and (b) after preloading.

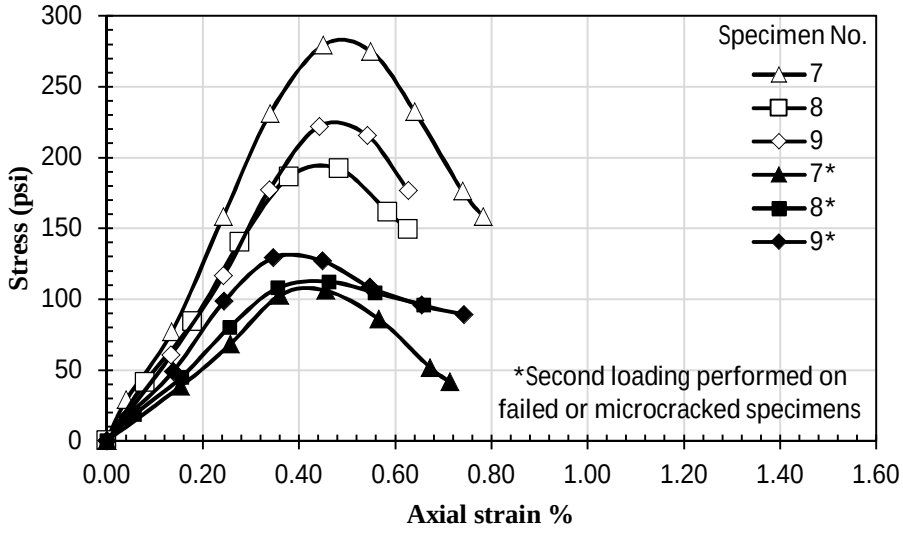

Figure 4-5 Stress-strain curves before and after microcracking of CMS specimens in Trial 3 for the 330th MN soil.

Table 4-5 Unconfined compressive strengths and moduli of failed CMS specimens for the 330th MN soil subjected to second loading.

Trial No.	Specimen No.	Specimen age	Compressive strength (psi)	Average strength (psi)	Modulus, E_{50} (ksi)	Average modulus, E_{50} (ksi)	Strength reduction	Modulus, E_{50} reduction
Trial 3	7	50 hours	279	231	65.8	54.0	50%	42%
	8		192		49.1			
	9		222		47.0			
Trial 3	7*	52 hours	106	116	26.0	31.3		
	8*		112		30.0			
	9*		129		37.9			

Note: *Second loading performed on failed or microcracked specimens

In Trial 4, three additional CMS specimens were microcracked. Figure 4-6 (a) presents their stress-strain curves. After the microcracking process, the specimens of Trial 4 were returned to the moisture room to continue the curing process and to allow the specimens for strength gain. After seven-day curing, the specimens of Trial 4 were tested for the UC strengths, and their stress-strain curves are presented in Figure 4-6 (b). The average strength of these three CMS specimens was 230 psi. In other words, the seven-day UC strength of the microcracked specimens were the same as the ultimate UC strength at 2-day of un-cracked specimens. Moreover, the seven-day UC strength of the microcracked specimens was approximately 75% of the design strength of the CMS mix (i.e., 300 psi). This finding is similar to that for the strength of the CMS layer with micro-cracks in the field at the age of seven days.

Table 4-6 summarizes the UC strengths of the CMS specimens before and after microcracking for Trial 4. Figure 4-7 shows the CMS specimen No. 3 of Trial 4 before microcracking, after microcracking at 48-hour curing, and after UC testing at seven-day curing. Micro-cracks were observed on the CMS specimens after the microcracking process. Based on the test procedure adopted and the test results obtained in this study, it is recommended that the microcracking process in the laboratory should be controlled as loading of the CMS specimen passing the peak compressive strength by less than 0.1% axial strain and releasing the load soon after.

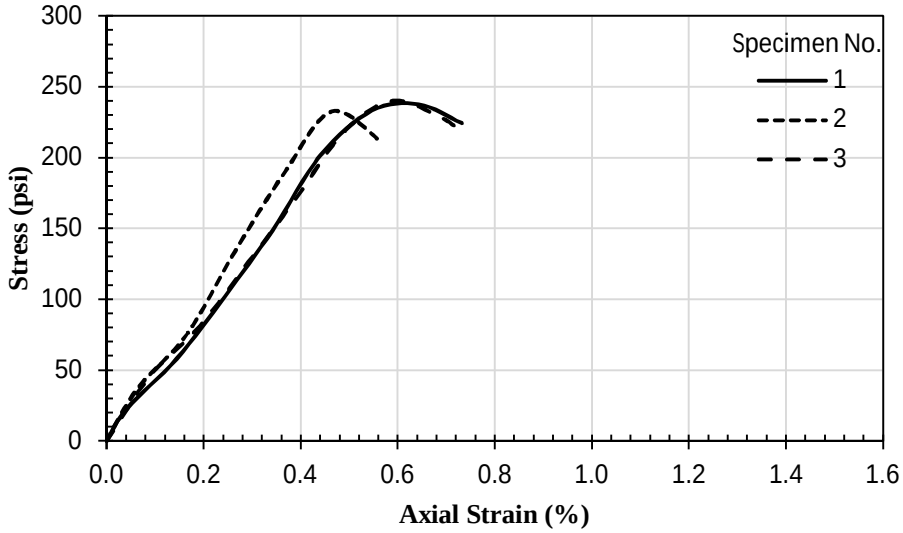

(a)

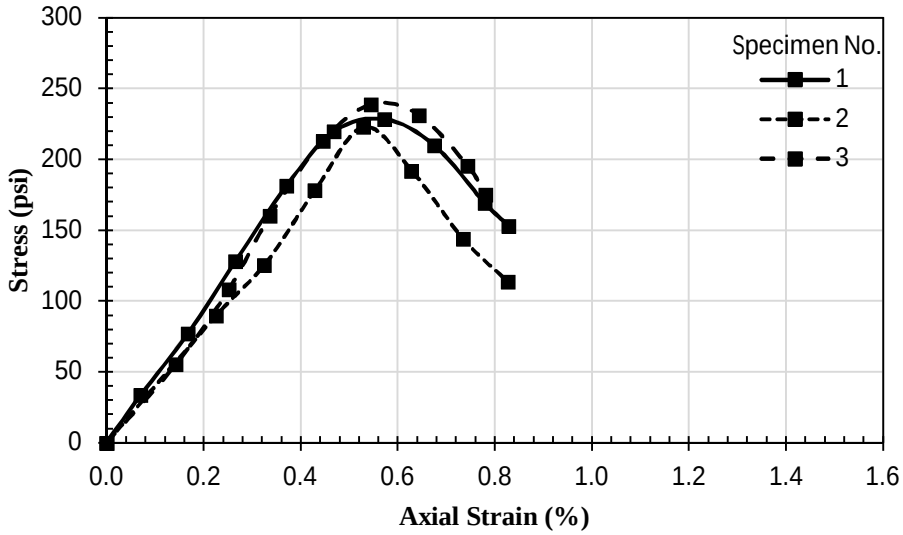

(b)

Figure 4-6 Stress-strain curves of CMS specimens at 5% cement in Trial 4 for the 330th MN soil: (a) during the microcracking process after 2-day curing and (b) after the microcracking process after 7-day curing.

Table 4-6 UC strengths of CMS specimens before and after microcracking for the 330th MN Soil.

Trial No.	Specimen No.	Compressive strength (psi)	Average strength (psi)	Compressive strength (psi)	Average strength (psi)
Specimen age		**48 hours**		**7 days**	
Specimen Condition		**After initial compaction**		**After microcracking**	
Trial 4	1	238	237	228	230
	2	233		223	
	3	240		239	

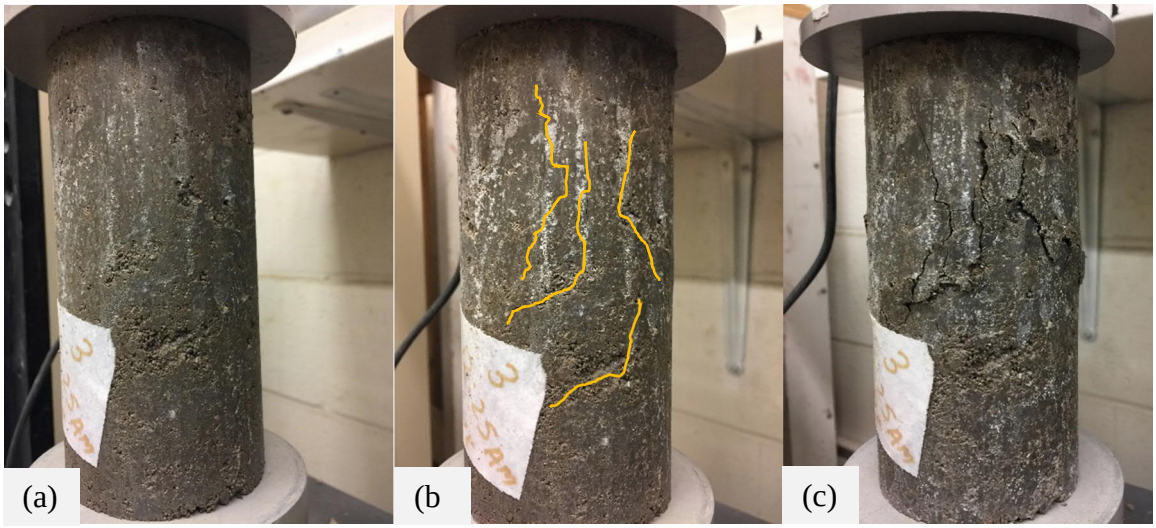

Figure 4-7 CMS specimen No. 3 of Trial 4 for the 330th MN soil: (a) before microcracking, (b) after microcracking at 48-hour curing, and (c) after UC testing at seven-day curing.

Table 4-7 shows the effects of the micro-cracks on the UC strength and modulus (E_{50}) after the 7-day moist curing period. The un-cracked specimens of Mix No. 2 had a higher UC strength and a lower modulus (stiffness) than those of the microcracked specimens of Trial 4. The average UC strength of the microcracked specimens was approximately 75% that of the un-cracked specimens. However, the microcracked specimens had the moduli approximately 150% that of the un-cracked specimens since the specimens were preloaded during the microcracking process.

Furthermore, the modulus to strength ratio of the un-cracked specimens after 7-day curing was approximately 100, which is the same as suggested by Han (2015) for soil-cement. On the other hand, the ratio of modulus to strength for the microcracked specimens increased to approximately 200 since they were preloaded. These results indicate that the presence of the micro-cracks made the specimen weaker but stiffer.

Table 4-7 Effects of microcracks in CMS specimens on the UC strength and modulus (E_{50}) at 7-day curing for the 330th MN soil.

Specimen Condition	Specimen No.	Compressive strength (psi)	Average strength (psi)	Modulus, E_{50} (ksi)	Average modulus, E_{50} (ksi)	Modulus to strength ratio
Un-cracked specimens (Mix No. 2)	1	290	305	21.0	30.6	100
	2	306		32.1		
	3	349		40.0		
	4	337		27.2		
	5	242		32.5		
Microcracked specimens (Trial 4)	1	228	230	48.9	44.4	193
	2	223		39.6		
	3	239		44.6		

Wet-Dry Cycle Test Results

The results of wet-dry cycle tests of CMS specimens for the 330th MN soil are presented in this section. The procedure for the wet-dry cycle test was described earlier in Section 3.3.5. The wet-dry cycle test was conducted to evaluate the climatic effect on the properties of CMS with or without microcracking during its service life. Figure 4-8 shows the volumetric change of one un-cracked specimen and one microcracked specimen after twelve cycles of wetting and drying. In general, even though small maximum volumetric changes (-0.6% after wetting cycles and -0.9% after drying cycles) were measured, negative volumetric changes indicate a shrinkage behavior for

both specimens. Also, the microcracked specimen had a slightly larger tendency for volumetric change due to easy infiltration and loss of water through microcracks. Considering the 330th MN soil is a coarse-grained soil; its shrinkage potential is low. Figure B-3 and Figure B-4 in Appendix B present the density and moisture content variations, respectively, during these cycles for both specimens. Figure 4-9 presents the mass loss results of an un-cracked specimen after twelve cycles of wetting, drying, and brushing as recommended in ASTM D559. With increasing number of wet-dry cycles, the specimen mass loss increased to approximately 7% of the initial specimen mass after the 12th cycle. Since the specimens had small diameter and height, they could not simulate the shrinkage of CMS to form large cracks in field; therefore, this test may not be representative for a field condition and it should be cautioned to interpret the results from this test.

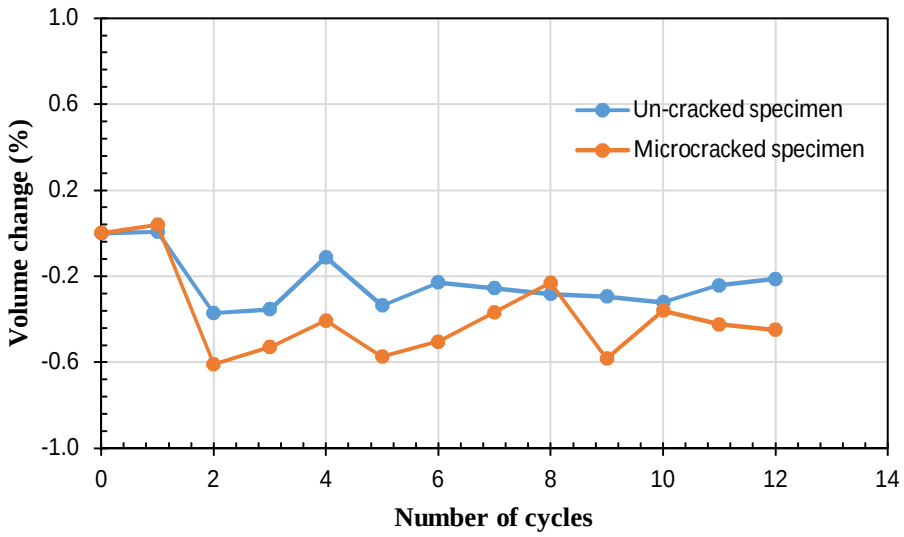

(a)

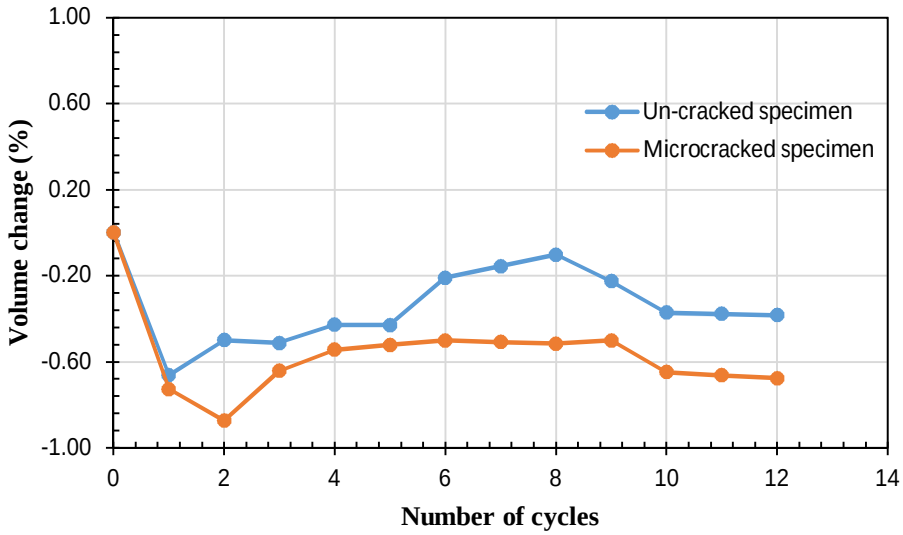

(b)

Figure 4-8 Volume change during the wet-dry test cycle based on: (a) wet condition and (b) dry condition.

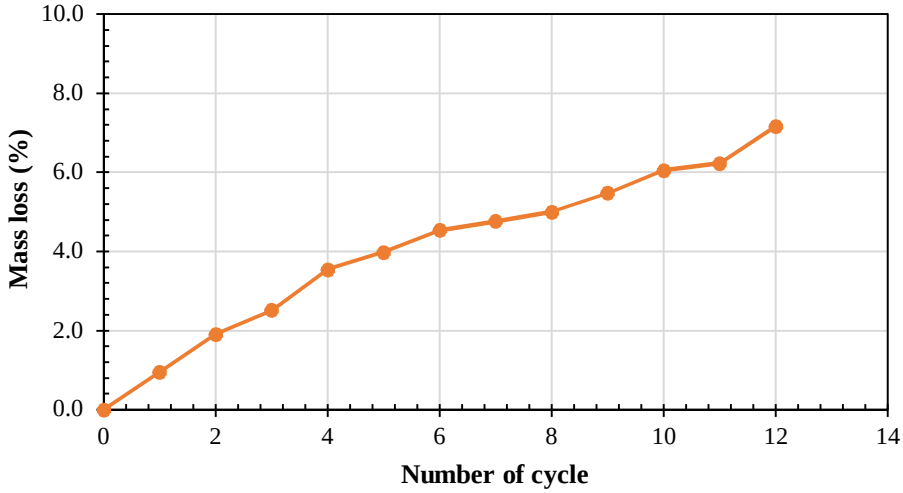

Figure 4-9 Mass loss for the brushed specimen calculated after a complete wet-dry cycle for all cycles.

Hydraulic and Electrical Conductivity Results

This section discusses the effects of microcracking on hydraulic and electrical conductivity of CMS specimens. Figure 4-10 shows the hydraulic conductivity (i.e., permeability) of one un-cracked specimen and one microcracked specimen at different effective stresses. These effective stresses represent different burial depths from the surface. In general, the un-cracked specimen had lower hydraulic conductivity than the microcracked specimen for all effective stresses. Also, the hydraulic conductivity for both un-cracked and microcracked specimens decreased as the effective stress increased because the specimen was compressed under higher confining pressure. The rate of decrease in the hydraulic conductivity for the microcracked specimen was higher than that for the un-cracked specimen as the effective pressure tended to compress and close the microcracks in the specimen.

Figure 4-11 presents the electrical conductivity of one un-cracked specimen and one microcracked specimen in terms of their electrical resistivity at different degree of saturation. The degree of saturation of the specimen changed as the specimen was cured for 7 days in the moisture room and placed in the hydraulic conductivity test chamber. Figure 4-11 shows that the micro-cracks increased the specimen electrical resistivity when the microcracked specimen was not fully saturated (<100%) as compared to the un-cracked specimen. However, at the degree of saturation (i.e., 100%), the microcracked specimen had lower electrical resistivity than that for the un-cracked specimen. It should be noted that the saturation process of the reconstituted specimen prior to permeability testing lasted approximately eight days. Therefore, the hydraulic conductivity testing on the microcracked and un-cracked specimens was initiated when the age of the specimens was 16 days after being reconstituted.

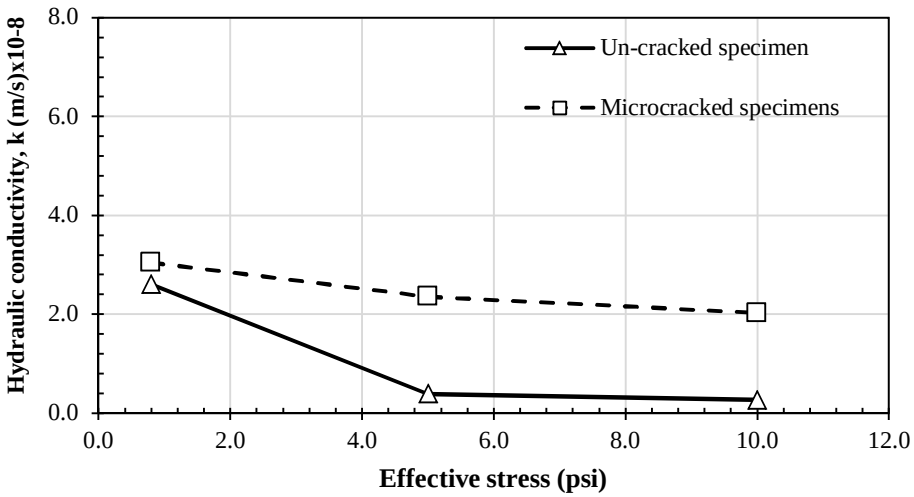

Figure 4-10 Hydraulic conductivity variation with different effective pressure.

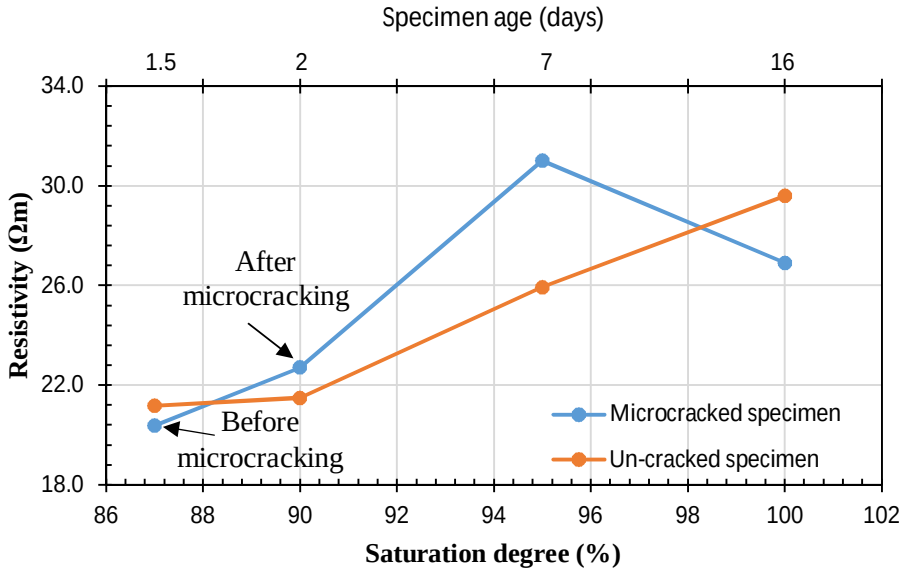

Figure 4-11 Resistivity variation with degree of saturation and age of CMS specimens for the 330th MN soil.

4.2.2 **87th SG Soil**

Following the recommendation for the microcracking procedure found based on the 330th MN soil, six UC specimens of CMS at the desired cement content of 5.5% for the 87th SG soil were prepared and tested (or microcracked) after 48-hour moist curing. Table 4-8 provides the UC test results. The average UC strength of CMS after 48-hour curing was 155 psi, or 74% of the 7-day strength. Figure 4-12 presents the stress-strain curves of the UC tests of the CMS specimens at 5.5% cement content after 48-hour curing.

Table 4-8 Unconfined compressive strength of CMS at 5.5% cement after 48-hour curing.

Group No.	Specimen No.	Compressive strength (psi)	Average strength (psi)
Group 1	1	154	155
	2	152	
	3	152	
Group 2	4	160	
	5	148	
	6	162	

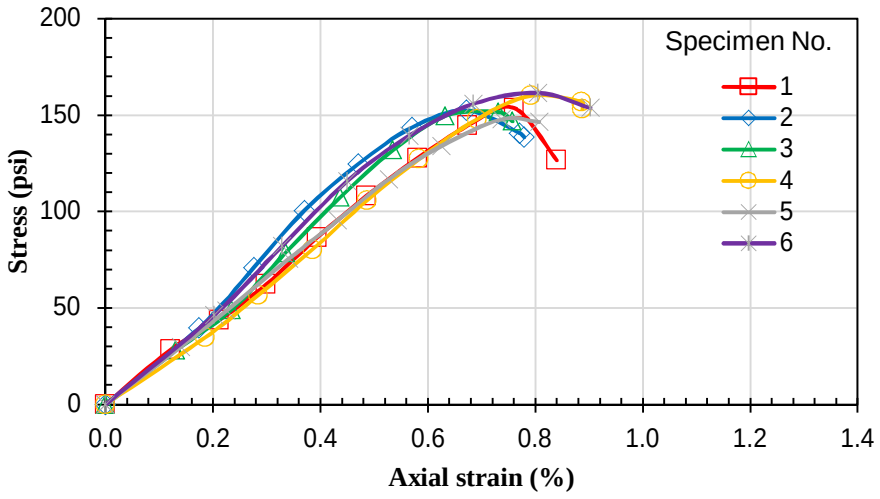

Figure 4-12 Stress-strain curves of CMS at 5.5 % cement after 48-hour curing for the 87th SG soil.

The specimens of Group 1 were microcracked by loading them to the ultimate UC strength after 48-hour curing time and then tested for the UC strength after a 2-hour waiting period. The UC tests of the second loading performed on failed or microcracked specimens from Group 1 showed the strength and modulus (E_{50}) reductions by approximately 28% and 9%, respectively, as shown in Figure 4-13 and Table 4-9.

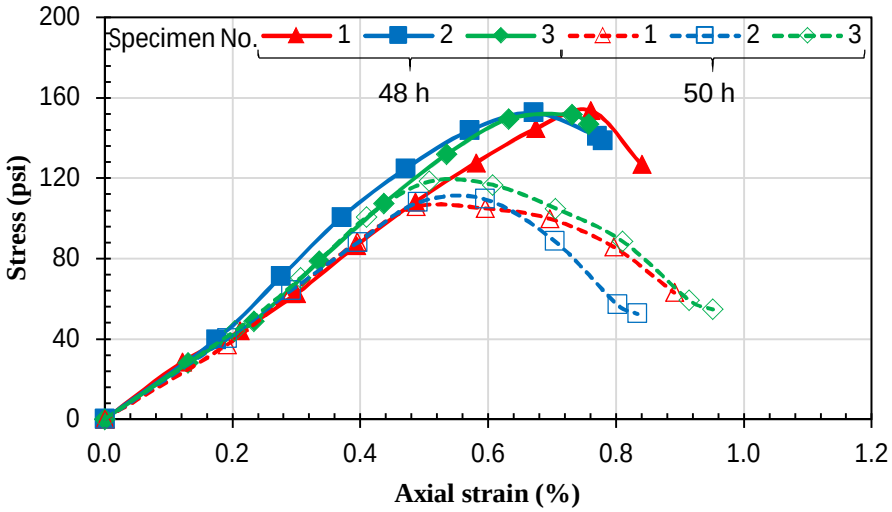

Figure 4-13 Stress-strain curves before and after microcracking of CMS specimens in Group 1 for the 87th SG soil.

Table 4-9 Unconfined compressive strengths and moduli of failed CMS specimens for the 87th SG soil subjected to second loading.

Group No.	Specimen No.	Specimen age	Compressive strength (psi)	Average strength (psi)	Modulus, E_{50} (ksi)	Average modulus, E_{50} (ksi)	Strength reduction	Modulus, E_{50} reduction
Group 1	1	48 hours	154	153	21.7	23.4	28%	9%
	2		152		26.2			
	3		152		22.2			
Group 1	1	50 hours	106	111	20.4	21.3		
	2		110		21.2			
	3		118		22.5			

In Group 2, three UC specimens of the CMS were microcracked, and their stress-strain curves are shown in Figure 4-14 (a). After the microcracking process, the specimens of Group 2 were returned to the moisture room to continue the curing process and to allow the specimens for strength gain. After seven-day curing, these specimens were tested for the UC strengths, and their stress-strain curves are presented in Figure 4-14 (b). The average strength of these three CMS specimens was 151 psi. In other words, the seven-day UC strength of the microcracked specimens was approximately the same as the two-day UC strength of un-cracked specimens. Moreover, the seven-day UC strength of the microcracked specimens were 72% of the design strength of the CMS mix (i.e., 210 psi). Table 4-10 summarizes the UC strengths of the CMS specimens before and after microcracking for Group 2. Figure 4-15 shows the CMS specimen No. 4 of Group 2 before microcracking, after microcracking at 48-hour curing, and after UC testing at seven-day curing.

Table 4-11 shows the effects of the micro-cracks on the UC strength and modulus (E_{50}) after the 7-day moist curing period. The un-cracked specimens of Mix No. 2 had a higher UC strength and a lower modulus (stiffness) than those of the microcracked specimens of Group 2.

The average UC strength of the microcracked specimens was approximately 74% that of the un-cracked specimens. However, the microcracked specimens had the moduli approximately same as that of the un-cracked specimens even though the specimens were preloaded during the microcracking process. Furthermore, the modulus to strength ratio of the un-cracked specimens after 7-day curing was approximately 160, and that for the microcracked specimens increased to approximately 219. These results indicate that the presence of the micro-cracks made the specimen weaker but slightly stiffer.

Table 4-10 UC strengths of CMS specimens before and after microcracking for the 87th SG soil.

Group No.	**Specimen No.**	**Compressive strength (psi)**	**Average strength (psi)**	**Compressive strength (psi)**	**Average strength (psi)**
Specimen age		**48 hours**		**7 days**	
Specimen Condition		**After initial compaction**		**After microcracking**	
Group 2	4	160	157	149	151
	5	148		154	
	6	162		150	

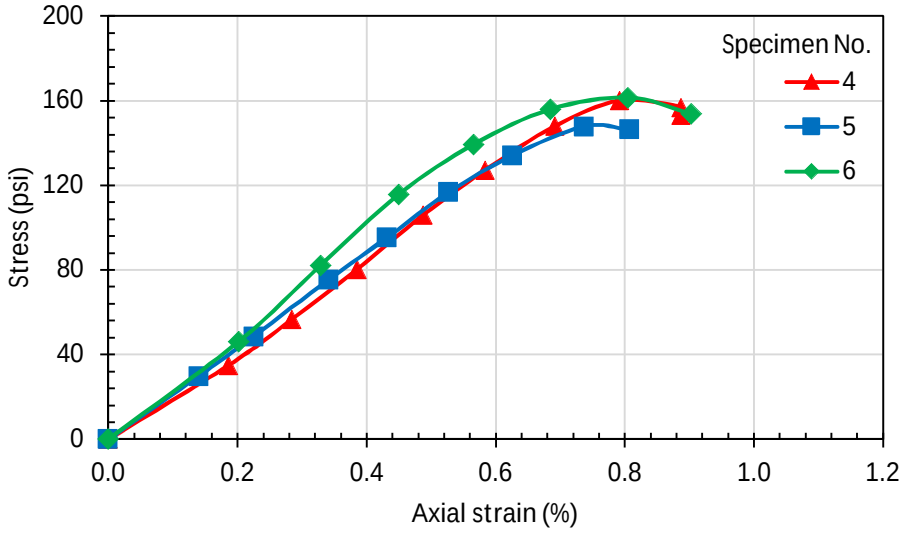

(a)

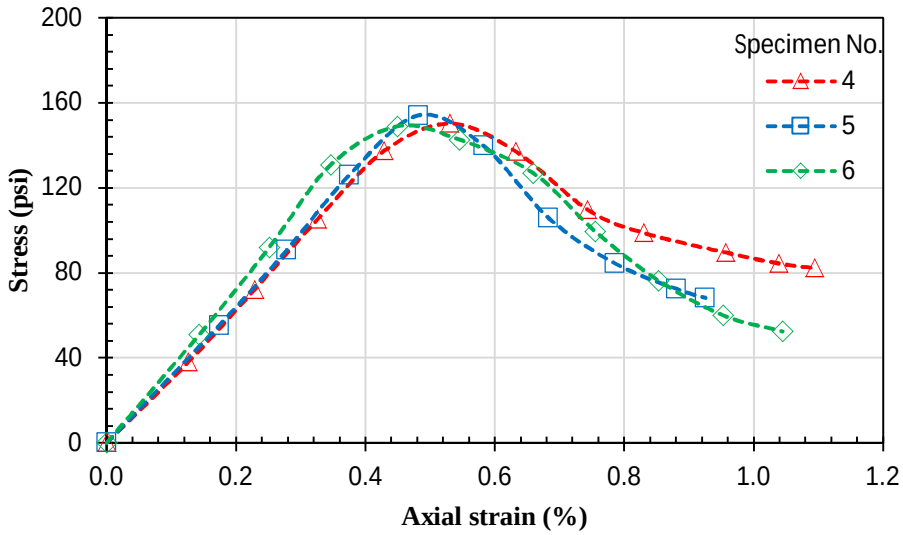

(b)

Figure 4-14 Stress-strain curves of CMS specimens at 5.5% cement in Group 2 for the 87th SG soil: (a) during the microcracking process after 2-day curing, and (b) after the microcracking process after 7-day curing.

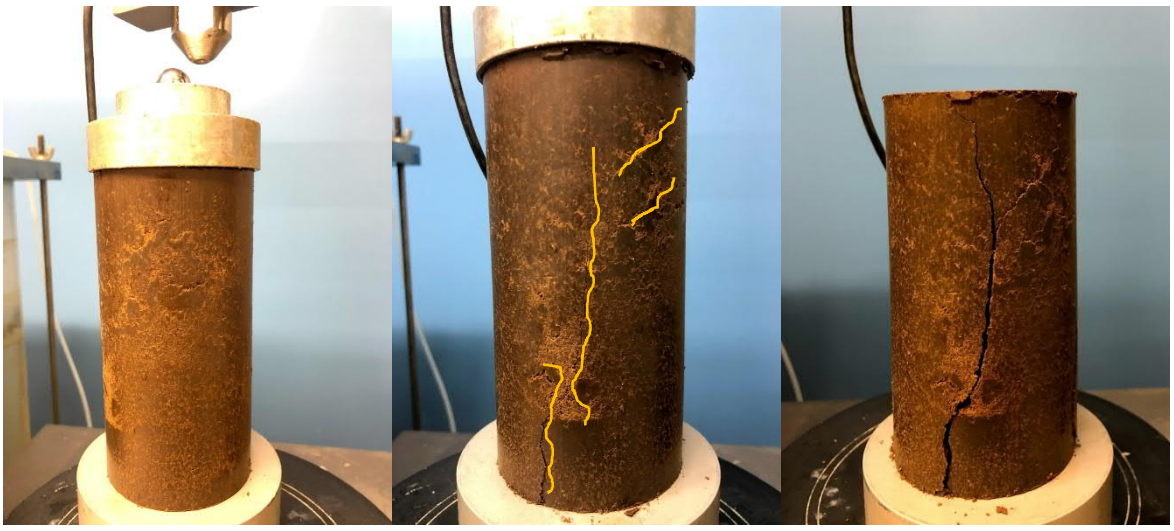

(a) (b) (c)

Figure 4-15 CMS specimen 4 of Group 2 for the 87th SG: (a) before microcracking, (b) after microcracking at 48-hour curing, and (c) after UC testing at seven-day curing.

Table 4-11 Effects of microcracks in CMS specimens on the UC strength and modulus (E_{50}) at 7-day curing for the 87th SG soil.

Specimen Condition	**Specimen No.**	**Compressive strength (psi)**	**Average strength (psi)**	**Modulus, E_{50} (ksi)**	**Average modulus, E_{50} (ksi)**	**Modulus to strength ratio**
Un-cracked specimens (Mix No. 2)	1	194	202	29.8	32.6	160
	2	200		32.7		
	3	211		35.0		
Microcracked specimens (Group 2)	4	149	151	35.8	33.1	219
	5	154		32.1		
	6	150		31.5		

CHAPTER 5 FIELD STUDY

5.1 ELECTRICAL RESISTIVITY

The effect of microcracking was evaluated in the field by measuring the in-situ resistivity before and after microcracking. The Wenner 4-pin method as described in ASTM Test Method G57 was used to evaluate the field electrical resistivity before and after microcracking along a site located in Hutchinson, Kansas and South 87th Street site in Sedgwick County. The on-site soils stabilized at the Hutchinson site comprised of clayey sand with gravel, which is similar to the soil encountered along the 330th MN site.

The 4-pin resistivity method developed by Wenner (1915), involves the use of 4 pins driven into the ground as shown in Figure 5-1. A current is applied to the outer pins, and the voltage between the inner pins is measured. The resistivity is a function of the current, voltage, and spacing of the electrodes (equal to the depth of the test). The resistivity equation is show Equation 5-1.

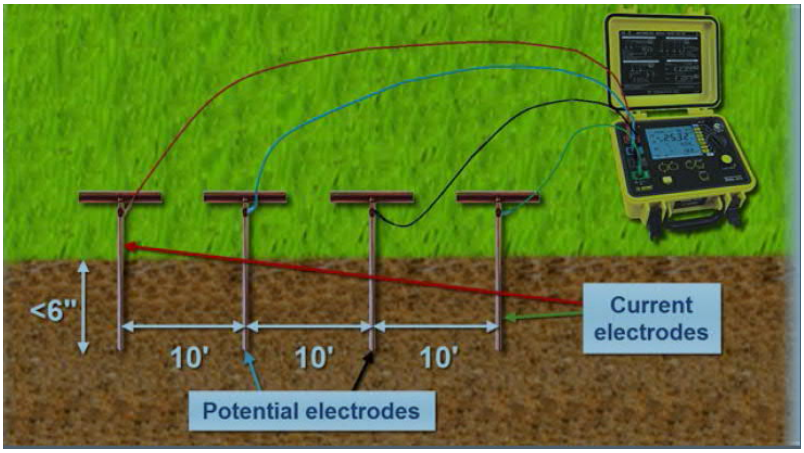

Figure 5-1 Typical Wenner 4-pin setup.

$$\rho = 2\pi \times a \times (\Delta\phi / I) \qquad \text{(Equation 5-1)}$$

where ρ= resistivity,

a = spacing between the electrodes,

$\Delta\phi$ = the voltage, and

I = applied current.

The current is usually applied using an instrument that supplies alternating current, otherwise polarization effects occur at the electrodes that can alter the reading. The field electrical resistivity results collected along the site in Hutchinson, KS and 87th SG before and after microcracking are presented in Table 5-2 and Table 5-1, respectively. These results did not show a clear correlation between the electrical resistivity and the microcracking process. Also, these results may indicate that the effect of microcracking on the electrical resistivity is within the accuracy of its measurement.

Table 5-1 Field electrical resistivity before and after microcracking on the Hutchinson site.

Site Location	**GPS Coordinates (Latitude, Longitude)**	**Test Condition**	**Pin Spacing (ft)**	**Resistance, (ohms)**
Hutchinson, KS	Coordinates not available	Before Microcracking	0.25	17.63
			0.5	12.91
			0.75	8.48
			1.0	7.57
		After Microcracking	0.25	17.98
			0.5	12.89
			0.75	9.93
			1.0	8.14

Table 5-2 Field electrical resistivity before and after microcracking at the 87th SG soil.

Site Location	GPS Coordinates (Latitude, Longitude)	Test Condition	Pin Spacing (ft)	Resistance, (ohms)
87th SG	37.533541, -97.210226	Before Microcracking	0.25	40.8
			0.5	19.3
			0.75	15.7
			1.0	11.1
		After Microcracking	0.25	4.5
			0.5	9.6
			0.75	8.6
			1.0	9.3
	37.533554, -97.212308	Before Microcracking	0.25	23.0
			0.5	19.1
			0.75	13.8
			1.0	10.2
		After Microcracking	0.25	22.4
			0.5	16.1
			0.75	13.0
			1.0	10.5

5.2 LIGHT WEIGHT DEFLECTOMETER TEST

The light weight deflectometer (LWD) is a portable non-destructive testing device as an alternative to the FWD. The LWD test is a dynamic plate loading test that is typically used to determine the dynamic deformation modulus (E_{lwd}) of soil by measuring the deflection of the loading plate. The test consists of the soil subjected to a pulse load applied via a disk-shaped steel plate or aluminum plate. The loading mechanism consists of a drop weight that falls along a rod and hit the top of the plate as shown in Figure 5-2. The mass of the dropping weight and the size of the loading plate vary in terms of product models. There are two types of commonly-used LWD devices, Dynatest 3031 and ZFG 3.0 (Zorn LWD), which have different working procedures. Dynatest 3031 gives stiffness values for each drop, while ZFG 3.0 requires three preloading drops and then three more drops are required to provide three deflection values and an average modulus [Average modulus

= 1.5×150×0.1/ (Average deflection)]. The LWD testing was performed in accordance with ASTM procedure E2583 (2015).

The LWD system is equivalent to a two degree of freedom mass-spring-damper system during the loading and rebound until the moment that the impact load becomes zero, after which the system decouples. The LWD equipment used in this study is the Zorn ZFG 3.0 LWD. This test equipment does not have a load cell and assumes a constant applied load of 1.59 kips (7.07 kN) when the weight is dropped from a full height of 28.5 inches (0.724 m) on soils with different stiffness values. The rate of the movement at the center of the plate is recorded by a velocity sensor. The maximum displacement is calculated by means of single integrals of the velocity. The load history and peak load are estimated based on the mass and the drop height. The modulus determined by the LWD is calculated using Equation 5-2 based on the Boussinesq equation:

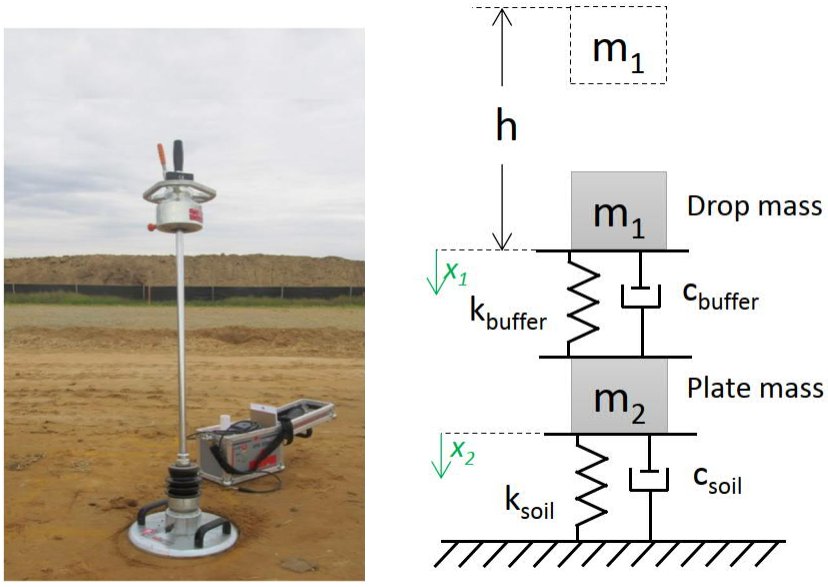

(a) (b)

Figure 5-2 The Zorn LWD device: (a) photo and (b) schematics of the LWD and subgrade system (two degree of freedom).

$$E = \frac{2k_s}{Ar_0}(1 - \nu^2) \quad \text{(Equation 5-2)}$$

where A = the stress distribution factor,

ν = the Poisson's ratio,

$k_s = \left|\frac{F_{peak}}{w_{peak}}\right|$, F_{peak} = peak load, w_{peak} = maximum displacement, and

r_0= plate radius.

Equation 5-2 assumes the subgrade to be an isotropic, linearly elastic, and homogeneous semi-infinite continuum. Terzaghi et al. (1996) defined the stress distribution under a plate as a function of plate rigidity and soil type. Table 5-3 denotes the typical stress distribution factor (A) for different type of soils under the LWD plate.

Table 5-3 Stress distribution factors for different types of soil.

Soil Type	Factor (*A*)	Stress Distribution Shape
Uniform (mixed soil)	π	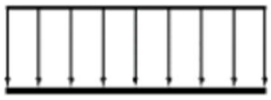
Granular material (parabolic)	3π/4	
Cohesive (inverse parabolic)	4	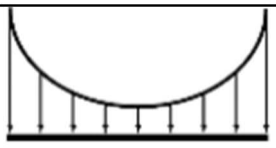

5.2.1 **Light Weight Deflectometer Test Results**

For both 330th MN and 87th SG sites described earlier in Section 3.2.1, the LWD tests were performed along the test sections. Figure 5-3 shows the LWD test locations and results for 330th MN. Figure 5-3(b) shows that the microcracking process, which was achieved by applying three passes of a roller compactor, reduced the dynamic modulus by approximately 17% to 67% as compared to that before microcracking. Figure 5-4 shows the LWD test locations and results for 87th SG. Figure 5-4 (b) shows the effects of modifying the subgrade with 5.5% cement as the LWD modulus increased for all locations after mixing with cement. Also, Figure 5-4 (c) demonstrates that microcracking reduced the dynamic moduli by approximately 22% to 56% as compared to those before microcracking.

(a)

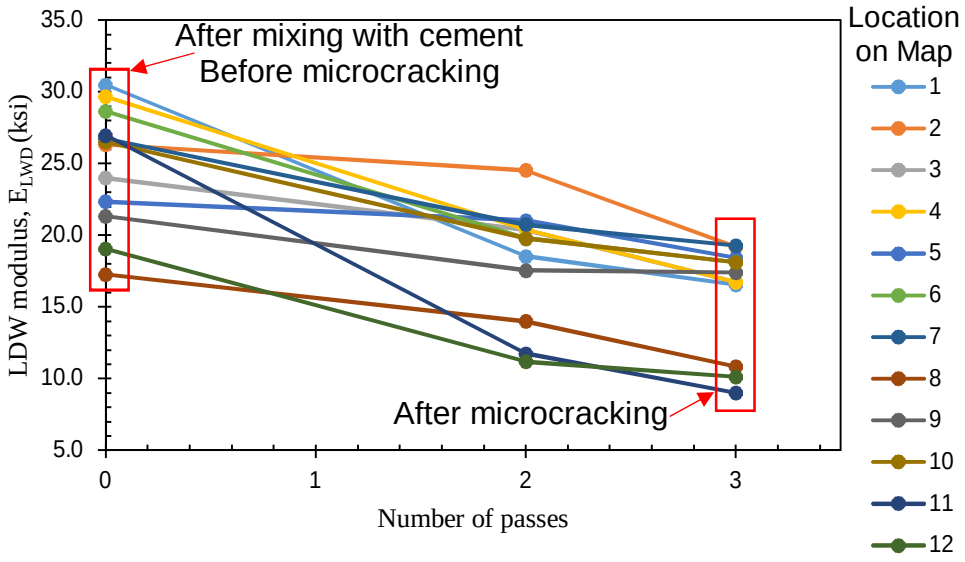

(b)

Figure 5-3 LWD tests conducted for the 330th MN project: (a) testing locations and (b) effect of microcracking.

(a)

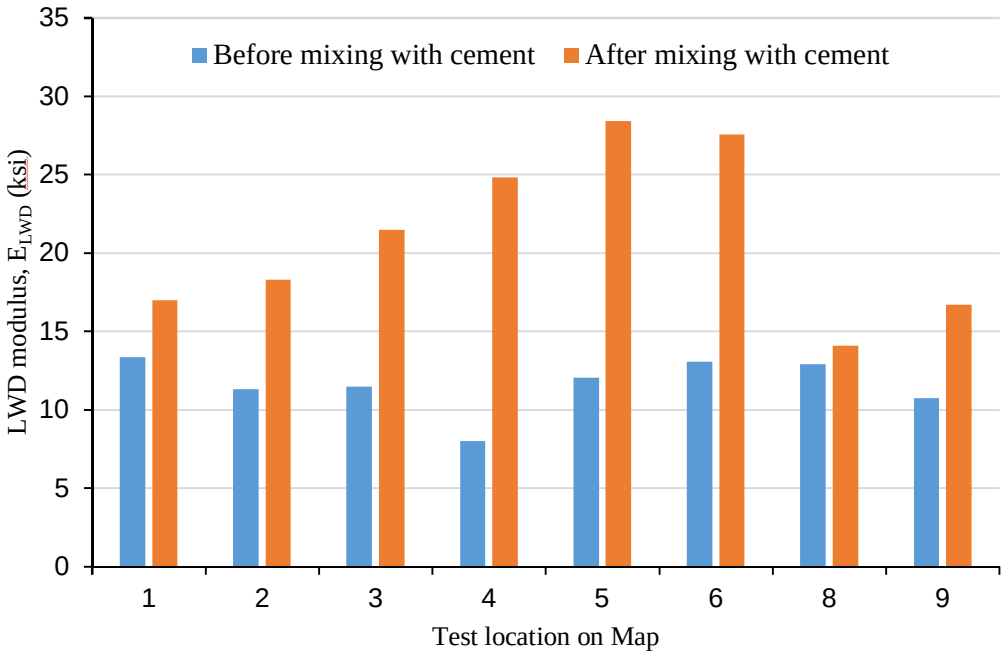

(b)

Figure 5-4 LWD tests conducted for the 87th SG project: (a) testing locations, (b) effect of cement, and (c) effect of microcracking.

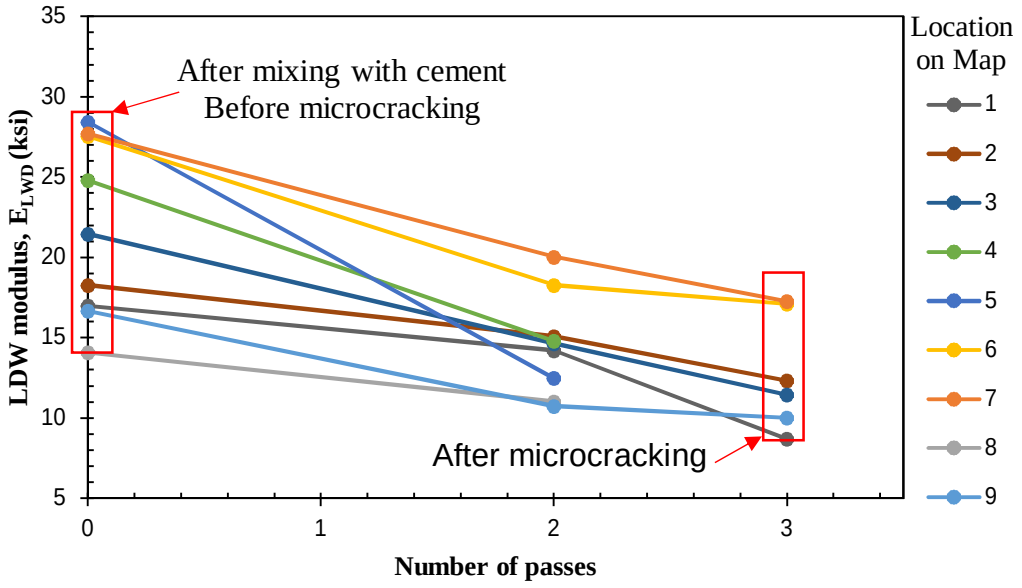

(c)

Figure 5.4 LWD tests conducted for the 87th SG project: (a) testing locations, (b) effect of cement, and (c) effect of microcracking (continued).

5.3 FALLING WEIGHT DEFLECTOMETER (FWD)

The FWD is a non-destructive pavement test that applies loads ranging from 1,500 to 27,000-lbs simulating moving wheel loads. This test is considered worldwide as one of the most effective tools for measuring pavement surface deflections. It is used by most highway agencies to evaluate the pavement performance, identify potential problems, and calculate the pavement layer moduli and the subgrade resilient modulus, which can be used for estimating the pavement structural capacity. The FWD is a trailer-mounted device which applies a load to the pavement surface through a circular plate with a diameter of 11.8 inches (300 mm) positioned on the pavement surface as shown in Figure 5-5. A mass is dropped onto the plate with a rubber pad generating a uniform impulse load on the pavement. This pulse load simulates the magnitude and duration of

a rolling vehicle wheel (at a speed ranging from 30 to 50 mph) and is measured with a load cell mounted on top of the loading plate. The magnitude of the pulse load on the pavement surface can be varied by altering either the mass of the drop weight or the drop height. Varying the drop mass and/or height during the FWD test provides a direct opportunity to evaluate the stress-dependent behavior of the materials in the pavement structure. The drop load at approximately 9,000 lbs is used in the analysis using the ELMOD V.6 (Evaluation of Layer Moduli and Overlay Design) software, which corresponds to the expected single wheel load from an equivalent single axle. The pavement responses (surface deflections) due to the load are measured by a series of deflection sensors (known as geophones) mounted at various distances from the loading point. The FWD main advantage is that it can closely approximate the effect of a moving wheel load, both in magnitude and duration.

The components of an FWD system include: a hydraulic system, a loading weight and a plate, a load cell, deflection sensors, and a control system. Seven deflection sensors located at distances of approximately 0, 12, 18, 24, 36, 48, and 60 inches away from the center of the loading plate were used in the FWD testing performed for this study. Once the load is applied, the actual load is measured by a precise heavy-duty load cell installed above the loading plate. The deflections measured by the seven sensors (D1 thru D7) under one drop are acquired and stored. The measured deflection at each sensor location is called the deflection basin. The shape of the deflection basin depends on the thickness and stiffness of the pavement layers and the subgrade. The deflection sensors at the farther distances respond primarily to the subgrade characteristics, while the deflection sensor at the center responds to the combined characteristics of the subgrade and upper pavement layers.

Utilizing the deflections measured by the FWD sensors, the resilient moduli of flexible pavement layers are determined using backcalculation software, for instance, ELMOD V.6 (a back-calculation software developed by Dynatest). The backcalculated moduli represent the estimated current in-situ moduli, which can be input into mechanistic-empirical equations to estimate the remaining life of the pavement and aid in evaluating the timing for maintenance and rehabilitations needs.

(a)

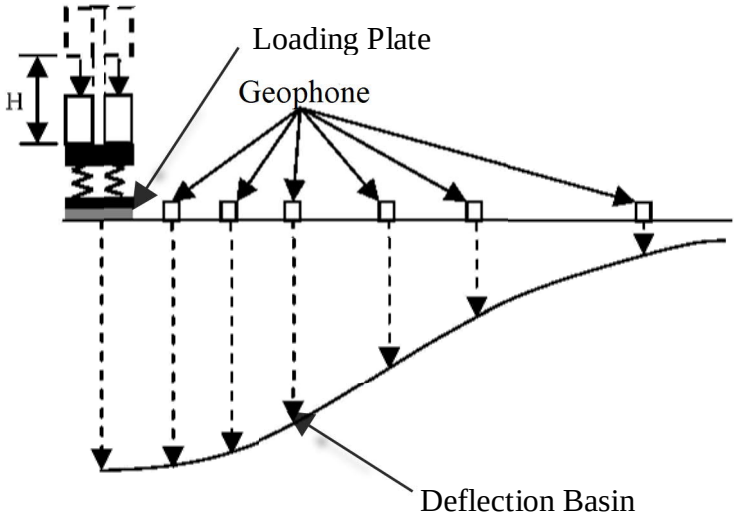

(b)

Figure 5-5 FWD: (a) equipment (b) deflection basin.

In this study, the Jils FWD equipment was used to measure the surface deflections along 330th MN and 87th SG. The field testing along 87th SG and 330th MN alignments were performed by KDOT personnel on October 30th and October 31, 2018, respectively. The FWD testing was performed in accordance with the ASTM D4694-09 "Standard Test Method for Deflections with a Falling-Weight-Type Impulse Load Device" and ASTM D4695–03 "Standard Guide for General Pavement Deflection Measurements". The deflection tests consisted of one seating drop and three recording drops per test location. A test load of 9,000 lbs in accordance with the KDOT Specification was used. The FWD testing was performed at an interval of approximately 100 feet along each lane (eastbound and westbound) and approximately 50 feet in a staggered pattern for both lanes. The testing was divided into two sections, eastbound (EB) and westbound (WB) lanes. The testing length for each section was approximately 1 mile. Test locations were along the right wheel of the driving lane. A total of 103 testing points along the existing 87th Street with 51 at EB lane and 52 at WB lane were performed. Also, a total of 104 testing points along the existing 330th Road with 52 at EB lane and 52 at WB lane were performed. The FWD test locations, the deflections at the center plate, and the temperatures at 87th SG and 330th sites are shown in Table C-1 and Table C-2, respectively, of Appendix C.

Following the FWD testing, four pavement cores were obtained by KDOT personnel from each site. The thicknesses of the asphalt pavements, identified from the collected pavement cores along 87th SG and 330th MN sites, were 2 and 3 inches, respectively. Note that the back-calculation procedure for the FWD data is sensitive and dependent on the thickness of the provided individual pavement layers. Subgrade visual classification for each site was provided by Terracon Consultants based on the information presented in geotechnical engineering report No. 01175084

dated October 18, 2017 and geotechnical engineering report No. 01185091 dated July 6, 2018 for the 330th MN and 87th SG sites, respectively.

5.4 BACK-CALCULATION ANALYSIS

Back-calculation is the approach used for computing pavement layer moduli and the subgrade resilient modulus based on pavement deflection data generated by FWD (Muench, et al. 2003). The back-calculation process is started by assuming the initial moduli of pavement layers. The values are usually estimated based on engineer's experience or equations. After assuming the initial layer moduli, pavement surface deflections can be calculated using pavement response models. The calculated deflections are then compared to the measured values. An iterative process is implemented by adjusting the pavement layer moduli to have a good match (within some tolerable error) between the measured and calculated deflections. Typical measured and calculated deflections (from the back-calculated moduli) at different radial distances are shown in Figure 5-6.

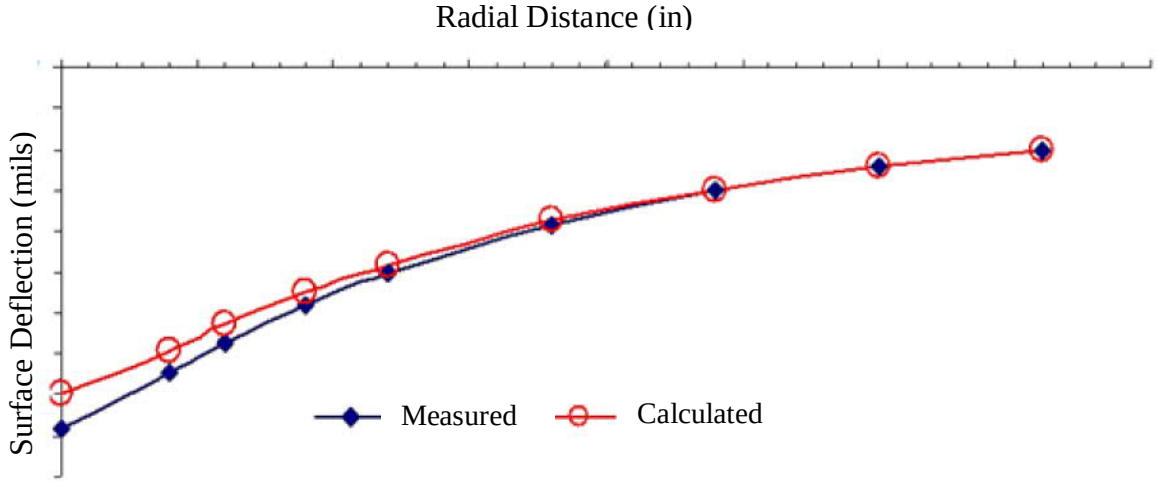

Figure 5-6 Typical layer modulus back-calculation (Marecos et al. 2018).

The basic flowchart of a backcalculation program is presented in Figure 5-7. The main components in the backcalculation process include (Lytton, 1989):

- Layer thickness and loads: thickness of each layer and load levels applied on the pavement surface,
- Measured deflections: surface deflections measured during FWD tests,
- Seed moduli: initial moduli used to compute theoretical surface deflections,
- Deflection calculation: use pavement response models to calculate theoretical deflections, and
- Error check: compare calculated and measured deflections.

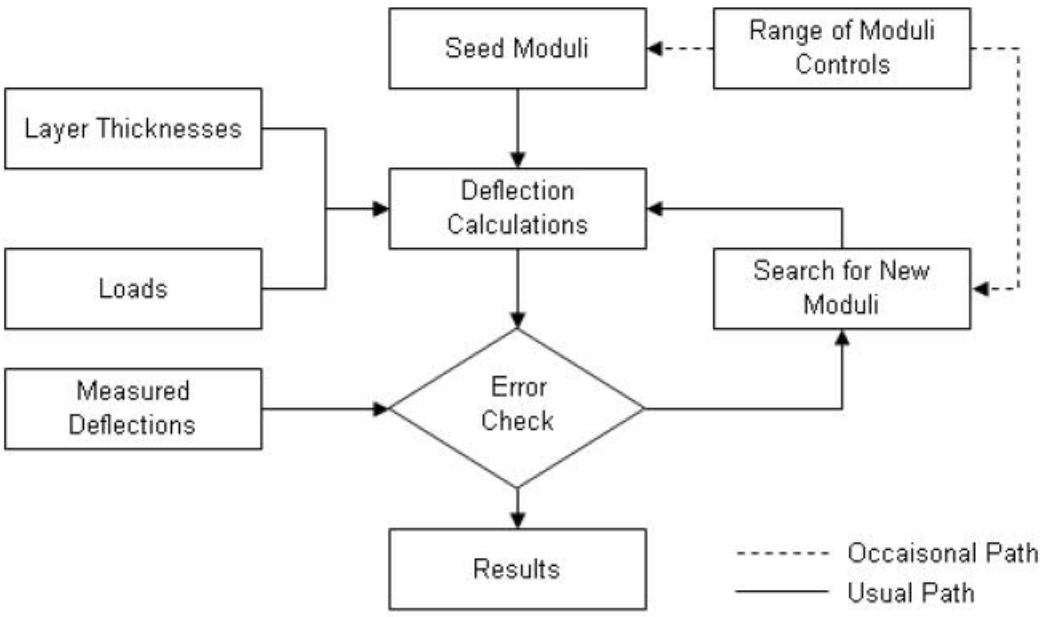

Figure 5-7 Backcalculation flowchart (Lytton, 1989).

5.4.1 **ELMOD**

ELMOD (Evaluation of Layer Moduli and Overlay Design) Version 6.0 is a window-based software package developed by Dynatest International A/S that is used to backcalculate the modulus of each layer in a three- or four-layer pavement system. There are three backcalculation options available in this program: Linear Elastic Theory (LET), Finite Element Method (FEM), and Method of Equivalent Thickness (MET). Basically, different forward analysis methods are used in these three options. The LET method uses WESLEA for forward analysis, the FEM uses an axi-symmetric finite element program to calculate the theoretical deflections, while the MET makes use of the Odemark-Boussinesq transformation formula to determine the equivalent thickness. For ELMOD V. 6.0 MET, the multilayer pavement structure is transformed into an equivalent single layer of equivalent stiffness using Equation 5-3.

$$h_e = h_1 \sqrt[3]{\frac{E_1}{E_2} + \frac{1-\nu_2^2}{1-\nu_1^2}} \qquad \text{(Equation 5-3)}$$

where E_1 = the modulus of the upper layer;

ν_1 = the Poisson's ration of the upper layer;

E_2 = the modulus of the lower layer;

ν_2 = the Poisson's ration of the lower layer;

h_1 = the thickness of the upper layer

ELMOD V.6 considers possible non-linearity of the subgrade to improve the fit between measured and calculated deflection basins. This feature generally removes the so-called the

"compensating layer effect," which can introduce large errors if the moduli are computed assuming only linearly elastic materials (Ullidtz et al. 1995).

5.4.2 **Backcalculation Results**

ELMOD V.6 was used for the back-calculation of the FWD raw data in this study. Deflection basin analysis was also carried out. The deflection values of the overall pavement structure (D1, deflection sensor at the center of loading plate) and the deflections related to the base layer (D2 and D3, deflection sensors at 12-inch and 18-inch offsets from D1) on all test stations were used to compare the performance of the micro-cracked sections. A flexible pavement cross section was considered in the back-calculation ELMOD V.6 including an asphalt layer and a cement-modified soil layer on top of an infinite half-space subgrade layer.

The selected pavement layer thicknesses and the assumed Poisson's ratios used in the back-calculation performed for 87th SG and 330th MN are shown in Table 6-5 of Chapter 6. Table C-1 and Table C-2 in Appendix C present the FWD testing data for 87th SG and 330th MN sites. The normalized center deflections versus station locations for 87th SG and 330th MN are plotted in Figure 5-8 and Figure 5-9, respectively.

Asphalt is a viscoelastic material whose modulus depends on the testing temperature and duration of loading. The stiffness of the asphalt layer decreases as the temperature increases (FHWA, 2017). Therefore, correcting the HMA modulus to a standard temperature was required for analysis purposes. A standard temperature of 68 °F is recommended by the Federal Highway Administration (FHWA, 2017) and was adopted for this research. This temperature has been also used by KDOT for other projects in Kansas. As no detailed information was available on the asphalt concrete material and no attempts have been made at deriving the master curve from

repeated testing of representative points at different temperatures, Equation 5-4 was used to adjust the asphalt concrete modulus to a reference temperature of 68 °F. This equation is the default equation in ELMOD V. 6.0 and is based on the Bells equation developed by Baltzer and Jansen (1994) for the asphalt temperature correction.

$$E = e^{A\times(t-t_{REF})} \times E_{REF} \qquad \text{(Equation 5-4)}$$

where t_{Ref} = the reference temperature, 68 °F,

t = the asphalt concrete (AC) temperature at time of testing,

A = -0.036= constant,

E = the backcalculated AC modulus at the tested temperature, and

E_{Ref} = the adjusted AC modulus to the reference temperature.

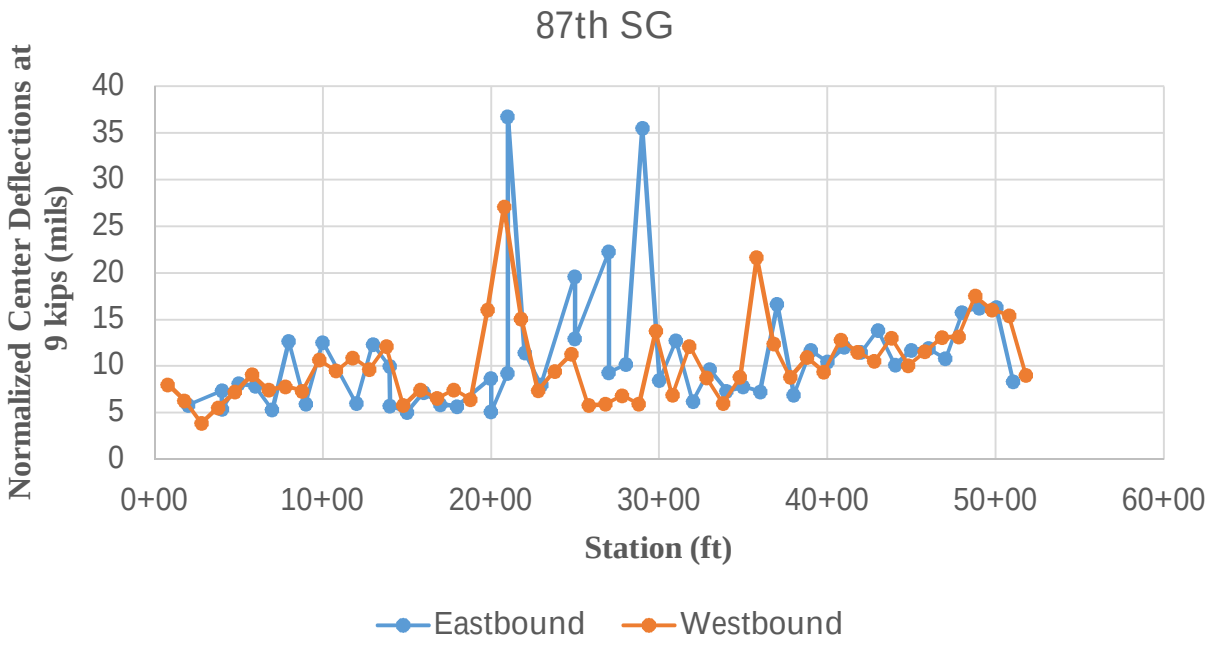

Figure 5-8 87th Street normalized deflections.

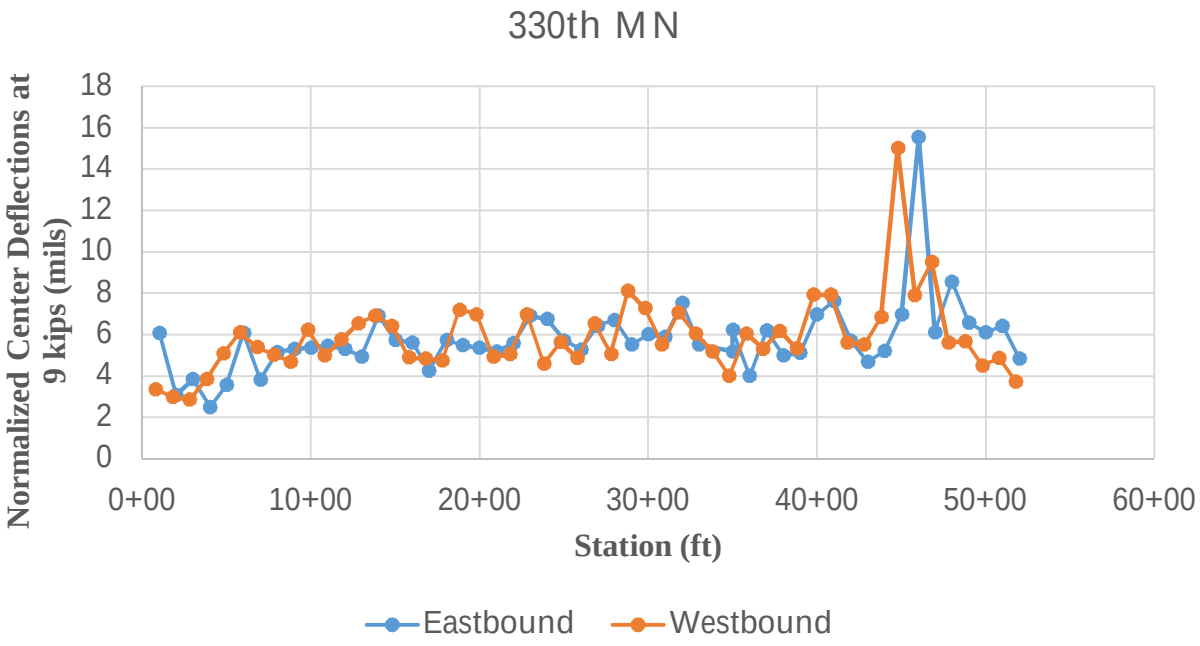

Figure 5-9 330th MN normalized deflections.

The back-calculated moduli with the station locations for eastbound and westbound of 87th SG are presented in Table C-3 and Table C-4, respectively. Also, the back-calculated moduli with the station locations for Eastbound (EB) and Westbound (WB) of 330th MN are presented in Table C-5 and Table C-6, respectively. The three-layer system moduli versus stations for 87th SG and 330th MN are plotted in Figure 5-10 and Figure 5-11, respectively. E1, E2, and E3 in these tables and figures represent the moduli of the asphalt layer, the cement-modified soil layer, and the native subgrade layer.

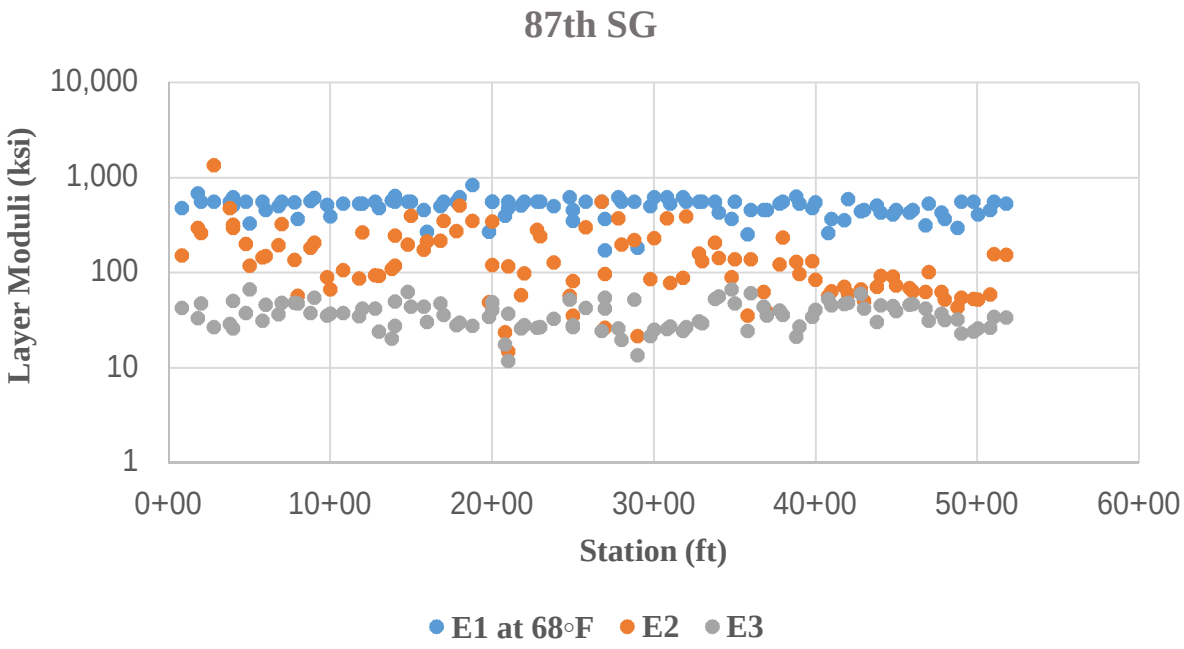

Figure 5-10 Layer moduli for 87th SG.

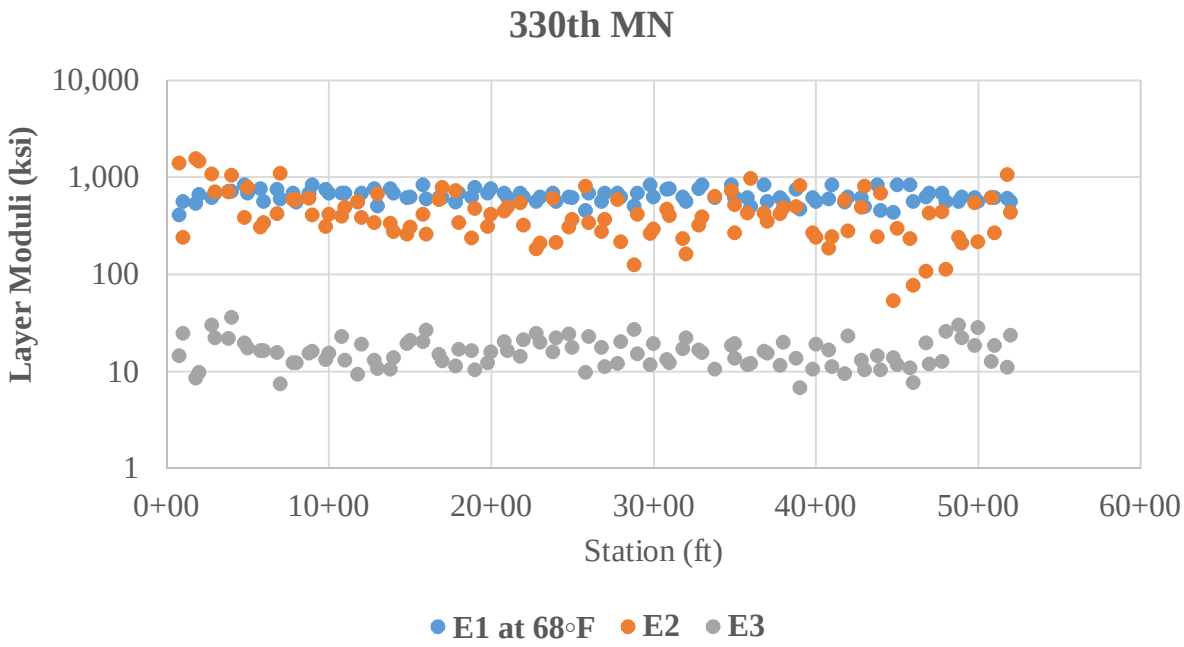

Figure 5-11 Layer moduli 330th MN.

Figure 5-10 show that there were some variations of the moduli at different stations for each layer at the 87th SG site. This variation could be attributed to construction variability. Figure 5-11 shows that the moduli at different stations for each layer at the 330th MN site are more uniform. The average modulus of each layer in addition to the modulus corresponding to the 84th percentile (i.e., one standard deviation for a log-normal distribution) for 87th SG and 330th MN are presented in Table 5-4. This table shows that the average backcalculated modulus of the HMA layer at 330th MN was approximately 30% higher than that at 87th SG and the average backcalculated modulus of the CMS layer at 330th MN was over three times higher than that on 87th SG. It should be noted that the 7-day UC strength test results of the reconstituted specimens at 330th MN were only 50 percent higher than those at 87th SG soil. However, the backcalculated subgrade modulus on 87th SG site was more than two times higher than that on 330th MN. This difference was also found in the laboratory CBR tests performed for both sites. The pavement properties describe in the previous table were later utilized in the KENLAYER analysis to determine the pavement responses for each pavement section.

Table 5-4 Layer moduli with 84th percentile.

Back-calculated Layer Moduli E, (ksi)	**87th SG**			**330th MN**		
	Mean	**Standard Deviation**	**84th Percentile**	**Mean**	**Standard Deviation**	**84th Percentile**
Asphalt Concrete @ 68 °F	485	1.293	375	636	1.167	545
CMS	121	2.194	55	391	1.802	217
Subgrade	35	1.392	25	15	1.395	11

Based on a log-normal distribution, = $84th\ Percentile = \frac{Average}{Standard\ Deviation\ Factor}$

5.5 RESILIENT MODULUS FORMULAE AND CONSTANTS

Three mathematical formulae summarized in Table 5-5, including the one recommended by the mechanistic-empirical design guide (NCHRP 1-28A), were evaluated for the reconstituted specimens using the soils from 330th MN and 87th SG sites as well as the specimens cored from the 330th MN site. Multiple regression analysis of all standard testing stresses and corresponding resilient modulus values was used to obtain material constants k_1, k_2, and/or k_3. The formulae were calibrated to provide best data "fits" between resilient modulus and testing stresses. The formula proposed by the mechanistic-empirical design guide is recommended but not required so all three formulae were evaluated to determine which formula provides the best data "fit" between resilient modulus and testing stresses.

Table 5-5 Published formulae to characterize resilient modulus.

Reference	Model Identification	Independent Variables	Model Equation
Seed et al. (1967)	**M1**	θ (Bulk Stress)	$M_r = k_1(\theta)^{k_2}$
Moossazadeh and Witczak (1981)	**M2**	σ_d (Deviator Stress)	$M_r = k_1(\sigma_d)^{k_2}$
NCHRP (National Cooperative Highway Research Program) Project 1-28A	**M3**	θ, τ (Bulk Stress and Octahedral Shear Stress)	$M_r = k_1 P_a \left(\frac{\theta}{P_a}\right)^{k_2} \left(\frac{\tau_{oct}}{P_a} + 1\right)^{k_3}$

where M_r = the resilient modulus,

θ = the bulk stress = $\sigma_1 + \sigma_2 + \sigma_3 = \sigma_d + 3\sigma_c$,

σ_1 = the major principal stress,

σ_2 = the intermediate principal stress = σ_3,

for M_r tests on cylindrical specimens, $\sigma_3 = \sigma_c$ confining pressure,

$\sigma_1 - \sigma_3 = \sigma_d$ = the deviator stress,

$|\tau_{oct}|$= the octahedral shear stress = $\frac{1}{3}\sqrt{(\sigma_1 - \sigma_2)^2 + (\sigma_1 - \sigma_3)^2 + (\sigma_2 - \sigma_3)^2}$,

$|\tau_{oct}| = \frac{\sqrt{2}}{3}\sigma_d$,

P_a = normalizing stress (i.e., atmospheric pressure=14.7 psi), and

k_1, k_2, k_3 = regression constants (obtained by fitting resilient modulus test data to the equation).

The model (**M1**) proposed by Seed et al. (1967) is typically used for unbounded granular base. In this formula, increasing the bulk stress "θ" would result in a higher resilient modulus. This phenomenon is also called stiffening or hardening of the material (i.e., an increase in the deviator stress causes an increase in the resilient modulus). Therefore, the constants, k_1 and k_2, are always positive. Since the cement modified soils after microcracking could behave like an unbounded granular material, this formula was considered in the evaluation of the laboratory resilient modulus data.

Moossazadeh and Witczak (1981) proposed the formula **M2** in Table 5-5. For a fine grade soil, the modulus generally decreases with the increase of the deviator stress because k_2 is negative.

The formula **M3** included in the mechanistic empirical design guide (MEPDG) is a generalized one, which includes three constants, k1, k2, and k3.

5.5.1 **Regression Analysis**

Regression analysis was conducted using the optimization technique - Solver in MS Excel. In performing the non-linear optimization, the initial values of the unknown parameters k_1, k_2 and/or k_3 are fed into the spreadsheet. Therefore, to obtain these initial values for the parameters k_1, k_2 and k_3 (where applicable), RLT test results were fitted to the formulae in Table 5-5 by performing a linear regression in the log-log scale. The k_1, k_2 and/or k_3 constants obtained by linear regression

were then used as the seed values for a nonlinear optimization performed using Solver in MS Excel for fitting the RLT test results to the formulae in the arithmetic scale. As a result, the values for k_1, k_2 and k_3 were obtained.

5.5.2 **Laboratory Reconstituted Specimens**

The resilient modulus results for the reconstituted specimens prepared in the laboratory at the desired cement contents are summarized in Table C-7 through Table C-14 in Appendix C. The resilient modulus versus bulk stress curves for the uncracked and cracked reconstituted specimens from 87th SG site are plotted in Figure C-1 through Figure C-4. The resilient modulus versus bulk stress curves for the uncracked and cracked reconstituted specimens from 330th MN are plotted in Figure C-5 through Figure C-8. It is evident that the resilient modulus values increase with the confining pressure and the deviatoric stress. This result is consistent with that in Hanifa et al. (2015), i.e., higher confining stresses resulted in higher resilient moduli. The analysis of these test data will be presented later.

In addition, the resilient modulus versus deviator stress curves for the uncracked and cracked reconstituted specimens from 87th SG site are plotted in Figure C-9 through Figure C-12. The resilient modulus versus deviator stress relationships for the uncracked and cracked reconstituted specimens from 330th MN are plotted in Figure C-13 through Figure C-16. Figure C-9 through Figure C-16 show that the resilient moduli of the materials from 87th SG and 330th MN increased with the increase of the deviator stress. This CMS behavior is similar to that obtained by the Louisiana Department of Transportation and Development (Zhang, 2015).

5.5.3 **Cored Specimens form 330th MN**

Table 5-6 through Table 5-9 summarize the laboratory resilient modulus data of the microcracked specimens cored from the 330th MN site on October 31, 2018. The resilient modulus values, $M_{r,}$ varied between 25 and 60 ksi, which fall within the range published by Hanifa et al. (2015). It is obvious that the higher confining stress resulted in the higher resilient modulus. These test results also show that the M_r values increased with the increase of the deviatoric stresses. Therefore, this material behaved as a stress-hardening material.

Table 5-6 Resilient modulus of cracked CMS specimen No. 1 cored from 330th MN Site.

Parameter	**Chamber Confining Pressure**	**Actual Applied Cyclic Stress**	**Actual Applied Contact Stress**	**Resilient Modulus**
Designation	σ_3	σ_{cyclic}	$\sigma_{contact}$	M_r
Unit	psi	psi	psi	psi
Sequence 1	6	1.73	0.20	45,519
Sequence 2	6	3.50	0.40	49,939
Sequence 3	6	5.29	0.61	53,121
Sequence 4	6	7.10	0.81	55,842
Sequence 5	6	8.86	1.04	58,512
Sequence 6	4	1.73	0.19	35,901
Sequence 7	4	3.52	0.39	39,333
Sequence 8	4	5.30	0.60	42,490
Sequence 9	4	7.11	0.79	45,891
Sequence 10	4	8.88	1.00	49,619
Sequence 11	2	1.73	0.18	25,211
Sequence 12	2	3.53	0.37	28,097
Sequence 13	2	5.34	0.56	31,395
Sequence 14	2	7.13	0.77	34,843
Sequence 15	2	8.89	0.98	38,316

Table 5-7 Resilient modulus of cracked CMS specimen No. 2 cored from 330th MN Site.

Parameter	Chamber Confining Pressure	Actual Applied Cyclic Stress	Actual Applied Contact Stress	Resilient Modulus
Designation	σ_3	σ_{cyclic}	$\sigma_{contact}$	M_r
Unit	psi	psi	psi	psi
Sequence 1	6	1.66	0.24	35,926
Sequence 2	6	3.38	0.44	39,188
Sequence 3	6	5.08	0.65	41,673
Sequence 4	6	6.77	0.87	44,381
Sequence 5	6	8.46	1.06	47,118
Sequence 6	4	1.67	0.20	33,680
Sequence 7	4	3.36	0.42	36,988
Sequence 8	4	5.08	0.63	39,414
Sequence 9	4	6.79	0.84	42,053
Sequence 10	4	8.51	1.04	44,891
Sequence 11	2	1.65	0.18	31,047
Sequence 12	2	3.36	0.39	33,824
Sequence 13	2	5.07	0.61	36,275
Sequence 14	2	6.81	0.81	38,811
Sequence 15	2	8.53	1.01	41,631

Table 5-8 Resilient modulus of cracked CMS specimen No. 4 cored from 330th MN Site.

Parameter	Chamber Confining Pressure	Actual Applied Cyclic Stress	Actual Applied Contact Stress	Resilient Modulus
Designation	σ_3	σ_{cyclic}	$\sigma_{contact}$	M_r
Unit	psi	psi	psi	psi
Sequence 1	6	1.11	0.46	56,245
Sequence 2	6	2.69	0.69	57,179
Sequence 3	6	4.35	0.91	58,386
Sequence 4	6	6.02	1.14	60,316
Sequence 5	6	7.67	1.35	62,061
Sequence 6	4	1.25	0.43	45,306
Sequence 7	4	2.94	0.60	46,697
Sequence 8	4	4.65	0.78	48,346
Sequence 9	4	6.33	1.01	50,616
Sequence 10	4	8.00	1.22	52,780
Sequence 11	2	1.49	0.27	30,661
Sequence 12	2	3.17	0.47	33,788
Sequence 13	2	4.88	0.65	36,258
Sequence 14	2	6.54	0.88	39,021
Sequence 15	2	8.21	1.10	41,789

Table 5-9 Resilient modulus of cracked CMS specimen No. 6 cored from 330th MN Site.

Parameter	Chamber Confining Pressure	Actual Applied Cyclic Stress	Actual Applied Contact Stress	Resilient Modulus
Designation	σ_3	σ_{cyclic}	$\sigma_{contact}$	M_r
Unit	psi	psi	psi	psi
Sequence 1	6	1.73	0.21	48,821
Sequence 2	6	3.48	0.42	51,958
Sequence 3	6	5.24	0.63	52,523
Sequence 4	6	7.03	0.83	53,739
Sequence 5	6	8.80	1.03	55,144
Sequence 6	4	1.74	0.20	39,500
Sequence 7	4	3.52	0.40	42,085
Sequence 8	4	5.32	0.59	44,204
Sequence 9	4	7.07	0.81	46,185
Sequence 10	4	8.84	1.01	47,920
Sequence 11	2	1.71	0.20	28,768
Sequence 12	2	3.51	0.38	31,757
Sequence 13	2	5.33	0.58	34,143
Sequence 14	2	7.11	0.80	36,495
Sequence 15	2	8.88	1.00	38,737

The constants for the formulae M1, M2, M3 and the M_r values of the cored specimens collected from 330th MN site are presented in Table 5-10, Table 5-11, and . Also, the resilient modulus test results for the four cored specimens collected from the 330th MN site are plotted in Figure 5-12

Table 5-10 Constants for the formula M1 and resilient modulus for the cored specimens collected from 330th MN site.

Soil Specimens No.	k_1	k_2	R^2	M_r @ θ = 10 psi
330th MN cored specimen 1 –cracked	5,863.4	0.696	0.99	29,117
330th MN cored specimen 2 –cracked	18,319.5	0.271	0.69	34,191
330th MN cored specimen 4 –cracked	8,813.9	0.607	0.97	35,659
330th MN cored specimen 6 –cracked	9,042.0	0.555	0.99	32,454
Average	**10,509.7**	**0.532**	**0.91**	**32,855**

Table 5-11 Constants for the formula M2 and resilient modulus for the cored specimens collected from 330th MN site.

Soil Specimens No.	**k_1**	**k_2**	**R^2**	**M_r @ σ_d = 4 psi**
330th MN cored specimen 1 –cracked	30,404.1	0.197	0.22	39,952
330th MN cored specimen 2 –cracked	30,272.1	0.169	0.73	38,264
330th MN cored specimen 4 –cracked	42,873.5	0.067	0.04	47,046
330th MN cored specimen 6 –cracked	35,521.9	0.121	0.13	42,009
Average	**34,768**	**0.14**	**0.28**	**41,818**

Table 5-12 Constants for the formula M3 and resilient modulus for the cored specimens collected from 330th MN site.

Soil Specimens No.	**k_1**	**k_2**	**k_3**	**R^2**	**M_r @ θ = 10 psi and τ = 1.89 psi**
330th MN cored specimen 1 –cracked	2,570	0.710	-0.099	1.00	28,199
330th MN cored specimen 2 –cracked	2,220	0.184	0.915	0.99	33,730
330th MN cored specimen 4 –cracked	3,275	0.667	-0.648	1.00	34,194
330th MN cored specimen 6 –cracked	2,841	0.753	-0.939	0.99	27,699
Average	**2,726**	**0.578**	**-0.193**	**0.99**	**31,119**

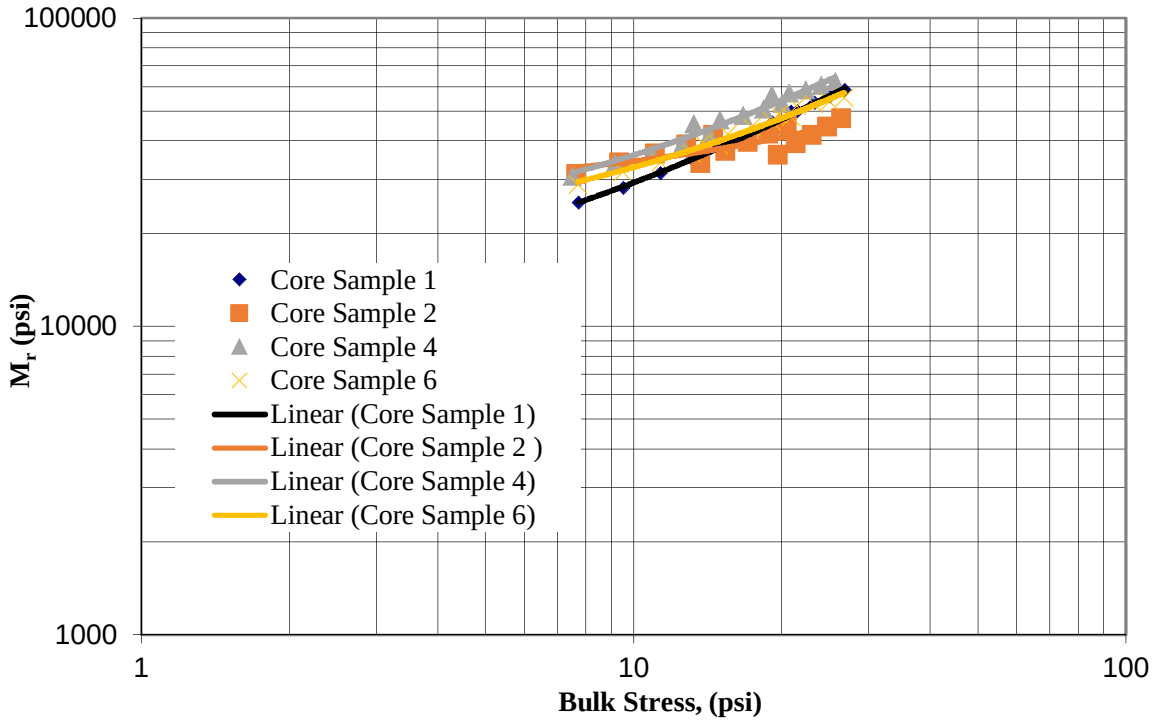

Figure 5-12 Resilient modulus versus bulk stress of the cored core specimens collected from 330th MN.

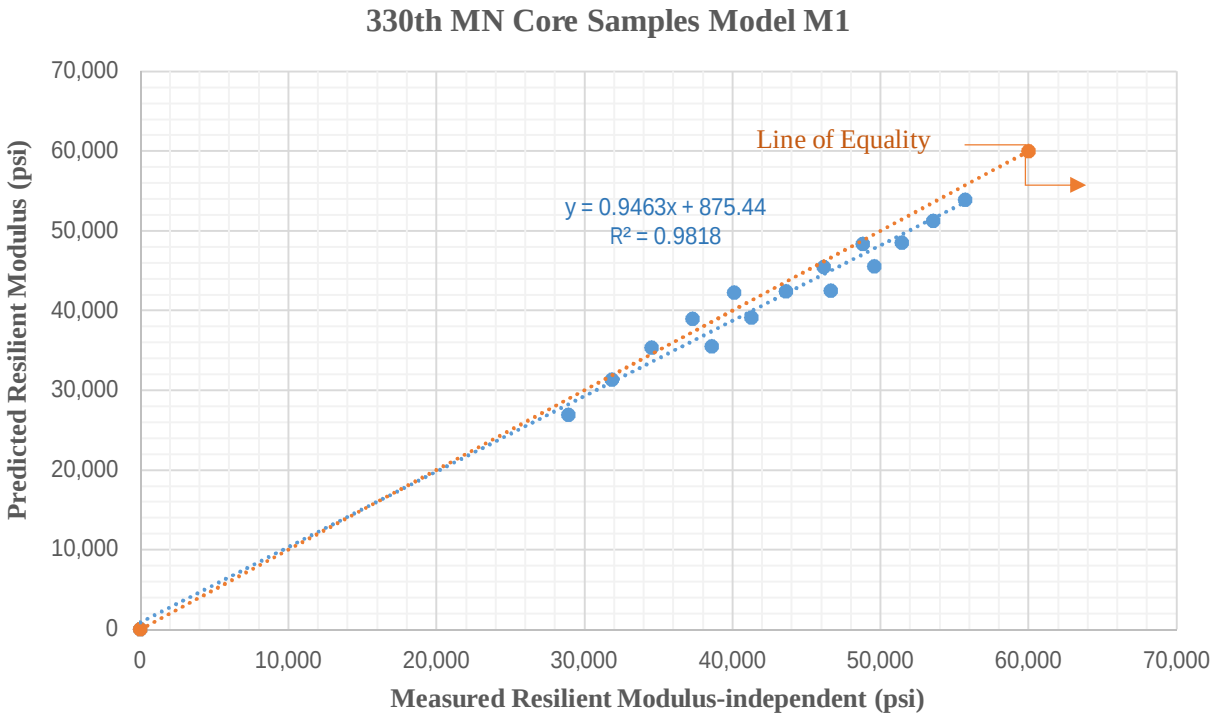

Figure 5-13 Predicted Mr using formula M1 versus laboratory measured Mr for the cored core specimens collected from 330th MN.

The predicted resilient modulus using formula M1 and the average resilient modulus of the CMS cored specimens from 330th MN site are plotted in Figure 5-13. However, the predicted resilient modulus using Model M2 and the average resilient modulus of the CMS cores collected from 330th MN for the confining pressures of 6, 4, and 2 psi are plotted in Figure 5-14. Also, the resilient moduli of the cored specimen calculated using M1, M2 and M3 models in this study are presented in Figure 5-15. It should be noted that the average resilient moduli of the cored specimens from 330th MN site were approximately 25 percent higher than those of the reconstituted specimens in the laboratory when compared using model M1 and M3, and about 50 percent higher when compared using model M2. However, the average UC strengths for the cored specimens from 330th MN site were approximately 10 percent higher than the average UC strength of the reconstituted specimens in the laboratory.

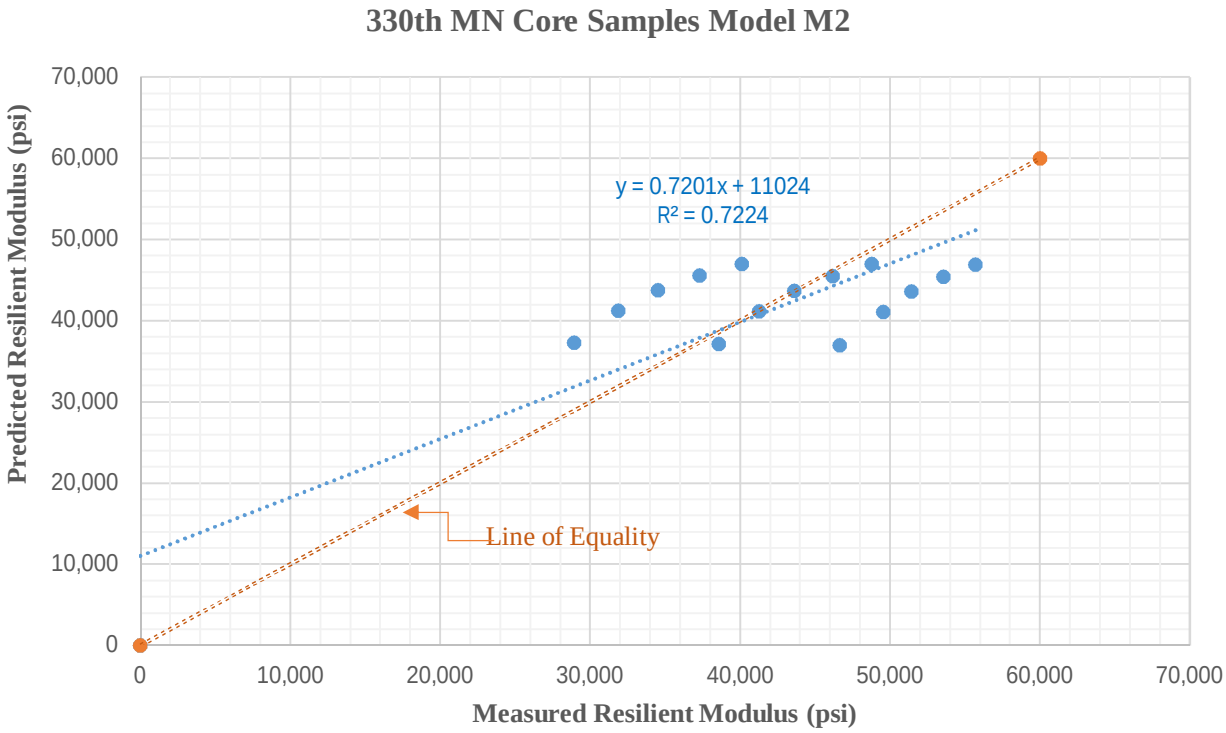

Figure 5-14 Predicted M_r using Model M2 versus laboratory measured M_r for the cored specimens collected from 330th MN.

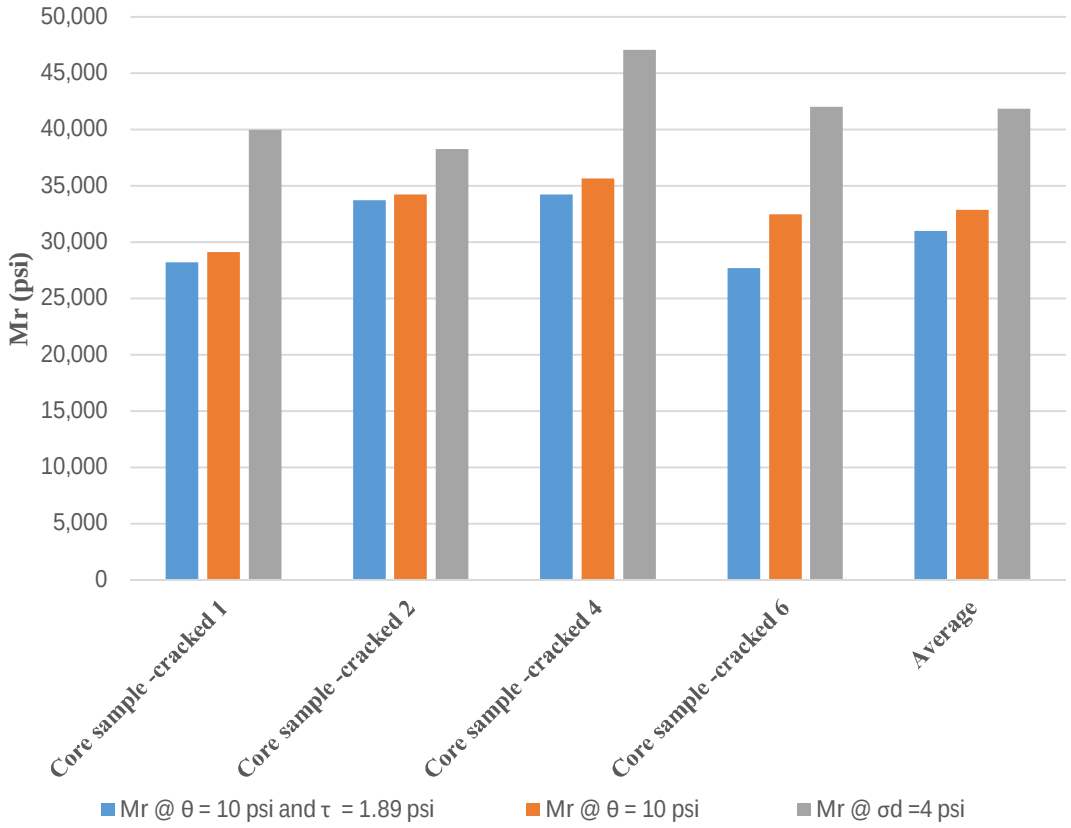

Figure 5-15 Resilient moduli of the cored specimens from 330th MN site.

5.5.4 **Effect of Microcracking on Resilient Modulus**

This study evaluated the effect of microcracking on the resilient modulus M_r values at a specific stress level: a bulk stress of approximately 10 psi and/or an octahedral shear stress of 1.89 psi as suggested by FHWA (2019), using the formulae discussed earlier. Also, a deviatoric stress of approximately 4 psi was considered for the formula M2. The formula constants and the M_r values at the aforementioned stresses are summarized in Table 5-13, Table 5-14 and Table 5-15 and plotted in Figure 5-16 through Figure 5-22.

The effect of microcracking on the resilient modulus was observed on two selected specimens per soil. Figure 5-23 shows that the average M_r values of the microcracked specimens were slightly higher than those of the uncracked specimens. This finding is consistent with the

effect of microcracking on E_{50} as previously discussed based on the laboratory data. It should be noted that this finding is based on two replicates. Therefore, it is highly recommended that additional resilient modulus testing be conducted to better assess the effect of microcracking on the resilient modulus.

Table 5-13 Constants and resilient modulus based on formula M1.

Soil Specimens No.	**k_1**	**k_2**	**R^2**	**M_r @ θ = 10 psi**
87th SG Un-cracked 1	7,787.6	0.407	1.0	19,879
87th SG Un-cracked 4	6,982.3	0.517	0.98	22,961
Average	**7,384.9**	**0.462**	**0.99**	**21,420**
87th SG Cracked 2	10,351.9	0.363	0.94	23,879
87th SG Cracked 3	7,563.3	0.443	0.95	20,975
Average	**8,957.6**	**0.403**	**0.94**	**22,427**
330th MN Un-cracked 1	9,261.7	0.46	0.99	26,711
330th MN Un-cracked 2	7,834.9	0.5	0.98	24,776
Average	**8,548.3**	**0.48**	**0.98**	**25,743**
330th MN Cracked 3	4,031	0.757	0.97	23,063
330th MN Cracked 4	10,078.1	0.45	0.96	28,404
Average	**7,054.6**	**0.603**	**0.96**	**25,733.5**

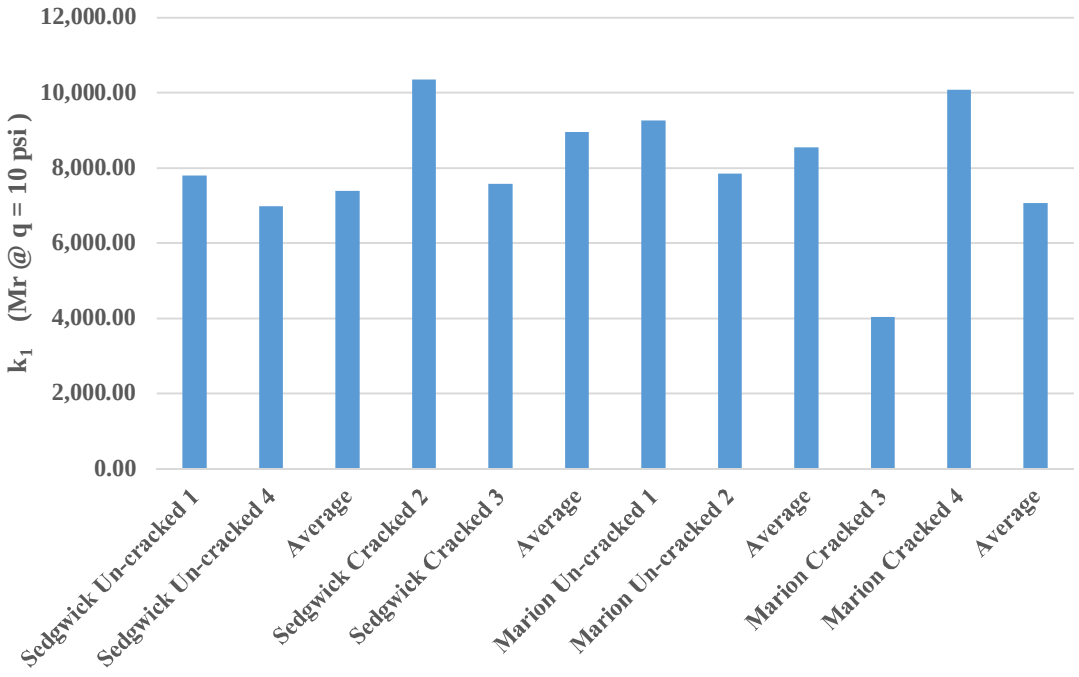

Figure 5-16 k_1 values (Mr @ θ = 10 psi - M1 Model)

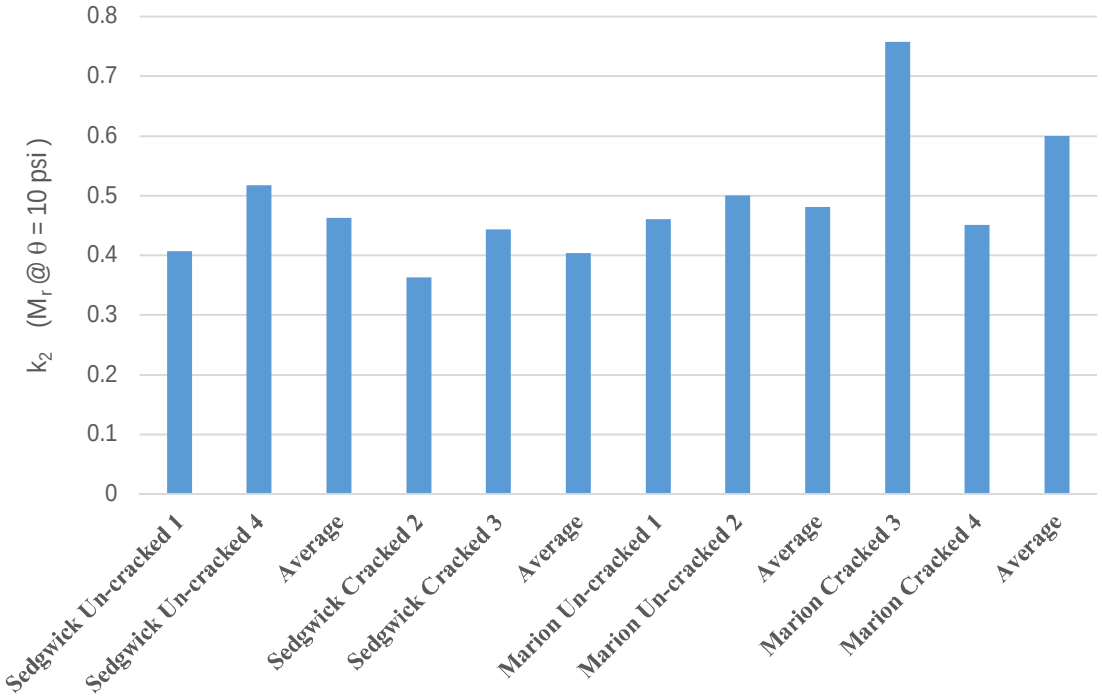

Figure 5-17 k_2 values (Mr @ θ = 10 psi - M1 Model).

Table 5-14 Resilient modulus test characteristics (M2 Model).

Soil Specimens No.	**k_1**	**k_2**	**R^2**	**M_r @ σ_d=4 psi**
87th SG Un-cracked 1	16,100	0.16	0.97	17,988
87th SG Un-cracked 4	17,635	0.21	0.97	20,398
Average	**16,867.5**	**0.185**	**0.97**	**19,193**
87th SG Cracked 2	19,934	0.14	0.87	24,204
87th SG Cracked 3	16,653	0.18	0.89	21,373
Average	**18,293.5**	**0.16**	**0.88**	**22,788**
330th MN Un-cracked 1	20,817	0.19	0.99	27,090
330th MN Un-cracked 2	19,005	0.21	0.96	25,427
Average	**19,911**	**0.2**	**0.975**	**26,258**
330th MN Cracked 3	15,576	0.31	0.98	23,938
330th MN Cracked 4	22,579	0.18	0.93	28,978
Average	**19,077.5**	**0.245**	**0.955**	**26,458**

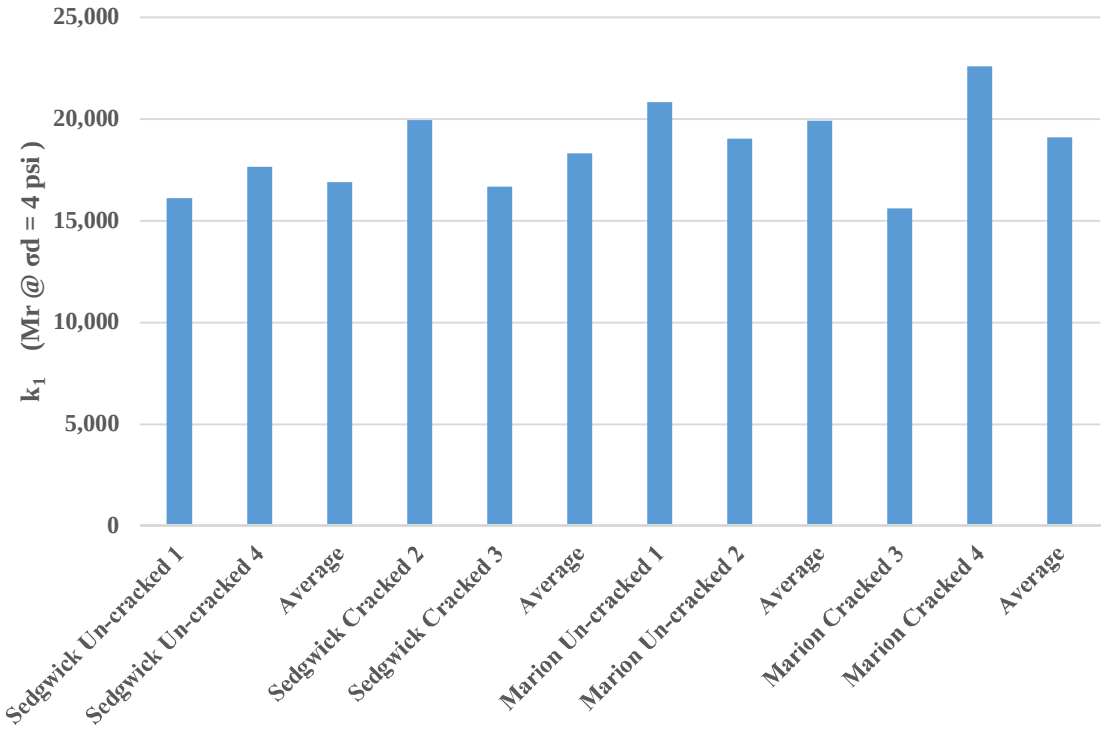

Figure 5-18 k_1 values (Mr @ σ_d = 4 psi M2 Model.

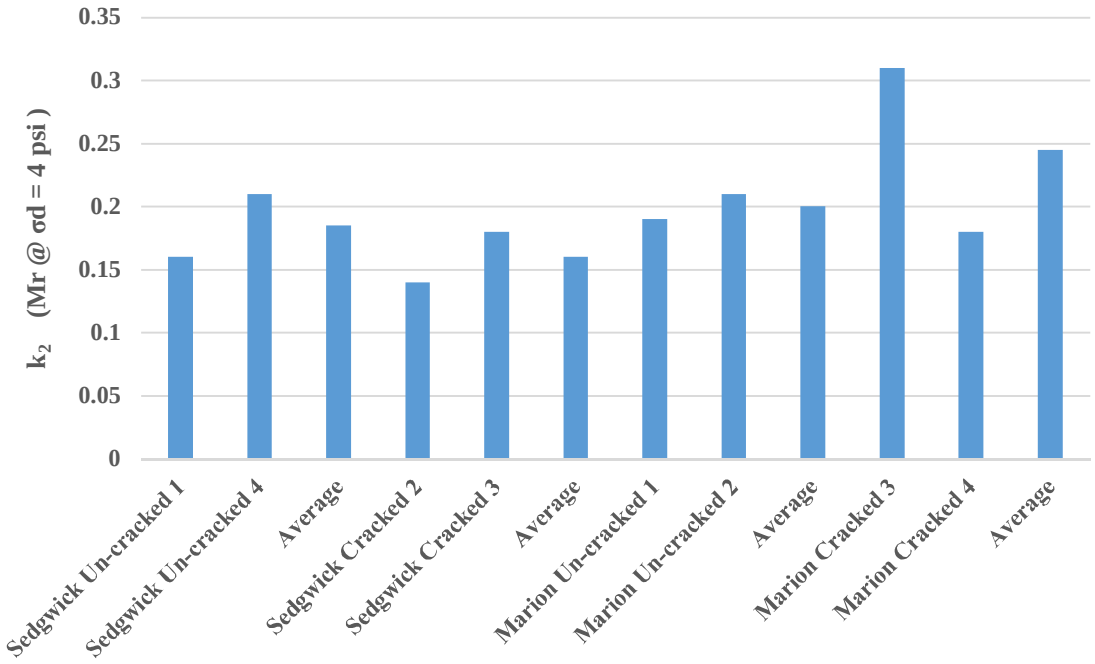

Figure 5-19 k_2 values (Mr @ $\sigma_d = 4$ psi M2 Model).

Table 5-15 Resilient modulus test characteristics (NCHRP M3 Model).

Soil Specimens No.	**k_1**	**k_2**	**k_3**	**R^2**	**$M_{r\,(psi)}$ @ θ = 10 psi and τ = 1.89 psi**
87th SG Un-cracked 1	1,284	0.145	0.708	0.96	19,308
87th SG Un-cracked 4	1,360	0.126	1.271	0.94	22,055
Average	**1,322**	**0.136**	**0.990**	**0.95**	**20,681**
87th SG Cracked 2	1,579	0.259	0.805	0.93	22,991
87th SG Cracked 3	1,271	0.100	1.049	0.94	20,268
Average	**1,425**	**0.180**	**0.927**	**0.93**	**21,630**
330th MN Un-cracked 1	1,539	0.064	1.319	0.98	25,712
330th MN Un-cracked 2	1,580	0.238	0.884	0.89	23,422
Average	**1,560**	**0.151**	**1.101**	**0.94**	**24,567**
330th MN Cracked 3	1,440	0.219	1.204	0.93	22,356
330th MN Cracked 4	1,785	0.159	0.938	0.90	27,453
Average	**1,612**	**0.189**	**1.071**	**0.91**	**24,904**

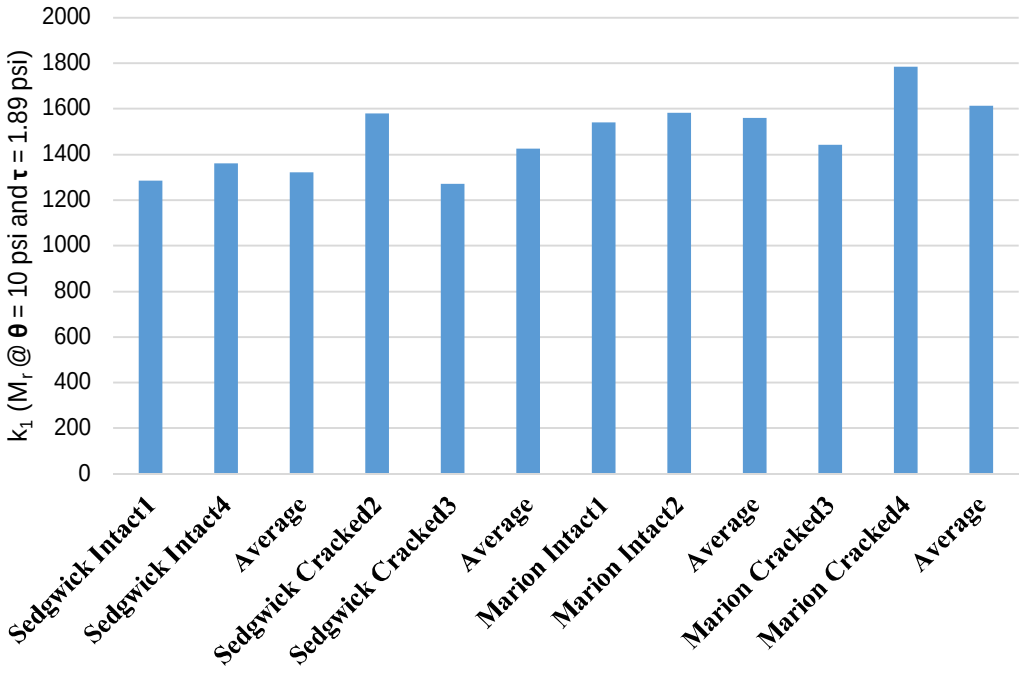

Figure 5-20 k_1 values (M_r @ θ = 10 psi and τ = 1.89 psi – M3 Model).

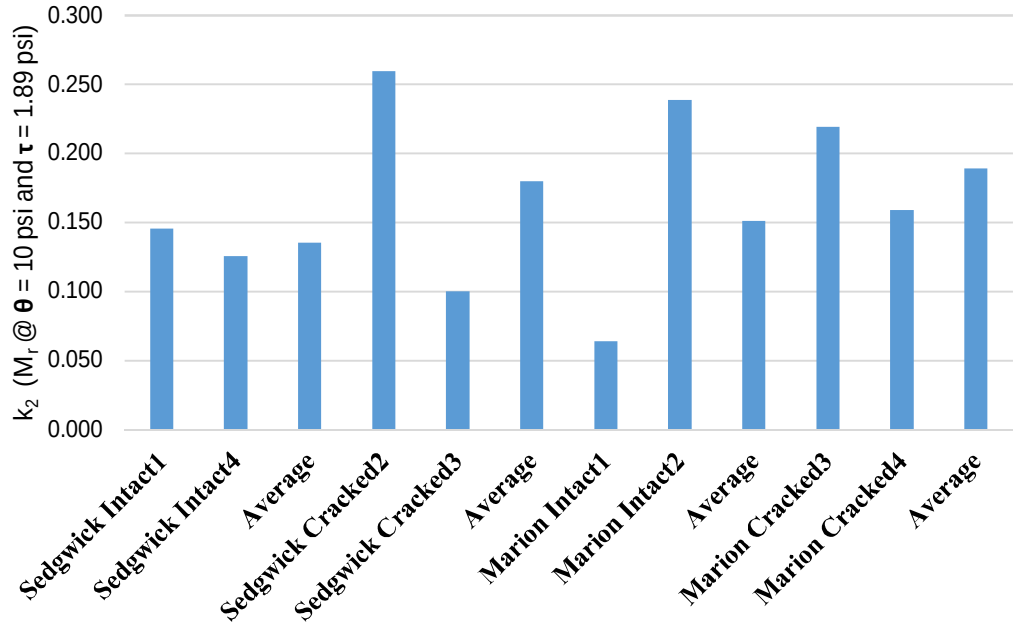

Figure 5-21 k_2 values (M_r @ θ = 10 psi and τ = 1.89 psi – M3 Model**).**

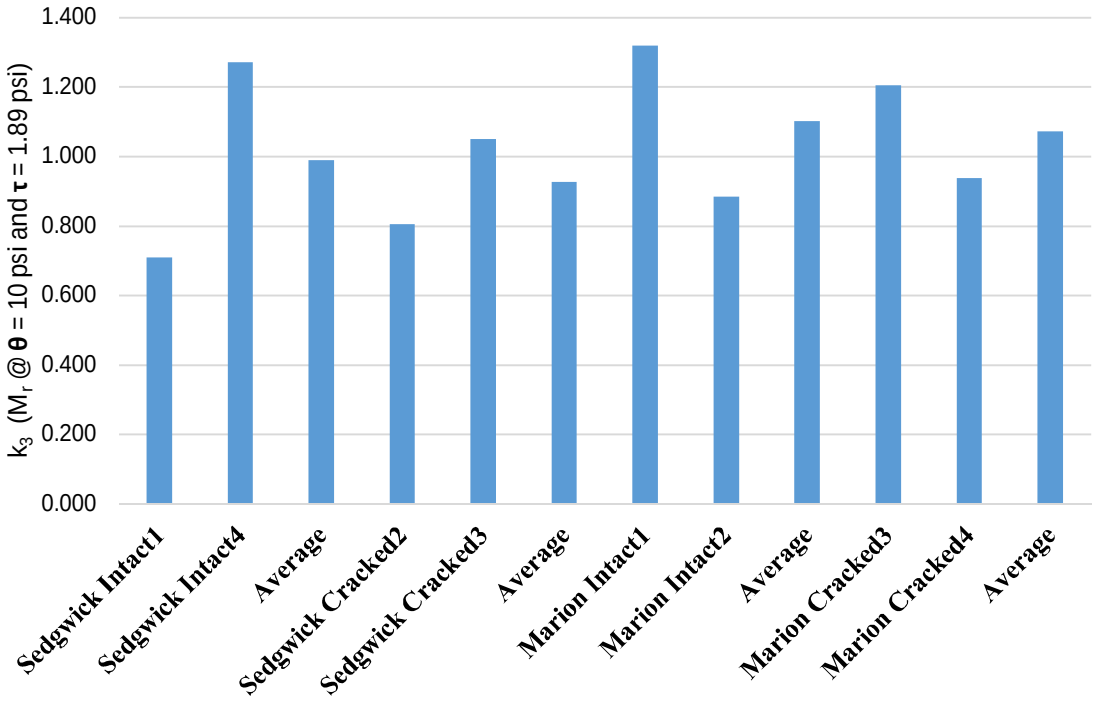

Figure 5-22 k_3 values (M_r @ θ = 10 psi and τ = 1.89 psi – M3 Model**).**

Figure 5-23 shows that the laboratory resilient moduli of the reconstituted specimens from 330th MN were higher than those from 87th SG. Also, the average resilient modulus of the cracked specimens from 87th SG was approximately 18 percent higher than that of the specimens that were without microcracking. However, this result was not obtained with the reconstituted specimens from 330th MN where the difference between the cracked and uncracked specimens was negligible. Also, the average resilient modulus ratio for all the specimens reconstituted from 330th to that for the specimens from 87th SG was approximately 0.17 for both Model M1 and Model M3 and 0.25 for M2 Model. In addition, the average resilient modulus of the cored specimens from 330th MN was approximately 20 to 50 percent higher than that of the specimens reconstituted in the laboratory.

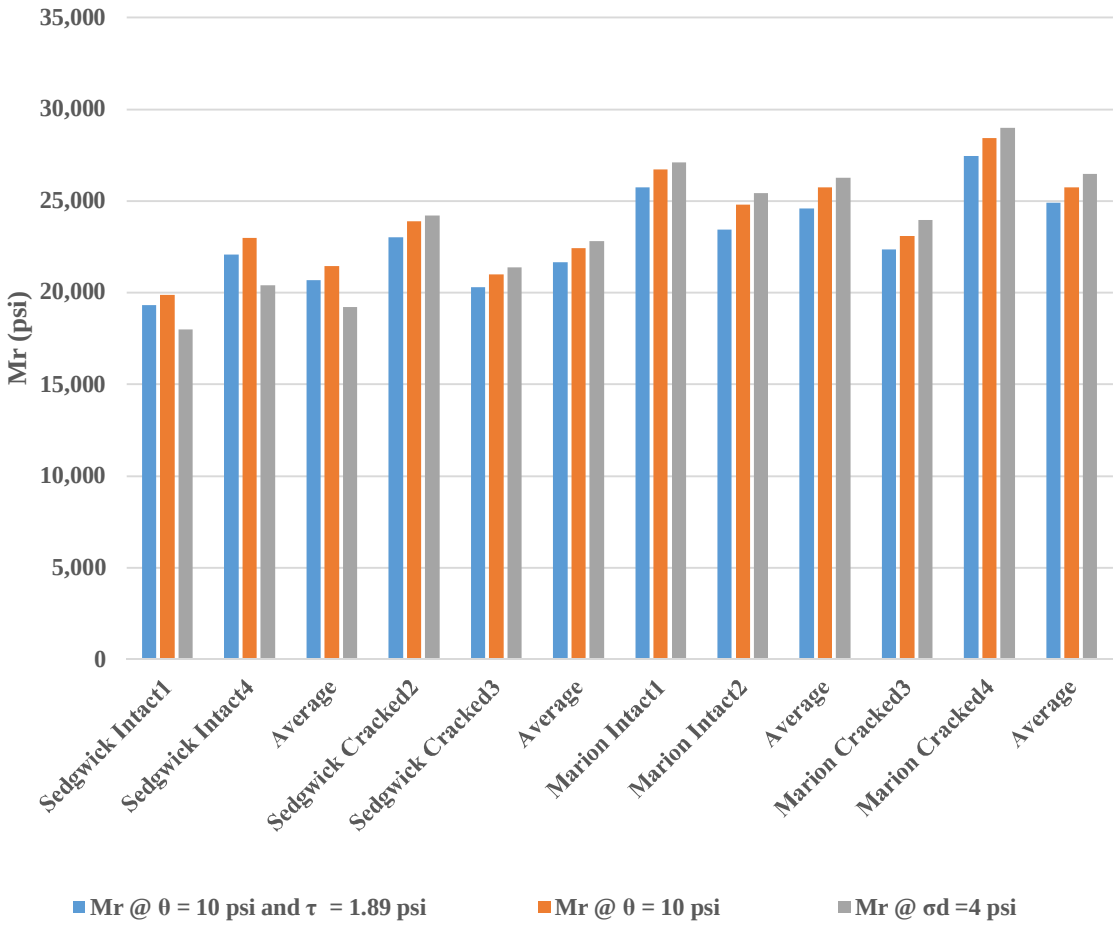

Figure 5-23 Resilient moduli of the reconstituted CMS specimens for 87th SG and 330th MN Soils.

5.5.5 **Resilient Modulus Correlated from Unconfined Compressive Strength**

Several studies, Thompson (1970) and Little and Yusuf (2001) have evaluated the correlations between the resilient modulus and the unconfined compressive strength of lightly stabilized materials. Rasul (2016) presented a correlation derived from the analysis of permanent deformations and unconfined compressive strengths as depicted in Equation 5-5. This equation was evaluated in this study in terms of the CMS.

$$M_r = (UCS)^{a+b*\sigma_d} \quad \text{(Equation 5-5)}$$

where M_r = the resilient modulus in psi,

UCS = the unconfined compressive strength in psi,

σ_d = the deviatoric stress in psi, and

a=1.573 and b=0.007 are regression parameters.

Table 5-16 presents a comparison of the unconfined compressive strength versus the resilient modulus for the cored CMS specimens collected from 330th MN in addition to the reconstructed specimens from 330th MN and 87th SG sites. Table 5-15 shows significant differences between the predicted resilient moduli using Equation 5-5 and the calculated resilient moduli using Models 1, 2 and 3. Toohey et al. (2013) also demonstrated the lack of a clear correlation between the resilient modulus and the unconfined compressive strength. Wooten and Foreman (2005), Terashi (2002), and Wilson (2013) have shown that the stiffness of the soil-cement increases with the age of the materials, the difference between the predicted resilient moduli using Equation 5-5 and the measured resilient moduli could be attributed to the age of the specimens that is not a variable in Equation 5-5.

Table 5-16 Measured versus predicted resilient moduli of CMS materials.

Soil Specimens No.	**UCS (psi)**	**Predicted M_r (psi) using** Equation 5-5	**Measured using M1 (psi)**	**Measured using M2 (psi)**	**Measured using M3 (psi) @ θ = 10 psi and τ = 1.89 psi**
330th MN Core Specimen 1	734	37,833	29,117	34,853	28,097
330th MN Core Specimen 2	734	37,575	34,191	34,034	33,824
330th MN Core Specimen 4	1,068	66,966	35,659	44,912	33,788
330th MN Core Specimen 6	355	11,850	32,454	38,630	31,757
Average	**722.8**	**38,556**	**32855.3**	**38107.3**	**31866.5**
87th SG Un-cracked 1	377	13,116	19,879	17,988	19,308
87th SG Un-cracked 4	511	21,529	22,961	20,398	22,055
Average	**444**	**17,323**	**21,420**	**19,193**	**20,681**
87th SG Cracked 2	519	21,909	23,879	24,204	22,991
87th SG Cracked 3	330	10,637	20,975	21,373	20,268
Average	**424.5**	**16,273**	**22,427**	**22,788**	**21,630**
330th MN Un-cracked 1	891	51,650	26,711	27,090	25,712
330th MN Un-cracked 2	855	48,794	24,776	25,427	23,422
Average	**873**	**50,222**	**25,743**	**26,258**	**24,567**
330th MN Cracked 3	594	27,226	23,063	23,938	22,356
330th MN Cracked 4	716	36,747	28,404	28,978	27,453
Average	**655**	**31,987**	**25,733.5**	**26,458**	**24,904**

CHAPTER 6 EVALUATION USING MECHANISTIC EMPIRICAL APPROACH

A better laboratory performance of a soil-cement mixture will not necessarily translate into a better performance in the field as the performance and life of a pavement system is highly dependent on the pavement structure and the characteristics (e.g., stiffness) of the pavement materials (Schaefer et.al, 2008). A mechanistic empirical design method represents the most advanced method for designing HMA pavements. This design entails the incorporation of both the climate variations and the traffic. The mechanistic portion is based on the mechanics of materials that relates an input, such as a wheel load, to an output or pavement response, such as stress, strain, or deflection. The empirical portion is when the response values are used to predict distresses based on laboratory relationships calibrated with field performance data.

Numerical modeling is widely used by pavement engineers to calculate the induced damage to pavement layers, including the asphalt layer, base and subgrade material. Based on linearly elastic theory, an analytical solution of layered semi-infinite half-space can be obtained. The assumptions are that stress-strain behavior is linearly elastic and the pavement domain has no limit in the horizontal direction. In the vertical direction, there is a horizontal stress-free surface at top of the medium while the bottom is extended to infinite depth.

Over the last few decades, several computer programs were developed for pavement analysis based on the multi-layer elastic theory. The available computer programs which can be used in pavement analysis and design include: BISAR, CHEVRON, KENLAYER, ELSYM5, Everstress, WESLEA and MEPDG. Typically, these software can compute the stresses, strains, and deflections under a circular surface load. The inputs of these software include: material

properties (modulus and Poisson's ratio), layer thickness, and load conditions (magnitude of load, radius, or contact pressure). The outputs include stresses, strains, and deflections.

6.1 SEASONAL AIR TEMPERATURES

The daily maximum, average, and minimum daily temperatures for the 87th SG and 330th MN sites for year 2018 were obtained from the National Centers for Environmental Information (formerly the National Climatic Data Center NCDC) and are presented in Figure 6-1.

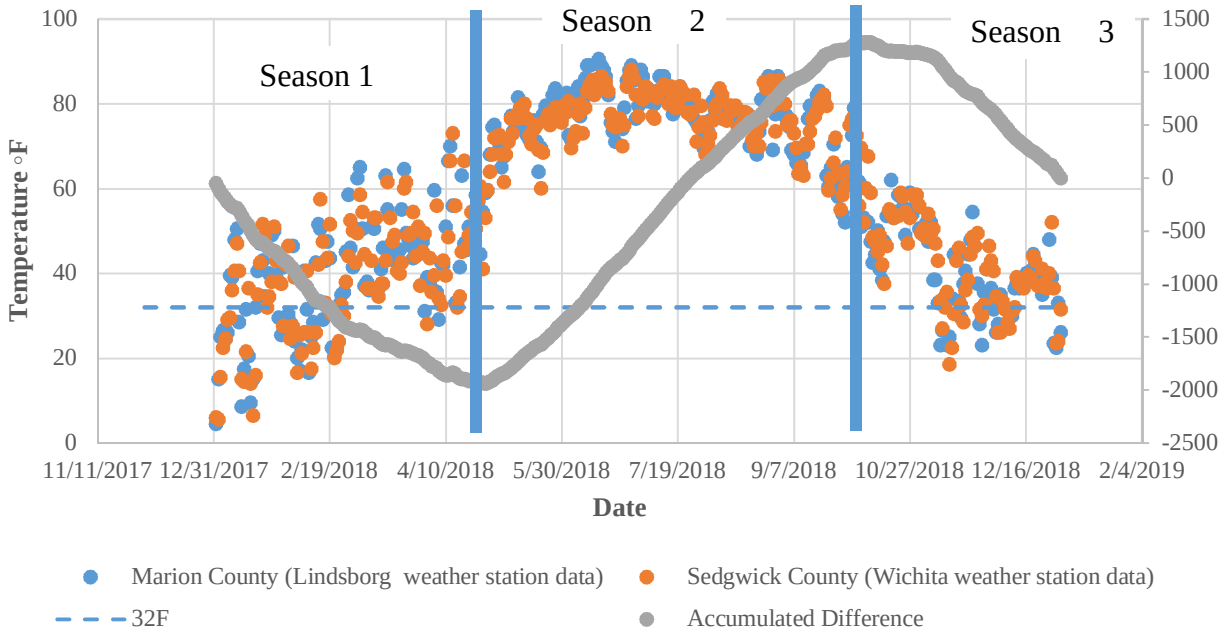

Figure 6-1 Accumulated difference method for seasonal determination.

The accumulated difference method is applied by collecting the average temperature for every day over one complete year. Afterwards, the average yearly temperature is computed and the difference between each day's temperature and the mean yearly temperature is computed. Finally, the accumulated difference is computed and plotted as a function of the days in that year.

This method allows us to divide the year into different seasons in order to apply the corresponding material characteristic for each season and account for seasonal variations and their effects. Every change in the behavior of the graph signals the start of a new season. Hence, based on Figure 6-1, the analysis year can be divided into three seasons, which are described in the following section.

Table 6-1 Three seasons in Kansas per the accumulated difference method.

Season	Start Date	End Date	Duration in Days	Duration in Weeks
1	January 1st	April 27th	116	16
2	April 27th	October 9th	165	24
3	October 10th	December 31st	84	12

The first season is the coldest, implying the highest modulus of elasticity of asphalt concrete (AC tends to have a more elastic behavior at low temperatures as opposed to a more viscous behavior at high temperatures). The second hot season corresponds to a low value for the modulus of elasticity of asphalt concrete, while the third season will have an intermediate modulus value. Furthermore, seasons 1 and 3 will include rain, implying a weaker subgrade as opposed to season 2 when the subgrade dries out and yields more strength. Table 6-1 presents the three-seasons data in Kansas per the accumulated difference method.

6.2 SEASONAL VARIATION

6.2.1 HMA Temperature and Modulus Variation

The most important environmental factor affecting surface deflections of flexible pavements is the temperature of the asphaltic layers (Kim et al. 1995; Park et al. 2002). The temperature can be measured directly by drilling holes into the pavement, but the procedure is time consuming and was not performed for this project. Also, multiple holes are needed to capture the temperature

gradient within the HMA layer. However, the pavement temperature was estimated based on correlations that use externally measurable variables (i.e. infrared surface temperature, average high and low air temperatures on the day before testing). The BELLS3 model as recommended by FHWA (2000) and depicted in Equation 6-1 was used in this study to estimate the mid-depth pavement temperature.

$$T_d = 0.95 + 0.892T_s + (\log d - 1.25) \times \left[1.83 \sin\left(2\pi\frac{A}{18}\right) - 0.448T_s + 0.621T_{avg}\right] + 0.042T_s \sin\left(2\pi\frac{B}{18}\right) \quad \text{(Equation 6-1)}$$

where d = the layer mid-depth (mm);

T_d= the pavement temperature at layer mid-depth (°C);

T_s= the infrared surface temperature (°C);

T_{avg}= the average of high and low air temperatures on the day before testing (°C); and

254 mm = 1 inch; (°F) = 1.8 (°C) + 32

A and B are computed as follows:

$$A = \begin{cases} t_d + 9.5 & \text{if } 0 \le t_d < 5 \\ -4.5 & \text{if } 5 \le t_d < 11 \\ t_d - 15.5 & \text{if } 11 \le t_d < 24 \end{cases}$$

$$B = \begin{cases} t_d + 9.5 & \text{if } 0 \le t_d < 3 \\ -4.5 & \text{if } 3 \le t_d < 9 \\ t_d - 13.5 & \text{if } 9 \le t_d < 24 \end{cases}$$

t_d= the time of the day (in decimal hours)

A and B are used as arguments to a pair of sin functions with 18-hour periods, and 15.5- and 13.5-hour phase lags, respectively.

The infrared pavement surface temperatures were measured at each test locations by the KDOT personnel at the time of testing. The average values of high and low air temperatures on the day before testing were obtained from the National Centers for Environmental Information (formerly the National Climatic Data Center NCDC) for the weather stations in Lindsborg, KS and Wichita, KS for 330th MN and 87th SG sites, respectively.

Since HMA stiffness is very sensitive to temperature and monitoring the pavement temperature was impossible at these sites, a correlation between the air temperature (readily collected parameter) and the pavement temperature was used for the analyses. The seasonal asphalt concrete temperature variation is assumed sinusoidal as given in Equation 6-2.

$$T = \frac{T_1+T_2}{2} + \frac{T_1-T_2}{2} \times sin\left(\frac{2\pi}{365} \times (D_0 - D) + \frac{\pi}{2}\right) \quad \text{(Equation 6-2)}$$

where T = the asphalt temperature in days number D, counted from January 1st,

T_1 = the maximum asphalt temperature during the year,

T_2 = the minimum asphalt temperature during the year,

D = the day number counted from January the 1st, and

D_0 = the day number corresponding to the maximum asphalt temperature.

A study has been conducted using the Long-Term Pavement Performance LTTP database over five sections in the US. These five sections as shown in Figure 6-2 are part of the LTTP seasonal monitoring program, which has an online database that has hourly recordings of air temperatures and asphalt temperatures at various depths. These sections are Alabama 01-0101, Arizona 04-0113, Montana 30-0114, Nebraska 31-0114, and New York 36-0801.

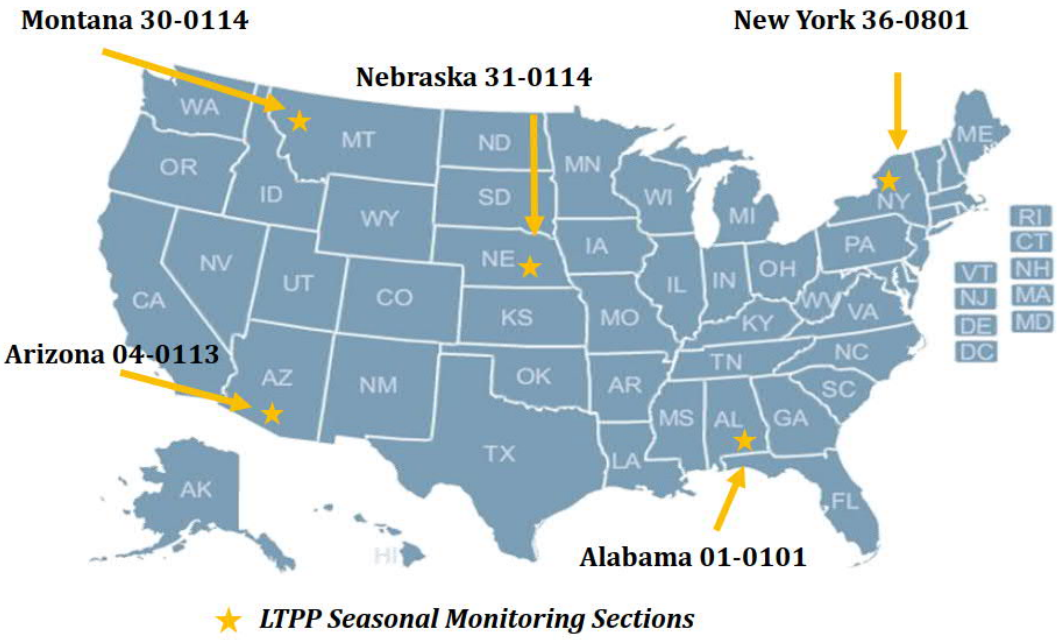

Figure 6-2 LTPP seasonal monitoring sections.

The maximum pavement temperature is found to be equal to 1.1 the maximum average daily air temperature; while the minimum pavement temperature is found equal to the minimum average weekly air temperature. This relationship is relatively constant for all the selected sites and hence is assumed applicable for Kansas.

Then given the air temperature for the year 2018 from the two weather stations in Lindsborg and Wichita, Kansas, the asphalt temperature can be estimated as depicted in Figure 6-3. The estimated HMA modulus for each season is presented in Table 6-2.

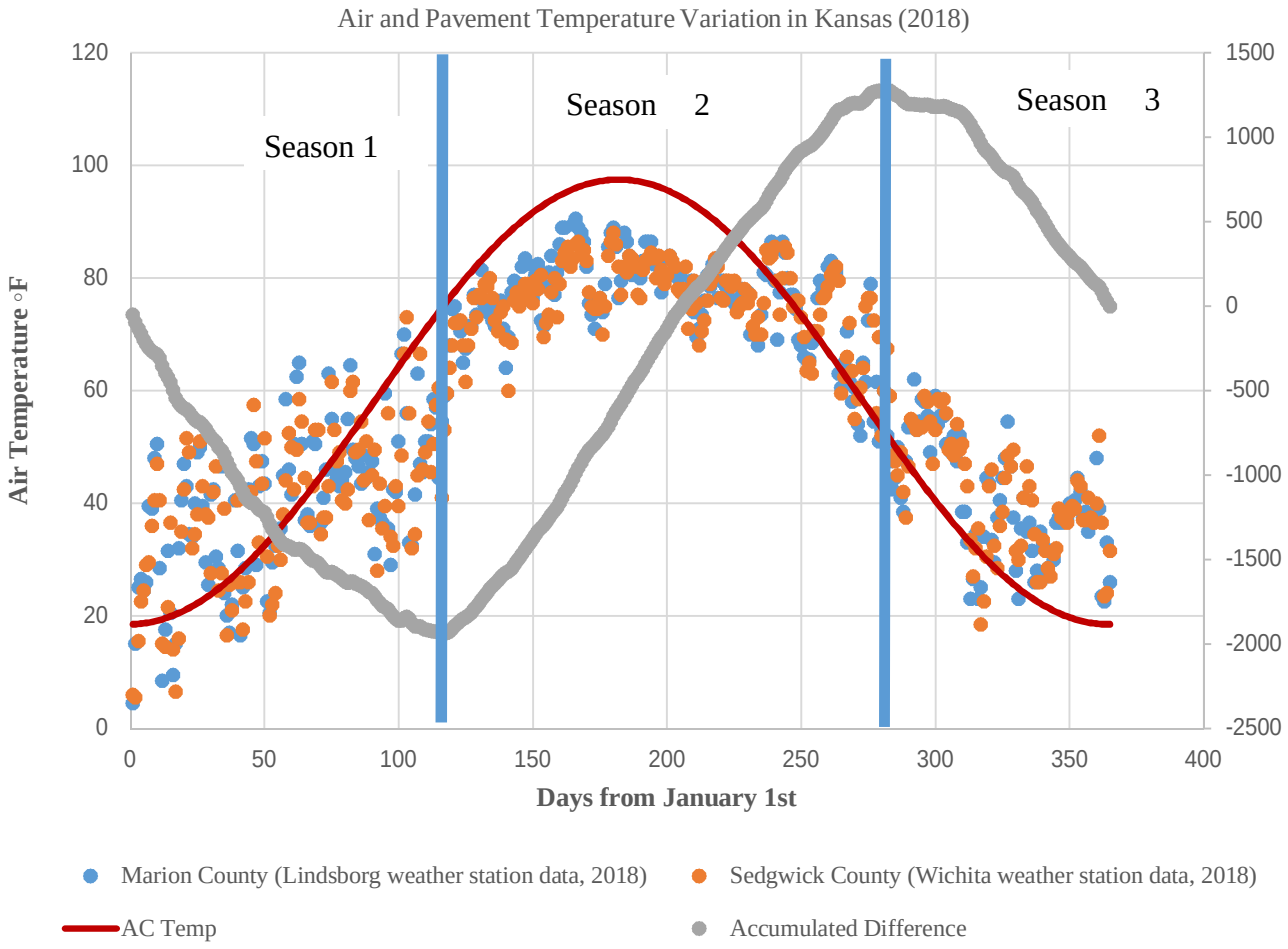

Figure 6-3 Air and pavement variations in Kansas for the Year 2018.

Table 6-2 Estimated HMA modulus for each season.

Site	Season	Duration in Days	Duration in Weeks	HMA Average temperature representing the season (°F)	$E_{1\ HMA}$ @ average temperature representing the season (using Equation 5-4 and FWD backcalculated modulus), ksi
330th MN	1	116	16	44	1,293
	2	165	24	77	394
	3	84	12	36	1,724
87th SG	1	116	16	44	889
	2	165	24	77	271
	3	84	12	36	1,186

6.2.2 **Subgrade Modulus Seasonal Variation**

The bearing capacity of flexible pavements is highly sensitive to environmental conditions. In cold regions like Kansas, pavement subgrade soils are susceptible to freezing in winter that is followed by thawing starting winter and through spring when the moisture of the subgrade is the highest when compared to the rest of the year. This moisture increase can significantly reduce the bearing capacity of the unbound subgrade layer. This poor support will result in an accelerated damage in the unbound layer. Sebaaly et al. (1994), Uhlmeyer et al. (1996), and Mehrotra (2011) showed that significant decrease in the resilient modulus of the subgrade could occur when the moisture content increases. This high moisture content decreases the modulus of the subgrade layer by almost 50% during the thawing seasons. Since Kansas undergoes several continuous freeze and thaw cycles during winter and through spring and no moisture measurement was performed through each season, the following subgrade modular factors were adopted in this study.

Since Kansas witnesses a moderate period with freezing, freeze and thaw effects are incorporated conservatively with the subgrade modular ratios of 0.6 for season 1, 0.85 for season 2, and 0.7 for season 3. These modular factors are taken under the assumption that thawing will last during seasons 1 and 3, while recovering during season 2.

6.3 ESAL

The traffic loads provided by the public work departments for 87th SG and 330th MN sites are shown in Table 6-3.

Table 6-3 ESALs over design life and per year for 87th SG and 330th MN.

Site	Design Life (years)	Equivalent Single Axle Load (ESAL) during design life	Equivalent Single Axle Load (ESAL) per year
87th SG	8	82,000	10,250
330th MN	20	548,687	27,435

Assuming equal traffic distribution through the year and knowing the number of weeks in each season, the seasonal repetitions are shown in Table 6-4.

Table 6-4 ESALs per season for each year.

Site	Season	Number of Weeks	Equivalent Single Axle Load (ESAL) per season
87th SG	1	16	3,154
	2	24	4,730
	3	12	2,366
330th MN	1	16	8,442
	2	24	12,662
	3	12	6,331

6.4 KENLAYER

KENLAYER is a computer program that can model pavement layers as linearly elastic, nonlinearly elastic or as Mohr-Coulomb elastoplastic materials (Huang 2004). The core of KENLAYER is the solution for an elastic multilayer system under a circular loaded area. The KENLAYER Computer Program can only be used to analyze flexible pavements with no joints. This program can use the superposition principle for multiple wheels. It can also use an iterative

technique to solve non-linear problems (Gedafa 2006). KENLAYER is based on the elastic theory. In a three-dimensional elastic analysis, the stress and strain are related to each other following the three-dimensional Hooke's law.

In this study, the pavement models were analyzed under two dimensional axisymmetric conditions where the three-dimensional Hooke's law equations can be reduced to the two-dimensional ones. In the KENLAYER software, it is assumed that the pavement sections extend indefinitely in the horizontal and the vertical directions.

6.4.1 **Analysis Approach**

The objective of this analysis is to evaluate the performance of flexible pavements on the CMS layer based on the laboratory findings and field NDT results. The mechanistic-empirical analysis was used in conjunction with the resilient modulus data of the CMS measured in the laboratory and backcalculated from the field data using the FWD tests for each site.

The mechanistic analysis was conducted to calculate the responses of the pavement system under an 18-kip single axle dual tire load (18,000 lbs/axle over 4 tires/axle). The tire contact pressure was assumed to be 100 psi for wheel spacing of 13 inches. The calculated contact radius of each tire under a wheel load of 4,500 lb was 3.8 inches. The analyses considered a three-layer pavement system for each site. The pavement thicknesses and material properties without seasonal variations for 330th MN and 87th SG sites are presented in Table 6-5.

Table 6-5 Pavement thicknesses and material properties without seasonal variations for 330th and 87th SG.

Site	Layer type	Thickness (in)	Poisson's ratio (v)	Material property	Layer modulus inputs
330th MN	HMA @ 68 °F	3	0.35	Linear elastic	E_{HMA}= 545 ksi
	CMS	12	0.35	Non-linear elastic	$M_r = k_1(\theta)^{k_2}$ Model M1 k_1 and k_2 from Table 5-13
	Subgrade	Semi-infinite	0.45	Linear elastic	E_3= 11 ksi
87th SG	HMA @ 68 °F	2	0.35	Linear elastic	E_{HMA}= 375 ksi
	CMS	10	0.35	Non-linear elastic	$M_r = k_1(\theta)^{k_2}$ Model M1 k_1 and k_2 from Table 5-13
	Subgrade	Semi-infinite	0.45	Linear elastic	E_3= 20.5 ksi

Since this analysis focused mainly on the effect of the CMS layer on the pavement performance, the HMA and the subgrade were modeled as linearly elastic materials with their E_{1HMA} and E_2 values as shown in Table 6-6. The resilient moduli of the subgrade were determined from the backcalculated E_3 moduli presented in Table C-3 through C-6 for each site. The pavement section details and seasonal material properties for 330th MN and 87th SG sites used in the KENLAYER analyses are presented in Table 6-6.

Table 6-6 Pavement thicknesses and seasonal material properties for 330th MN and 87th SG.

Site	Layer Type	Thickness (in)	Seasons	Average HMA Temperature (°F)	Layer modulus inputs
330th MN	HMA	3	1	44	E_{HMA}= 1,293 ksi
			2	77	E_{HMA}= 394 ksi
			3	36	E_{HMA}= 1,724 ksi
	CMS	12	1, 2, 3	--	$M_r = k_1(\theta)^{k_2}$ Model M1 k_1 and k_2 from Table 5-13
	Subgrade	Semi-infinite	1	--	$E_{3\ season\ 1} = 0.6\ E_3$
			2	--	$E_{3\ season\ 2} = 0.85E_3$
			3	--	$E_{3\ season\ 3} = 0.7\ E_3$
87th SG	HMA	2	1	44	E_{HMA}= 889 ksi
			2	77	E_{HMA}= 271 ksi
			3	36	E_{HMA}= 1,186 ksi
	CMS	10	1, 2, 3	--	$M_r = k_1(\theta)^{k_2}$ Model M1 k_1 and k_2 from Table 5-13
	Subgrade	Semi-infinite	1	--	$E_{3\ season\ 1} = 0.6\ E_3$
			2	--	$E_{3\ season\ 2} = 0.85E_3$
			3	--	$E_{3\ season\ 3} = 0.7\ E_3$

6.4.2 **Critical Responses from KENLAYER**

The KENLAYER program requires entering the locations of interest to compute pavement responses. A total of 24 locations for analysis and output were included in this study. These locations were distributed within and outside the loaded areas, forming a grid in the plane parallel to the transverse YZ-plane. The responses at the bottom of the HMA layer were used for fatigue

analysis; whereas the responses on top of the subgrade were used for permanent deformation analysis.

Based on the KENLAYER analyses of the pavement sections for each site under the 18-kip dual tire axel load, the critical tensile strain at the bottom of the HMA was located at the center of the tire and the critical vertical strain at the top of the subgrade was located at the mid-span of dual tires. The critical responses at the center of the tires and the mid-span of dual tires were calculated based on the material properties without any seasonal variations (including E_{1HMA} at 68 ^{o}F and the resilient modulus M1) for 330th MN pavement section as presented in Table 6-7 and Table 6-8, respectively. Similar results for 87th SG pavement section M1 are presented in Table 6-9 and Table 6-10, respectively.

Table 6-7 Critical responses for 330th MN pavement section at the center of the tires without seasonal variations of the subgrade.

Responses / **Depths, (in)**	**Vertical displacement (in)**	**Tensile strain, strain (10^{-6})**	**Compressive stress (psi)**	**Compressive strain, strain (10^{-6})**
0	0.0276	--	--	--
3	0.0268	**-274**	--	--
15	0.0216	-309	4.13	349

Table 6-8 Critical responses for 330th MN pavement section at the mid-span of dual tires without seasonal variations of the subgrade.

Responses / **Depths, (in)**	**Vertical displacement (in)**	**Tensile strain, strain (10^{-6})**	**Compressive stress (psi)**	**Compressive strain, strain (10^{-6})**
0	0.0271	--	--	--
3	0.0267	-214	--	--
15	0.0223	-331	4.47	**663**

Table 6-9 Critical responses for 87th SG pavement section at the center of the tires without seasonal variations of the subgrade.

Responses / **Depths, (in)**	**Vertical displacement (in)**	**Tensile strain, strain (10^{-6})**	**Compressive stress (psi)**	**Compressive strain, strain (10^{-6})**
0	0.0291	--	--	--
2	0.0287	**-413**	--	--
12	0.0205	-4319	8.35	810

Table 6-10 Critical KENLAYER responses for 87th SG pavement section at the mid-span of dual tires without seasonal variations of the subgrade.

Responses / **Depths, (in)**	**Vertical displacement (in)**	**Tensile strain, strain (10^{-6})**	**Compressive stress (psi)**	**Compressive strain, strain (10^{-6})**
0	0.0264	--	--	--
2	0.0265	-249	--	--
12	0.0216	-466	8.81	**846**

The critical responses (with seasonal variations, $E_{1\ HMA}$ and E_3 subgrade as shown in Table 6-6) at the center of the tires, the edge of the tire, and the mid-span of dual tires for 330th MN pavement section using the resilient modulus M1 are presented in Table 6-11, Table 6-12, and Table 6-13, respectively. Similar critical responses for 87th SG pavement section using the resilient modulus M1 are presented in Table 6-14, Table 6-15, and Table 6-16, respectively. The critical responses presented in Tables 6-11 through 6-16 are basesd on E_3 backcalculated from the FWD testing and adjusted for seasons 1, 2, and 3 as described in Section 6.2.2.

Table 6-11 Critical KENLAYER responses for 330th MN pavement section at the center of the tires with seasonal variations (E_3 correlated from the FWD data).

Responses / **Material, Depths (in)**	**Seasons**	**Vertical displacement (in)**	**Tensile strain, strain (10^{-6})**	**Compressive stress (psi)**	**Compressive strain, strain (10^{-6})**
HMA, (0)	1	**0.0248**	--	--	--
	2	**0.0222**	--	--	--
	3	**0.0218**	--	--	--
HMA, (3)	1	0.0244	**-198**	--	--
	2	0.0211	**-284**	--	--
	3	0.0215	**-169**	--	--
Subgrade (15)	1	0.0199	-270	3.93	**541**
	2	0.0160	-257	5.10	**498**
	3	0.0175	-236	4.04	**475**

Table 6-12 Critical KENLAYER responses for 330th MN pavement section at the edge of the tire with seasonal variations (E_3 correlated from the FWD data).

Responses / **Material, Depths (in)**	**Seasons**	**Vertical displacement (in)**	**Tensile strain, strain (10^{-6})**	**Compressive stress (psi)**	**Compressive strain, strain (10^{-6})**
HMA, (0)	1	**0.0252**	--	--	--
	2	**0.0216**	--	--	--
	3	**0.0222**	--	--	--
HMA, (3)	1	0.0249	**-189**	--	--
	2	0.0210	**-245**	--	--
	3	0.0221	**-163**	--	--
Subgrade (15)	1	0.0206	-285	4.20	**584**
	2	0.0166	-274	5.46	**538**
	3	0.0180	-248	4.32	**512**

Table 6-13 Critical KENLAYER responses for 330th MN pavement section at the mid-span of dual tires with seasonal variations (E_3 correlated from the FWD data).

Responses / **Material, Depths (in)**	**Seasons**	**Vertical displacement (in)**	**Tensile strain, strain (10^{-6})**	**Compressive stress (psi)**	**Compressive strain, strain (10^{-6})**
HMA, (0)	1	**0.0251**	--	--	--
	2	**0.0212**	--	--	--
	3	**0.0218**	--	--	--
HMA, (3)	1	0.0249	**-175**	--	--
	2	0.0206	**-204**	--	--
	3	0.0215	**-169**	--	--
Subgrade (15)	1	0.0207	-288	4.25	**592**
	2	0.0167	-277	5.52	**544**
	3	0.0175	-236	4.04	**475**

Table 6-14 Critical KENLAYER responses for 87th SG pavement section at the center of the tires with seasonal variations (E_3 correlated from the FWD data).

Responses / **Material, Depths (in)**	**Seasons**	**Vertical displacement (in)**	**Tensile strain, strain (10^{-6})**	**Compressive stress (psi)**	**Compressive strain, strain (10^{-6})**
HMA, (0)	1	**0.0203**	--	--	--
	2	**0.0195**	--	--	--
	3	**0.0180**	--	--	--
HMA, (2)	1	0.0201	**-305**	--	--
	2	0.0189	**-412**	--	--
	3	0.0178	**-267**	--	--
Subgrade (12)	1	0.0136	-295	9.21	**553**
	2	0.0108	-263	11.61	**488**
	3	0.0119	-255	9.39	**479**

Table 6-15 Critical KENLAYER responses for 87th SG pavement section at the edge of the tire with seasonal variations (E_3 correlated from the FWD data).

Responses / **Material, Depths (in)**	**Seasons**	**Vertical displacement (in)**	**Tensile strain, strain (10^{-6})**	**Compressive stress (psi)**	**Compressive strain, strain (10^{-6})**
HMA, (0)	1	**0.0199**	--	--	--
	2	**0.0174**	--	--	--
	3	**0.0178**	--	--	--
HMA, (2)	1	**0.0199**	**-268**	--	--
	2	0.0172	**-327**	--	--
	3	0.0177	**-238**	--	--
Subgrade (12)	1	0.0143	-317	9.85	**591**
	2	0.0114	-282	12.15	**505**
	3	0.0125	-274	10.09	**516**

Table 6-16 Critical KENLAYER responses for 87th SG pavement section at the mid-span of dual tires with seasonal variations (E_3 correlated from the FWD data).

Responses / **Material, Depths (in)**	**Seasons**	**Vertical displacement (in)**	**Tensile strain, strain (10^{-6})**	**Compressive stress (psi)**	**Compressive strain, strain (10^{-6})**
HMA, (0)	1	**0.0192**	--	--	--
	2	**0.0156**	--	--	--
	3	**0.0180**	--	--	--
HMA, (2)	1	0.0193	**-222**	--	--
	2	0.0158	**-223**	--	--
	3	0.0173	**-203**	--	--
Subgrade (12)	1	0.014	-321	9.92	**594**
	2	0.0114	-285	12.10	**498**
	3	0.0126	-278	10.18	**520**

The largest tensile strains at the bottom of the HMA layer for 330th MN and 87th SG at all seasons were located at the center of the tire. Also, the largest compressive strains on top of the subgrade for 330th MN and 87th SG at all seasons were located at the mid-span of dual tires.

6.5 DISTRESS PREDICTION MODELS

The distress prediction model is defined, by the World Road Association (Ferreira et al. 1999, 2004), as a mathematical representation that can be used to predict the future condition of pavements, based on current conditions, traffic, and climate. The analysis of a given pavement structure is based upon the accumulation of damage as a function of traffic and time. The primary distresses considered in this analysis are, fatigue cracking that is related to the magnitude of the tensile strain at the bottom of the HMA layer and permanent deformation (rutting) that depends on the compression strain on top of the subgrade. Distress models are the weak link in the mechanistic-empirical method because extensive field calibration and verification are needed to establish reliable field distress prediction.

AASHTO (2002) specified that pavements with one or more stabilized layers should be designed for fatigue cracking alone, but not for rutting because permanent deformation is often assumed to be zero in this standard (Rasul, 2015). However, Wu et al. (2011) showed that permanent deformation could still occur in pavements with stabilized soils. It is a fact that introducing the CMS layer in flexible pavements can reduce the rutting of HMA pavements as a result of minimal rutting in the subgrade, subbase, and base (Von Quintus et al. 2005). According to De Beer (1990), crushing damage may occur due to the repeated compressive strain at the top of the soil-cement, as shown in Figure 6-4. The crushing typically occurs in a thick, lightly cemented material and is directly related to the ratio of compressive stress to compressive strength. The same study showed that when the compressive stress to compressive strength ratio is less than 0.2, the crushing damage could be neglected. However, a compressive strain of 1% is considered as the failure strain for compression fatigue and the compressive strain is expected to increase as the load repetitions increase (De Beer, 1990). Theyse et al. (1996) reported that increasing the UCS increases the

compression fatigue life. Regarding the compression fatigue characterization, Theyse et al. (1995) suggested a 0.08-inch rut as the criterion for crushing initiation and a 0.4-inch rut for advanced rutting.

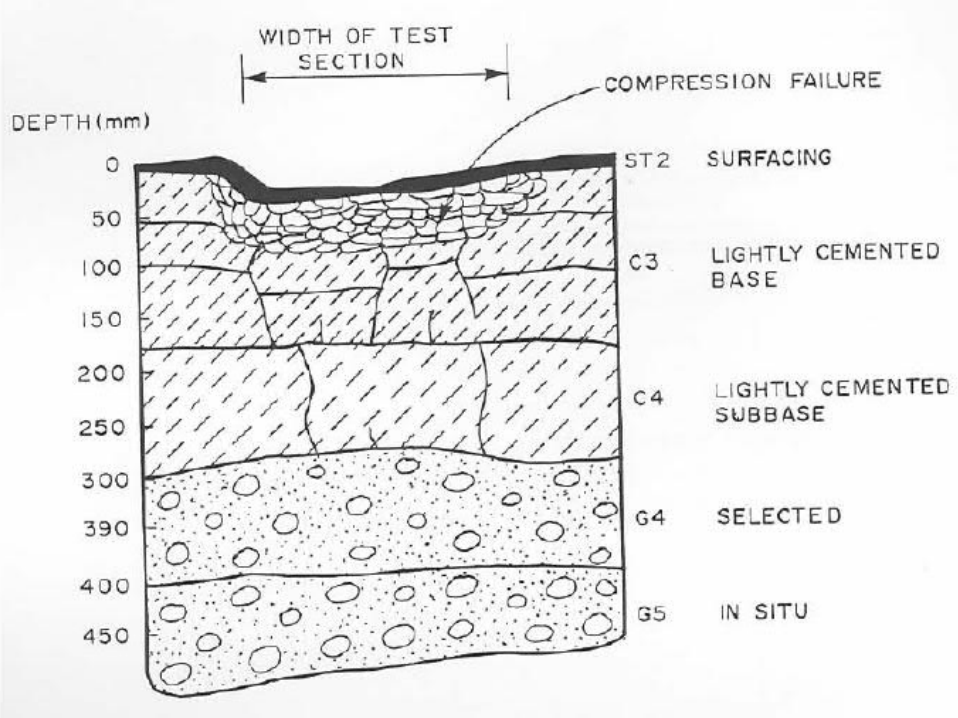

Figure 6-4 Crushing damage of lightly cemented soil (De Beer 1990).

Since the CMS layers at 87th SG and 330th MN site were not lightly cemented and their compressive stress to compressive strength ratios in this study are less than 0.2, evaluation of crushing damage to the CMS layers is not necessary and was not conducted. The Asphalt Institute (AI, 1982) recommended prediction models for tensile fatigue cracking and permeant deformation are described in the following sections.

6.5.1 **Fatigue Cracking Model**

This study used the Asphalt Institute (AI) fatigue model that relates the maximum horizontal tensile strain at the bottom of the asphalt layer and the modulus of the asphalt layer to the allowable number of repetitions. This model as presented in Equation 6-3 uses 45% fatigue cracking in the wheel-path area, or 20% of the total lane area as the failure criterion (AI, 1982).

$$N_f = f_1(\varepsilon_t)^{-f_2}(E)^{-f_3} \qquad \text{(Equation 6-3)}$$

where N_f = the allowable number of load repetitions,

E = the dynamic modulus of the asphalt mixture,

ε_t = the horizontal tensile strain at the bottom of the asphalt layer, and

$f_1 = 0.0796, f_2 = 3.291,$ and $f_3 = 0.854$ are the constants for a standard mix recommended by AI.

The major limitation of the above fatigue cracking model is that it can only provide the fatigue life in terms of the allowable number of load repetitions before reaching a pre-defined percentage of area cracked. According to this model, the pavements with similar modulus and tensile strain at the bottom of the asphalt layer will result in similar predicted fatigue lives.

6.5.2 **Permanent Deformation Model**

This study used the general model recommended by AI for permanent deformation as shown in Equation 6-4 to calculate the allowable number of load repetitions corresponding to the pre-defined permanent deformation. The permanent deformation model relates the compressive strain at the surface of the subgrade to the allowable number of load repetitions to control permanent deformation. It should be noted that the use of the compressive strain on the top of the subgrade

as a failure criterion is valid only when the permanent deformation is caused by the weak subgrade rather than the overlying layers (Huang, 2004).

$$N_d = f_4(\varepsilon_c)^{-f_5} \quad \text{(Equation 6-4)}$$

where N_d = the allowable number of load repetitions,

ε_c= the compressive strain on top of the subgrade, and

$f_4 = 1.365 \times 10^{-9}$ and $f_5 = 4.477$ are the constant for a standard mix recommended by AI.

6.5.3 **Damage Analysis Results for Fatigue and Permanent Deformation**

The critical compressive strains determined in Section 6.4.2 from KENLAYER were used to compute the number of repetitions until failure N through the model that allows the accumulation of damage and determination of possible distresses. Knowing the number of repetitions per year and the number of repetitions until failure, the remaining life of each layer was determined and checked against the design period of 8- and 20-years for 87th SG and 330th MN, respectively. Table 6-17 through

Table 6-18 summarize the allowable numbers of repetitions to fatigue failure N_f and permanent deformation failure N_d for the flexible pavements at 330th MN and 87th SG sites for three seasons.

The damage per season was calculated as the ratio of the actual number of load repetitions during the design life for a certain season to the critical allowable number of repetitions to failure for that season.

The remaining service life (RSL) is the anticipated number of years that a pavement is in an acceptable condition while accumulating enough functional or structural distresses under normal conditions, given that no further maintenance is performed, or the distress level is equal to an as-defined threshold value (Baladi, 1991). The remaining service life is the inverse of the total damage for all the seasons per year and the critical layer is the one with the shortest remaining life or the highest damage per year. The KENLAYER software was used to calculate the critical responses for evaluating the remaining life for all scenarios at 330th MN and 87th SG. The actual number of load repetitions per season is shown in Table 6-3. The remaining service lives for 330th MN and 87th SG for the three scenarios analyzed are presented in Table 6-17 and

Table 6-18.

Table 6-17 Allowable number of repetitions for the responses obtained from Tables 6.7 through 6.10.

Site	**Description**	**One Season**	**Estimated Remaining Service Life (years)**
330th MN	Total Design Traffic x10^{-3} (18-kip axle)	27.4	**8.5**
	N_f, HMA (millions)	5.3	
	Damage Ratio x 10^{-2}	0.52	
	N_d, Subgrade (millions)	0.23	
	Damage Ratio x 10^{-2}	11.83	
87th SG	Total Design Traffic x10^{-3} (18-kip axle)	10.25	**7.48**
	N_f, HMA	1.90	

	(millions)		
	Damage Ratio x 10^{-2}	0.54	
	N_d, Subgrade (millions)	0.08	
	Damage Ratio x 10^{-2}	13.37	

Table 6-18 Allowable number of repetitions for responses obtained from Tables 6.11 through 6.16.

Site	**Description**	**Seasons 1**	**Seasons 2**	**Seasons 3**	**Sum**	**Estimated Remaining Service Life (years)**
330th MN	Total Design Traffic x10^{-3} (18-kip axle)	8.44	12.66	6.33	27.43	**18.6**
	N_f, HMA (millions)	0.74	0.62	0.98	2.34	
	Damage Ratio x 10^{-2}	1.14	2.03	0.65	3.82	
	N_d, Subgrade (millions)	0.38	0.56	0.69	1.63	
	Damage Ratio x 10^{-2}	2.2	2.26	0.92	5.38	
87th SG	Total Design Traffic x10^{-3} (18-kip axle)	3.15	4.73	2.37	10.25	**56.39**
	N_f, HMA (millions)	2.45	2.51	2.99	7.95	
	Damage Ratio x 10^{-2}	0.13	0.19	0.08	0.40	
	N_d, Subgrade (millions)	0.38	0.79	0.69	1.86	
	Damage Ratio x 10^{-2}	0.83	0.60	0.04	1.77	

The estimated remaining lives presented in

Table 6-18 are based on the subgrade moduli backcalculated from the FWD data respectively. Considering the estimated remaining life, for 330th MN, presented in

Table 6-18 and the current age of the project, the pavement appears to be designed for a period of 20 years. This finding is similar to a study performed by Hossain et al. (1992) that demonstrated that the FWD testing is a viable choice for estimating the remaining service life. However, the remaining service life for 87th SG appears to be overestimated due to the relatively high modulus backcalculated for the subgrade at that site. This should be considered as a limited conclusion since the remaining service life for asphalt pavements can also be impacted by other environmental factors or failures related to the performance of the pavement materials that are unknown to us at the evaluated sites.

CHAPTER 7 CONCLUSIONS AND RECOMMENDATIONS

7.1 CONCLUSIONS

This study introduced a laboratory procedure to simulate the microcracking process adopted in the field for cement-modified soil (CMS) subgrade. The procedure utilized laboratory reconstituted unconfined compression (UC) test specimens, which were preloaded to different stress levels as compared with the unconfined compressive strength. It was found that when the preloading stress level was lower than the unconfined compressive strength, no microcrack was generated and their compressive strengths were not degraded. To microcrack CMS in the laboratory, this study found that the preloading stress level must be equal to the unconfined compressive strength of the CMS

specimen. The CMS specimens right after microcracking had UC strengths of approximately 50% of those before microcracking and moduli of approximately 42% of those before microcracking. However, the specimens microcracked after a 48-hour curing period had 70% of the strength of the un-cracked specimens at the same curing period and their moduli was approximately 150% of the moduli of the un-cracked specimens. Also, based on the UC strength observations of the 330th MN and 87th SG materials, it was clear that the average 7-day UC strength of the microcracked specimens was similar to the UC of the un-cracked specimens cured for 48 hours. The microcracked specimens had a modulus to strength ratio approximately two times the un-cracked specimens. Based on the finding from this research, it is recommended that to achieve a representative microcracking process in the laboratory, loading of a CMS specimen (cured for 48 hours) should continue past the peak compressive strength by less than 0.1% axial strain and then the load should be released to zero. After microcracking, the specimens should be returned to the curing room for further curing to a desired curing period.

Furthermore, the microcracking effects on the hydraulic conductivity and electrical resistivity were evaluated. The laboratory results of the reconstituted specimen from 330th MN site showed that microcracking increased the hydraulic conductivity of the specimen and reduced its electrical resistivity when the specimen was saturated. However, at a saturation degree of less than 100, microcracking increased the specimen electrical resistivity.

Light Weight Deflectometer (LWD) tests were conducted in the field before the subgrade mixed with cement, after mixed with cement, and after microcracking. The LWD results showed that adding cement increased the subgrade modulus. However, after applying three passes of roller compaction to generate the micro-cracks, the subgrade modulus dropped to approximately 40% its original value on average.

In addition, resilient modulus (M_r) tests were conducted on the reconstituted specimens with and without micro-cracks. Also, the resilient modulus testing was performed on four cored specimens from 330th MN. Three formulae were used to describe the resilient moduli of the CMS in this study. In summary, the average M_r values of the microcracked specimens were slightly higher than those of the uncracked specimens. This is consistent with the finding on the effect of microcracking on specimens' moduli (E_{50}) calculated from the UC tests (i.e., under static loading). However, the resilient moduli of four samples cored from 330th MN were approximately 25 percent higher than those of the reconstituted samples in the laboratory when compared using the formulae proposed by Seed et al. (1967) and NCHRP (I-28A), and approximately 50 percent higher when compared using the formula proposed by Moossazadeh and Witczack (1981). It should be noted that the average UC strengths of the cored samples from 330th MN site were approximately 10 percent higher than those of the reconstituted samples in the laboratory. The resilient modulus specimens from 87th SG and 330 MN showed hardening behaviors based on all three formulae used in this research.

The average backcalculated moduli of the HMA layer at 330th MN were approximately 30% higher than those at 87th SG and the average backcalculated moduli of the CMS layer at 330th MN were approximately three times higher than those at 87th SG. However, the 7-day UC strengths for the reconstituted samples at 330th MN were only 50 percent higher than those at 87th SG. Also, the backcalculated subgrade modulus at 87th SG site was more than two times higher than that at 330th MN. Similar difference was also observed in the laboratory CBR tests performed for both sites.

The pavement critical responses obtained from KENLAYER for 87th SG and 330th MN were obtained using the performance prediction models recommended by the Asphalt Institute for

fatigue failure and permanent deformation. The predicted remaining service lives (RSL) for 330th MN and 87th SG were approximately 18.5 years and exceeding 20 years, respectively, when the CMS properties characterized in the laboratory and HMA and subgrade backcalculated moduli from the FWD were used.

7.2 RECOMMENDATIONS

Based on the observations from this study, the following recommendations for cement modified subgrade (CMS) with microcracking are made:

1. To achieve a representative microcracking process in the laboratory, it is recommended that loading of the reconstituted CMS specimen (cured for 48 hours) should continue past the peak compressive strength by less than 0.1% axial strain and then the load should be released to zero. The microcracked specimens should be returned to the moisture room for continuing curing.
2. Run UC tests on the uncracked and cracked CMS specimens after seven days of moist curing. Determine the UC strengths and moduli (E_{50}) for both un-cracked and microcracked specimens and calculate the percentage reduction of the modulus and the modulus to strength ratio.
3. The estimated modulus reduction from the laboratory can be used as a reference for the light weight deflectometer (LWD) tests to evaluate the modulus reduction of the subgrade required to achieve microcracking in field.
4. Non-destructive methods have become more acceptable and available techniques to evaluate the modulus of chemically stabilized materials in both the laboratory and the field. These techniques have the potential to provide reliable moduli of pavement materials

compared with traditional methods (e.g., resilient modulus testing) and can provide comparable results under similar conditions in the laboratory and the field. Future studies are recommended to further evaluate the resilient modulus of CMS in the laboratory. It is also important to have a field study to evaluate the performance of a pavement structure with CMS layer, by using non-destructive techniques in the fields, such as falling weight deflectometer (FWD) and surface analysis of seismic wave (SASW). A comparison between the laboratory and field results would be beneficial in this research area.

5. In addition, even though the microcracking technology applied on some cement modified soil under HMA pavements demonstrated its effectiveness through the field deflection testing and the backcalculated in-situ moduli, additional field and laboratory evaluations are needed to evaluate its impact on the change in the cement content, and to improve the reliability of the microcracking effect. Also, future studies could explore the possibilities of microcracking using dynamic axial loading at different confining pressures in the tri-axial cell.

DISCLAIMER

Neither the developers of this work nor the University of Kansas assume any legal liability or responsibility for the accuracy, completeness, or usefulness of any information, product or process disclosed in this dissertation.

REFERENCES

ASTM E2853 – 2015, Standard Test Methof for Measuring Deflections with a Light Weight Deflectometer (LWD)

Baltzer, S. and J. M. Jansen, 1994, Temperature Correction of Asphalt-Moduli for FWD Measurements, Proceedings of the Fourth International Conference on Bearing Capacity of Roads and Airfields, MN, Vol. 1, 753-760.

Baladi, G. Analysis of Pavement Distress Data, Pavement Distress Indices, and Remaining Service Life. An Advanced Course in Pavement Management Systems, FHWA, Boston, MA, 1991.

Baltzer, S., Ertman-Larsen, H. J., Lukanen, S., and Stubstad, R. N. (1994). “Prediction of Asphalt Concrete Material Temperatures for Routine Load Deflection Measurements.” Proceedings of 4th International Conference on the Bearing Capacity of Roads and Airfields, Univ. of Minnesota, Vol. 1, Minneapolis, MN, pp. 401-412.

Bofinger, H. (1971). "The Behaviour of Soil-Cement Pavements with Special Reference to the Problem of Cracking." Proc., 4th Asian Regional Conference on Soil Mechanics and Foundation Engineering, Bangkok, Thailand.

Bofinger, H., Hassan, H., and Williams, R. I. T. (1978). "The shrinkage of fine-grained soil-cement." TRRL Supplementary Report 398. Transport and Road Research Laboratory (TRRL), Crowthorne, England.

Brandl, H. (1999). Mixed in Place Stabilisation of Pavement Structures with Cement and Additives. Proc., 12th European Conference on Soil Mechanics and Geotechnical Engineering, Rotterdam, Netherlands.

Bruinsma, J. E., Vandenbossche, J.M., Chatti, K., and Smith, K.D., (2017) Using Falling Weight Deflectometer Data with Mechanistic Empirical Design and Analysis, Volume II: Case Study Reports, Final Report, Submitted to FHWA, Publication NO. FHWA-HRT-16-010 March 2017.

Chen, W. F., and Mizuno, E. (1990). "Non-linear Analysis in Soil Mechanics, Theory and Implementation." Developments in Geotechnical Engineering." Vol. 53, 1990.

Cockrell, C. F., Muter, R. B., Leonard, J. W, and Anderson, R. E. (1970). "Application of floatation for recovery of calcium constituents from limestone modified fly ash," West Virginia University, Coal Resource Bureau and School of Mines.

Das, B. M. (1990). "Principle of Foundation Engineering," PWS-KENT publishing company, Boston.

Deacon, J. A., 1969. "Load Equivalency in Flexible Pavements," Proceeding, Association of Asphalt PavingTechnologists, Vol. 38, pp. 465-491.

FHWA 2015, "Using Falling Weight Deflectometer Data with Mechanistic-Empirical Design Analysis, Volume I, Ch. 2, Overview of Pavement Deflection Testing". https://www.fhwa.dot.gov/publications/research/infrastructure/pavements/16009/002.cfm , accessed November 10, 2019.

FHWA 2019, "Geotechnical Aspects of Pavements Reference Manual" https://www.fhwa.dot.gov/engineering/geotech/pubs/05037/05c.cfm, accessed June 2019.

FWA, T. F. 2006. The handbook of highway engineering, 6000 Broken Sound Parkway NW, Suite 300 Boca Raton, FL 33487-2742, Taylor & Francis Group, LLC.

D.S. Gedafa, Comparison of Flexible Pavement Performance Using Kenlayer and HDM-4, Midwest Transportation Consortium, Ames, Iowa, 2006.

George, K.P. (1968). Shrinkage Characteristics of Soil Cement Mixtures. University of Mississippi.

George, K.P. (1968). Final Report on the Study of Criteria for Strength and Shrinkage Control of Cement-Treated Bases. University of Mississippi.

George, K.P. (1973). Mechanism of Shrinkage Cracking of Soil-Cement Bases. In Highway Research Record 442, HRB, National Research Council, Washington, D.C., pp. 1–10.

George, K. P. (1968). Cracking in Pavements Influenced by Visoelastic Properties of Soil-cement. Presented at the 48th Annual Meeting of the Highway Research Board, Washington, D.C.

George, K.P. (2001). Soil Stabilization Field Trial. FHWA/MS-DOT-RD-01-133, Interim Report I, the University of Mississipi.

Han, J. (2015). Principles and Practice of Ground Improvement, John Wiley and Sons, Hoboken, NJ.

Halsted, G.E., Luhr, D.R., Adaska, W.S. 2006. Guide to Cement-Treated Base (CTB). Portland Cement Association. Skokie, IL.

Hanifa et al. 2015, "Design Values o Resilient Modulus for Stabilized and Non-Stabilized Base", Louisiana Transportation Research Center, July 2015.

Hossain, M. and Scofield, L.A. (1992) “Correlation Between Backcalculated and Laboratory-Determined Asphalt Concrete Moduli.” Transportation Research Record 1377, p. 67–76. Transportation Research Board, Washington, DC.

HUANG, Y. H. 2004. "Pavement Analysis And Design", 2nd edition,USA, Pearson Education Inc.

Al-Khoury, R., A. Scarpas, and C. Kasbergen. Dynamic Interpretation of FWD Test Results. In Transportation Research Record 1716, 2000, pp.49-54.

Kim, Y.R., B. O. Hibbs and Y. C. Lee. Temperature Correction of Deflections and Back-calculated Asphalt Concrete Moduli. In Transportation Research Record 1473, 1995, pp.55-62.

LITTLE, D. & YUSUF, M. 2001. Example Problem Illustrating the Application of the National Lime Association Mixture Design and Testing Protocol (MDTP) to Ascertain Engineering Properties of Lime Treated Subgrades for Mechanistic Pavement Design/Analysis. The National Lime Association, Federal Highway Administration and the Mississippi Department of Transportation, FHWA/MS-DOT-RD-01-129.

Litzka, J., and Haslehner, W. (1995). "Cold in-place recycling on low-volume roads in Austria." Proc., 6th International Conference on Low Volume Roads, Minneapolis, Minn.

Loulizi, A., Al-Qadi, I. L., Lahouar, S., and Freeman, T. E. (2001). “Data Collection and Management of the Instrumented Smart Road Flexible Pavement Sections.” Presented at the Transportation Research Board 81st Annual Meetings Paper # 01-2668, Washington, D.C., pp. 1-27.

Lytton, R. L., (1989). “Backcalculation of Pavement Layer Properties”, ASTM Special Technical Publication 1026, American Society for Testing and Materials, Philadelphia, 7-38.

Marecos, V., Fontul, S., Solla, M., Ludes Antunes, M. (2018). " Transport Infrastructures Assessment Using Multiple GPR Configurations ad FWD" Matec Web of Conferences 211 - modified.

Mehrotra A., (2011). " Evaluating the Influence of Moisture Variation on Resilient Modulus for Unsaturated Pavement Subgrades" Master's Thesis at the Louisiana State University..

Muench, S.T., Mahoney, J.P., and Pierce, L.M., (2003). “The WSDOT Pavement Guide Interactive”, Washington Department of Transportation (WSDOT), Olympia, WA. Retrieved June 12, 2009, from WSDOT Official Web site: http://training.ce.washington.edu/WSDOT/.

Muhunthan, B. and Sariosseiri, F. (2008). “Interpretation of Geotechnical Properties of Cement Treated Soils,” RR. FHWA Contract DTFH61-05-00008, Washington State University, Pullman, WA.

NCHRP (2004). “Guide for Mechanistic-Empirical Design of New and Rehabilitated Pavement Structures,” March 2004.

Noureldin,A.S., K. Zhu, S. Li, and D. Harris. Network Pavement Evaluation with Falling- Weight Deflectometer and Ground-Penetrating Radar. In Transportation Research Record 1860, 2003, pp. 90-99.

O’FLAHERTY, C. 2002. "Highways: The Location, Design, Construction and Maintenance of Pavements". Butterworth-Heinemann, Oxford, United Kingdom.

Park, H.M., Y. R. Kim, and S. Park. Temperature Correction of Multiload-Level, Falling-Weight Deflectometer Deflections. In Transportation Research Record 1806, 2002, pp.3-8.

Portland Cement Association (PCA) (2003). "Reflective Cracking in Cement Stabilized Pavements." Soil-Cement Information. Skokie, Ill.

Rasul, J.M. (2015). "Permanent Deformation of Stabilized Subgrade Soils" Bituminous Mixtures & Pavements iV - Nikolaides (Ed.): Taylor & Francis Group, London, ISBN 978-1-138-02866-1.

Schaefer, R. Vernon, White, J. David, Ceylan, Halil, Stevens, J. Larry "Design Guide for Improved Quality f Roadway Subgrade and Subbases, Iowa State University (2008).

Scullion, T. (2002). "Precracking of soil-cement bases to reduce reflection cracking: field investigation." Transportation Research Record: Journal of the Transportation Research Board, Washington, D.C., No. 1787, 22-30.

Sebaaly, P.E., Schoener, P., Siddharthan, R., and Epps, J., "Implementation of Nevada's Overlay Design Procedure," in *Proceedings, 4th International Conference on the Bearing Capacity of Roads and Airfields,* University of Minnesota, 1994.

Sebesta, S. (2005). "Use of microcracking to reduce shrinkage cracking in cement-treated bases." Transportation research record, 1936(1), 2-11.

Seed, H., Mitry, F., Monosmith, C., and Chan, C (1967). Prediction of pavement deflection from laboratory repeated load tests, NCHRP report 35, Transportation Research Board 500 Fifth Street, NW, Washington, DC.

Terashi, M. (2002). Long-term Strength Gain vs. Deterioration of Soils Treated by Lime and Cement. Proceedings of Deep Mixing Workshop, The International Workshop of Deep Mixing. 39-57.

Theyse, H. L., M. De Beer, and F. C. Rust. 1996. Overview of South African Mechanistic Pavement Design Method. Transportation Research Record 1539: 6-17

Theyse, H. L., M. De Beer, J. Prozzi, and C. J. Semmelink. 1995. TRH4 Revision Updating the Transfer Functions for the South.

Thompson, M. R. 1970. Quantitative Characterization of Cyclic Freezing and Thawing in Stabilized Pavement Materials. Highway Research Record.

Toohey M., N, Moonry A. M., Bearce G., R. " Relationship between Resilient Modulus and Unconfined Compressive Strength for Lime-Stabilized Soils. : ASCE Journal of Geotechnical and Geoenvironmental Engineering / Volume 139 Issue 11, Nov. 2013.

TUTUMLUER, E. & KIM, M. Considerations for nonlinear analyses of pavement foundation geomaterials in the finite element modeling of flexible pavements. Symposium on the Mechanics of Flexible Pavements, 2007.

Uhlmeyer, J.S., Mahoney, J.P., Hanek, G., Wang, G., Copstead, R.L., and Janssen, D.J., *Estimation of Seasonal Effects for Pavement Design and Performance—Volume 1*,Report No. FHWA-FLP-95-006, Federal Highway Administration, Washington, DC, August 1996.

ULLIDTZ, P. 1987. "Pavement Analysis. Developments in Civil Engineering", 19.

Ullidtz P., and Coetzee, N.F. (1995) “Analytical Procedures in Nondestructive Testing Pavement Evaluation.” Transportation Research Record 1482, National Research Council, Washington, D.C., pp.61-66.

US Army Engineer School (1992). “Military Soils Engineering,” Field Manual 5-410, Chapter 9, Soil Stabilization for Roads and Airfields, Department of the Army, Washington, DC, Dec. 23, 1992 http://faculty.unlv.edu/mjnicho/military_soils_fm5_410.pdf, Accessed November, 2012

Vanapalli, S. K., Fredlund, D. G., & Pufahl, D. E. (1999). The influence of soil structure and stress history on the soil–water characteristics of a compacted till.Geotechnique, 49(2), 143-159.

Von Quintus, H. L., J. Mallela, and J. Jiang. 2005. Expected Service Life and Performance Characteristics of HMA Pavements in LTPP. Asphalt Pavement Alliance (February).

Wenner, F. (1915). “A Method of Measuring Earth Resistivity”, Scientific Papers of the Bureau of Standards No. 258, October 11, Department of Commerce, Washington, DC

Wilson, William Herbert Jr. 2013. Strength Assessment of Soil Cement. Master's Thesis, Auburn University.

Wu, Z., Chen, X., & Yang, X. 2011. Finite Element Simulation of Structural Performance on Flexible Pavements with Stabilized Base/Treated Subbase Materials under Accelerated Loading (No.FHWA/LA. 10/452). Louisiana Transportation Research Center.

Wooten, L. and Foreman, B. (2005). Deep Soil Mixing for Seismic Remediation of the Clemson Upper and Lower Diversion Dams. Presented at the 25th USSD Annual Meeting and Conference.

Zhong, W., Yilong L. and Ferdous, I. (2018). "Minimizing SHrinkage Cracking in Cement-Stabilized Bases through Micro-Cracking"

APPENDICES

Appendix A Properties of Cement

ASH GROVE CEMENT COMPANY

1801 North Santa Fe
P.O. Box 519
Chanute, KS 66720
Phone: 620-433-3500
Fax: 620-431-3282

LOT # 2682

Type I/II (Low Alkali)

Production Period: July 1 thru July 31, 2017

Date: 8/17/2017

The following information is based on average test data during the production period. The data is typical of cement shipped from the Chanute, Kansas plant. Individual shipments may vary.

STANDARD REQUIREMENTS
ASTM C150/C150M-16, Tables 1 and 3

CHEMICAL

Item	A.S.T.M. Test Method	Spec. Limit	Test Result
SiO_2 (%)	C114	*A*	20.85
Al_2O_3 (%)	C114	6.0 max	4.18
Fe_2O_3 (%)	C114	6.0 max	3.07
CaO (%)	C114	*A*	64.41
MgO (%)	C114	6.0 max	2.13
SO_3 (%)	C114	3.0 max	2.91
Loss on ignition (%)	C114	3.5 max	2.24
Na_2O (%)	C114	*A*	0.20
K_2O (%)	C114	*A*	0.51
Insoluble Residue (%)	C114	1.5 max	0.42
CO_2 (%)	C114	*A*	1.64
Limestone (%)	C114	5.0 max	4.2
$CaCO_3$ in limestone (%)	C114	70 min	89.82
Potential compounds (%)[D]			
C_3S	C114	*A*	57
C_2S	C114	*A*	17
C_3A	C114	8.0 max	6
C_4AF	C114	*A*	9
$C_3S + 4.75\ C_3A$	C114	100 max	86

PHYSICAL

Item	A.S.T.M. Test Method	Spec. Limit	Test Result
Air content of mortar (volume %)	C185	12 max	7
Fineness (cm^2/g):			
Air permeability	C204	2600 min	3869
Autoclave expansion (%)	C151	0.80 max	0.01
Compressive strength (psi)			
1 Day	C109	*A*	2308
3 Days	C109	1740 min	3811
7 Days	C109	2760 min	4632
Time of setting (minutes) (Vicat)			
Initial: Not less than	C191	45	127
Not more than		375	127
Mortar Bar Expansion	C1038	*E, B*	0.006
Specific Gravity	C188	*A*	3.11

OPTIONAL REQUIREMENTS
ASTM C150/C150M-16, Tables 2 and 4

CHEMICAL

Item	A.S.T.M. Test Method	Spec. Limit	Test Result
$C_3S + C_3A$ (%)	C114	*A*	
Equivalent alkalies (%)	C114	0.60	0.54

PHYSICAL

Item	A.S.T.M. Test Method	Spec. Limit	Test Result
False set (%)	C451	*B*	85
Heat of hydration (kJ /kg)			
7 days	C186	*A*	

A = Not applicable.
B = Test result provided for information only.
C = Test results for this period not available.
D = Adjusted per Annex A1.6 M85
E = Required only if the SO_3 exceeds 3.0, in which case the expansion shall not exceed 0.020% at 14 days.

We certify that the above described cement, at the time of shipment, meets the chemical and physical requirements of ASTM C150/C150M-12 (Types I/II) and AASHTO M85-12 (Type I/II), or (other)_____specification.

Signature: Marc D. Melton

Marc D. Melton
Title: Chief Chemist

Figure A-1 Cement properties used in CMS at 330th MN.

ASH GROVE CEMENT COMPANY

1801 North Santa Fe
P.O. Box 519
Chanute, KS 66720
Phone: 620-433-3500
Fax: 620-431-3282

Type I/II (Low Alkali)

Production Period: July 1 thru July 31, 2017

Date: 8/17/2017

The following information is based on average test data during the production period. The data is typical of cement shipped from the Chanute, Kansas plant. Individual shipments may vary.

Additional Data

Inorganic Processing Addition Data	
Type	Limestone
Amount(%)	4.16
SiO_2 (%)	5.03
Al_2O_3 (%)	1.47
Fe_2O_3 (%)	1.2
CaO (%)	48.5
SO_3 (%)	0.06

Base Cement Phase Composition	
C_3S	59
C_2S	17
C_3A	6
C_4AF	10

Signature:

Marc D. Melton
Title: Chief Chemist

Figure A-1 Cement properties used in CMS at 330th MN (Continued).

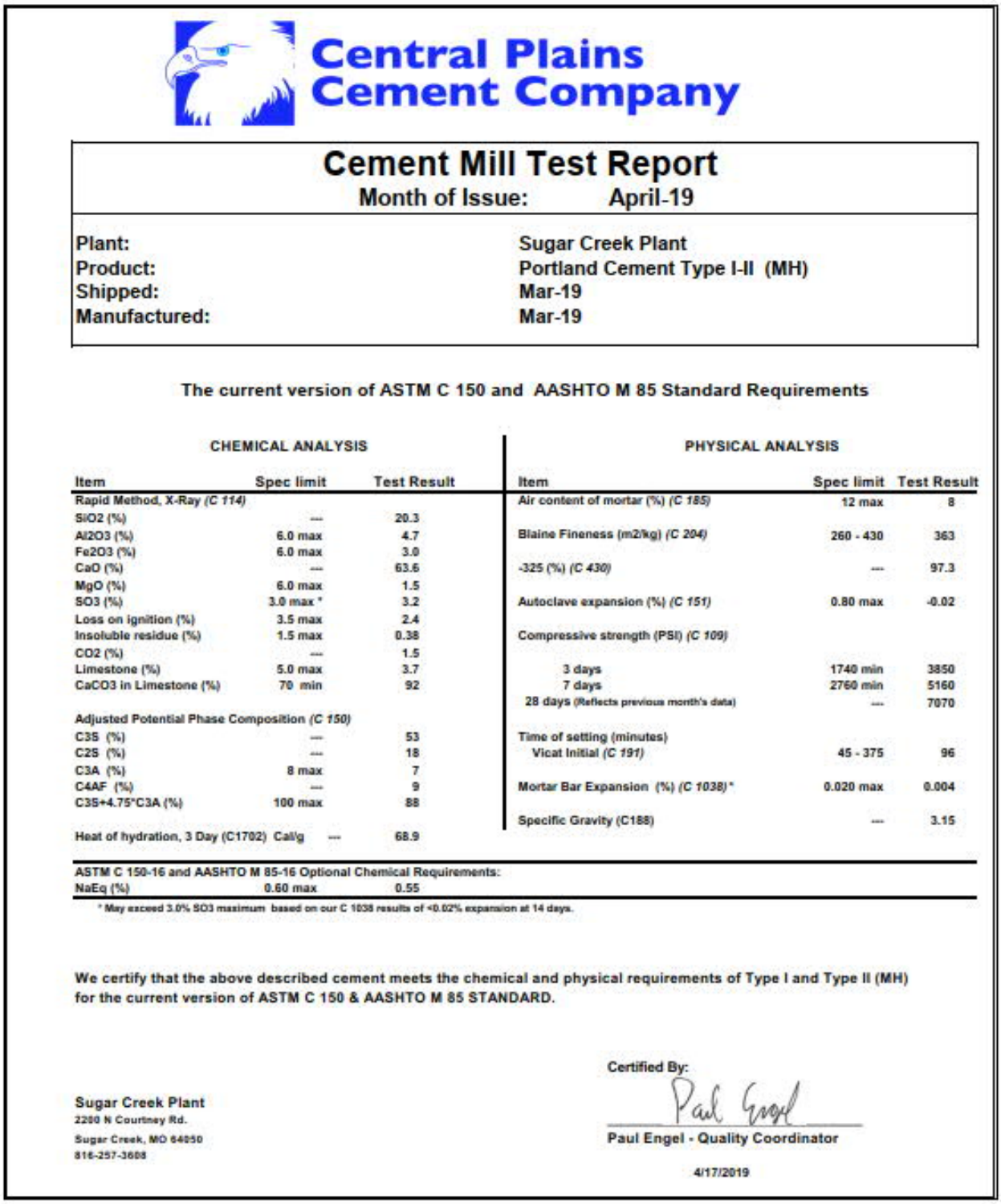

Central Plains Cement Company

Cement Mill Test Report

Month of Issue: April-19

Plant:	**Sugar Creek Plant**
Product:	**Portland Cement Type I-II (MH)**
Shipped:	**Mar-19**
Manufactured:	**Mar-19**

The current version of ASTM C 150 and AASHTO M 85 Standard Requirements

CHEMICAL ANALYSIS

Item	Spec limit	Test Result
Rapid Method, X-Ray *(C 114)*		
SiO2 (%)	---	20.3
Al2O3 (%)	6.0 max	4.7
Fe2O3 (%)	6.0 max	3.0
CaO (%)	---	63.6
MgO (%)	6.0 max	1.5
SO3 (%)	3.0 max *	3.2
Loss on ignition (%)	3.5 max	2.4
Insoluble residue (%)	1.5 max	0.38
CO2 (%)	---	1.5
Limestone (%)	5.0 max	3.7
CaCO3 in Limestone (%)	70 min	92
Adjusted Potential Phase Composition *(C 150)*		
C3S (%)	---	53
C2S (%)	---	18
C3A (%)	8 max	7
C4AF (%)	---	9
C3S+4.75*C3A (%)	100 max	88
Heat of hydration, 3 Day (C1702) Cal/g	---	68.9

PHYSICAL ANALYSIS

Item	Spec limit	Test Result
Air content of mortar (%) *(C 185)*	12 max	8
Blaine Fineness (m2/kg) *(C 204)*	260 - 430	363
-325 (%) *(C 430)*	---	97.3
Autoclave expansion (%) *(C 151)*	0.80 max	-0.02
Compressive strength (PSI) *(C 109)*		
3 days	1740 min	3850
7 days	2760 min	5160
28 days (Reflects previous month's data)	---	7070
Time of setting (minutes)		
Vicat Initial *(C 191)*	45 - 375	96
Mortar Bar Expansion (%) *(C 1038)* *	0.020 max	0.004
Specific Gravity (C188)	---	3.15

ASTM C 150-16 and AASHTO M 85-16 Optional Chemical Requirements:		
NaEq (%)	0.60 max	0.55

* May exceed 3.0% SO3 maximum based on our C 1038 results of <0.02% expansion at 14 days.

We certify that the above described cement meets the chemical and physical requirements of Type I and Type II (MH) for the current version of ASTM C 150 & AASHTO M 85 STANDARD.

Certified By:

Paul Engel - Quality Coordinator

4/17/2019

Sugar Creek Plant
2200 N Courtney Rd.
Sugar Creek, MO 64050
816-257-3608

Figure A-2 Cement properties used in CMS at 87th SG.

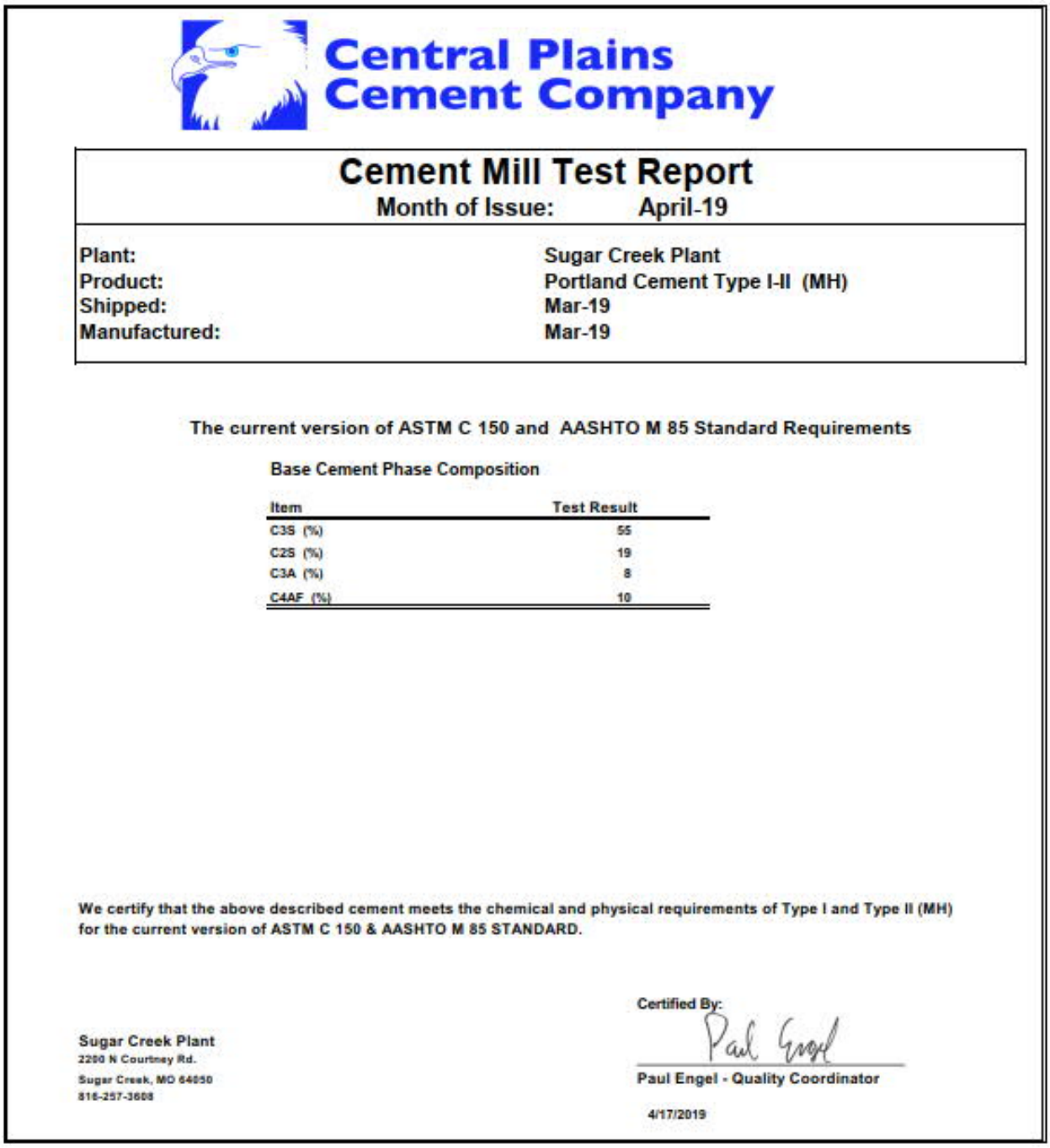

Central Plains Cement Company

Cement Mill Test Report

Month of Issue: April-19

Plant:	**Sugar Creek Plant**
Product:	**Portland Cement Type I-II (MH)**
Shipped:	**Mar-19**
Manufactured:	**Mar-19**

The current version of ASTM C 150 and AASHTO M 85 Standard Requirements

Base Cement Phase Composition

Item	Test Result
C3S (%)	55
C2S (%)	19
C3A (%)	8
C4AF (%)	10

We certify that the above described cement meets the chemical and physical requirements of Type I and Type II (MH) for the current version of ASTM C 150 & AASHTO M 85 STANDARD.

Certified By:

Paul Engel

Paul Engel - Quality Coordinator

4/17/2019

Sugar Creek Plant
2200 N Courtney Rd.
Sugar Creek, MO 64050
816-257-3608

Figure A-2 Cement properties used in CMS at 87th SG (Continued).

Appendix B Additional Figures Related to Chapter 4

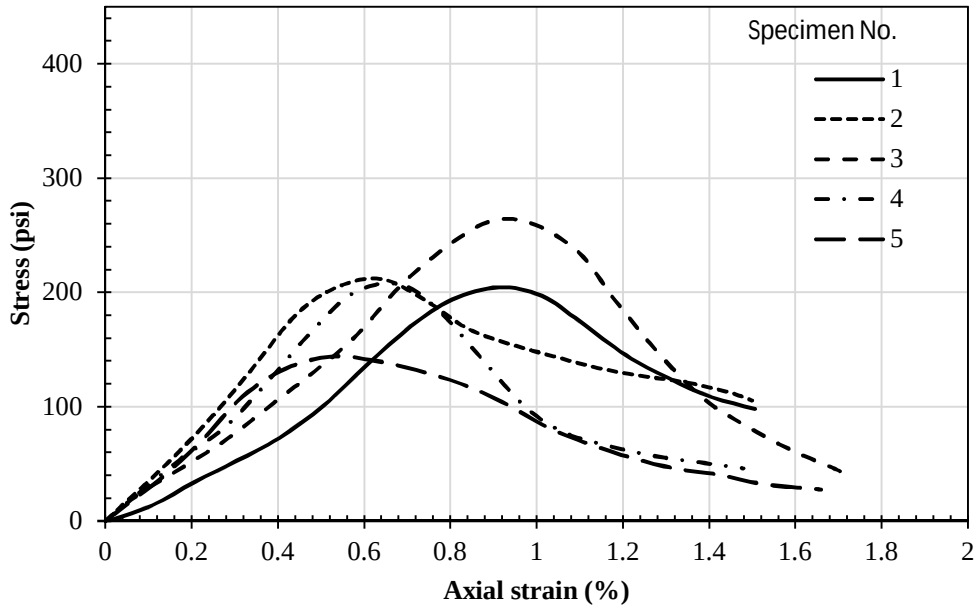

(a)

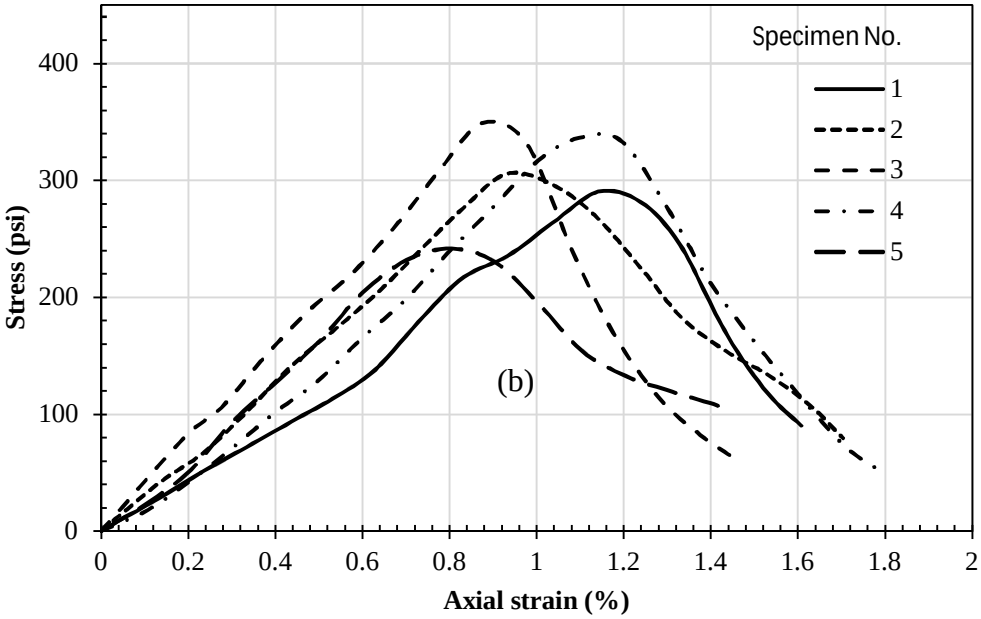

(b)

Figure B-1 Stress-strain curves of CMS specimens of 330th MN after seven-day curing at cement contents: (a) 3.5%, (b) 5.0%, and (c) 6.5%.

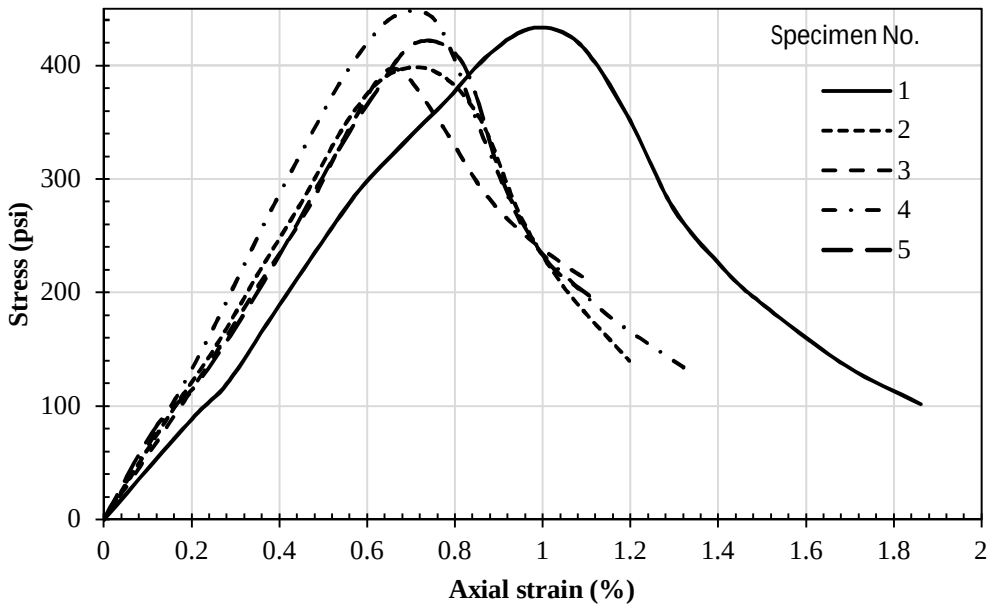

(c)

Figure B-1 Stress-strain curves of CMS specimens of 330th MN after seven-day curing at cement contents: (a) 3.5%, (b) 5.0%, and (c) 6.5% (Continued).

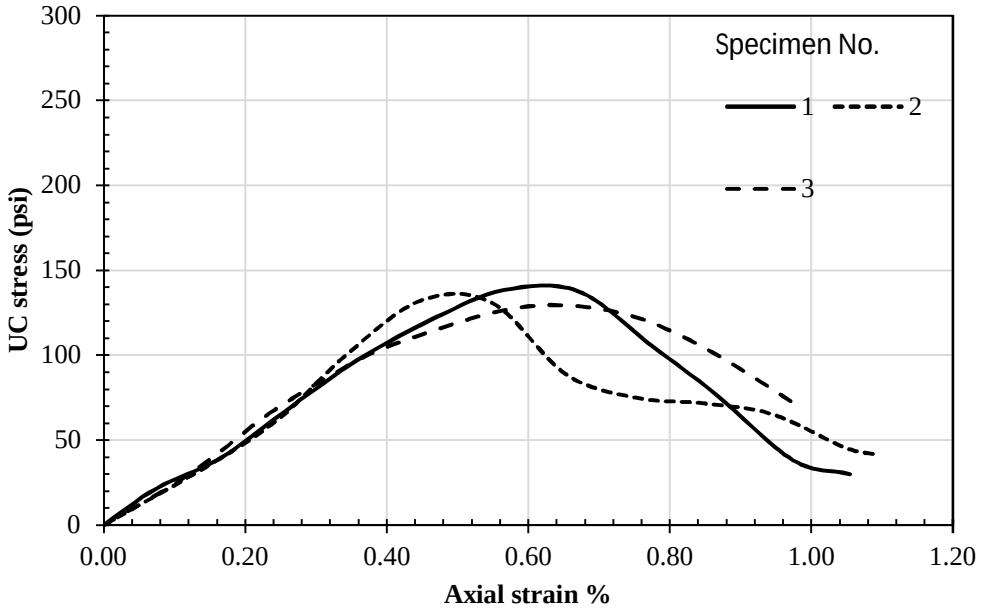

(a)

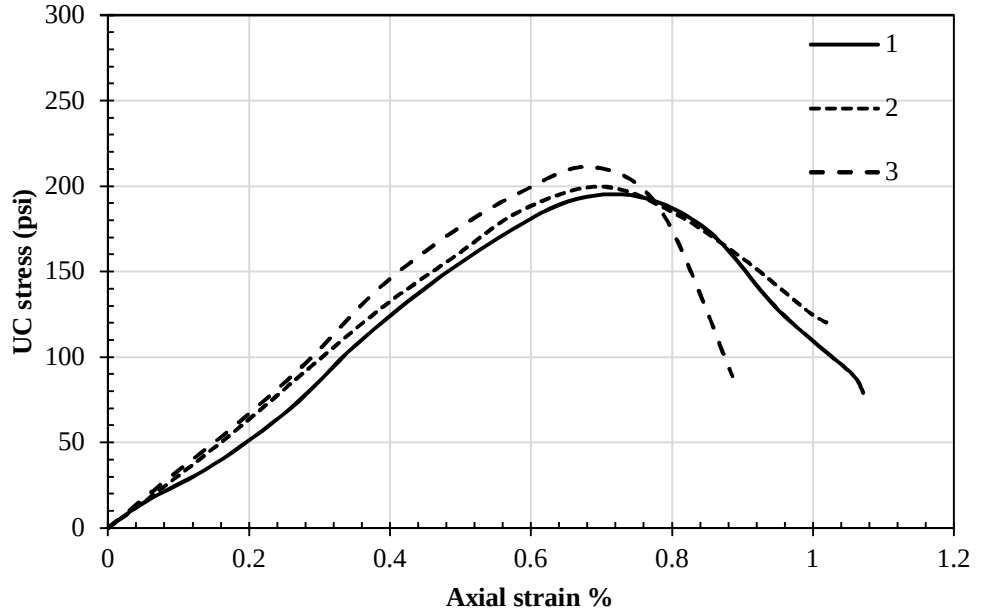

(b)

Figure B-2 Stress-strain curves of CMS specimens of 87th SG after seven-day curing at cement contents: (a) 4.0%, (b) 5.5%, and (c) 7.0%.

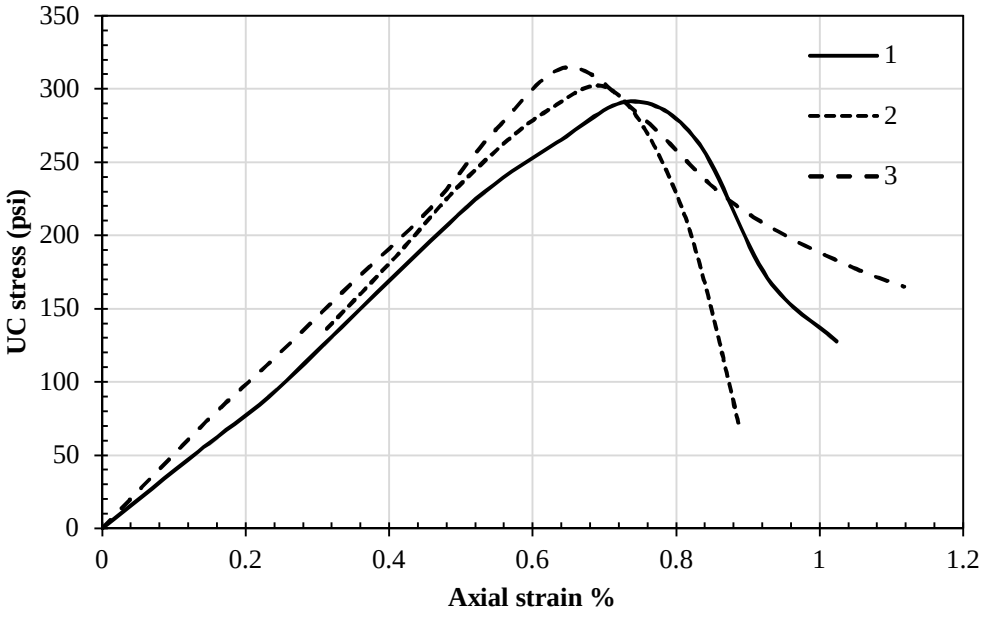

(c)

Figure B-2 Stress-strain curves of CMS specimens of 87th SG after seven-day curing at cement contents: (a) 4.0%, (b) 5.5%, and (c) 7.0% (Continued).

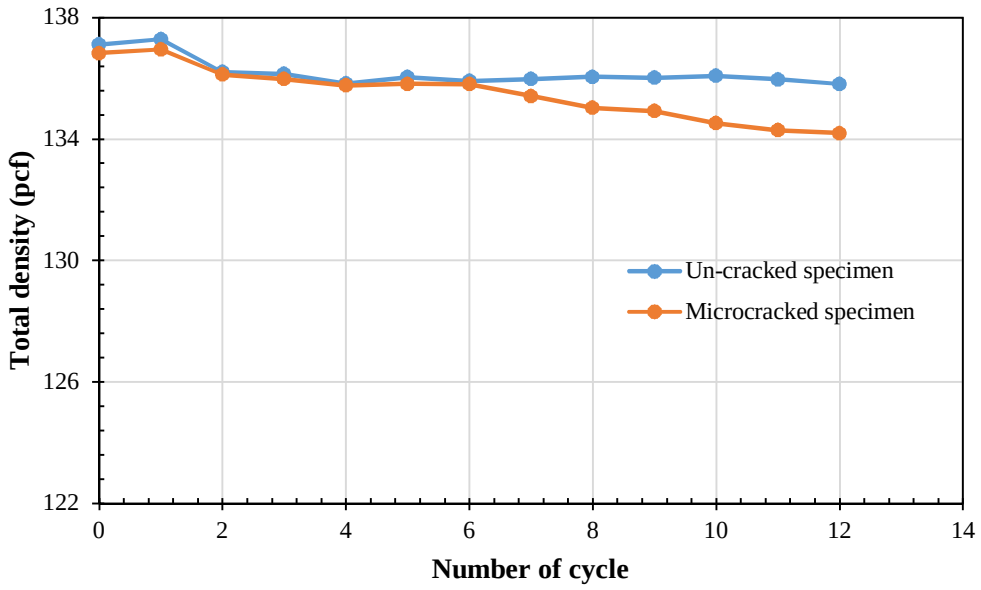

(a)

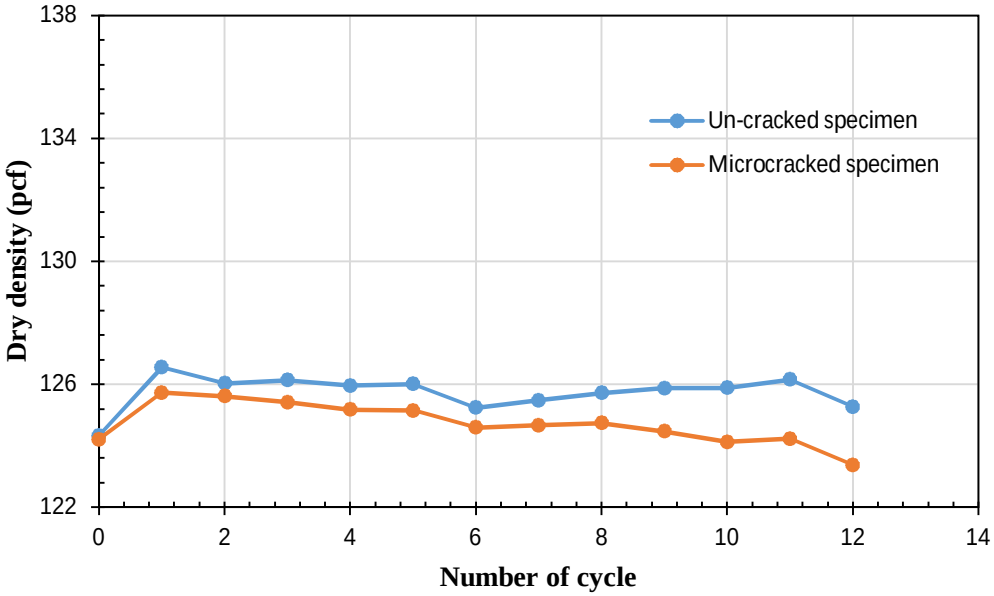

(b)

Figure B-3 Density variation during the wet-dry cycles (a) total density after wet cycles and (b) dry density after dry cycles.

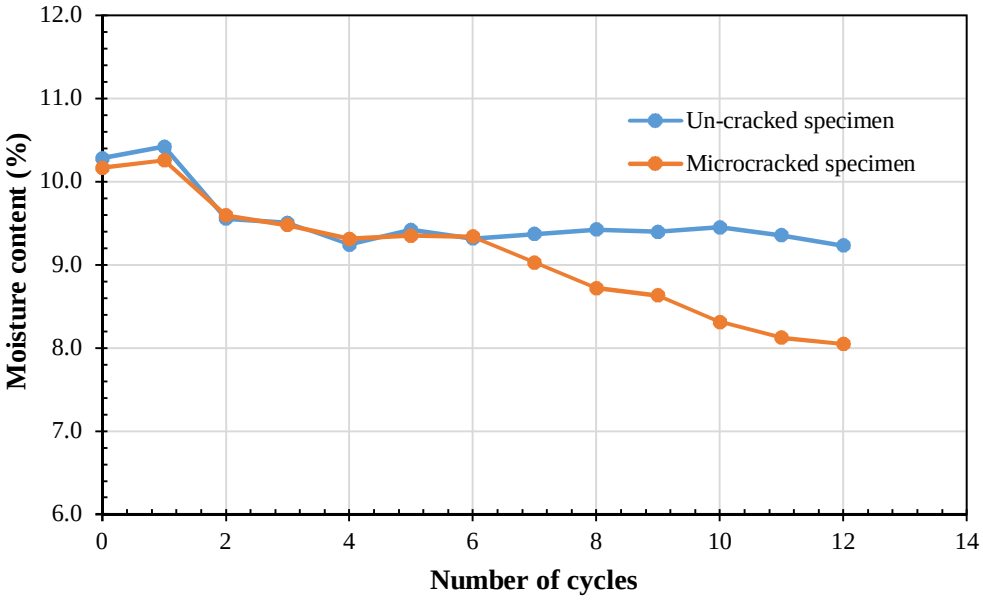

Figure B-4 Moisture variation after wet cycles.

Appendix C Data Related to Chapter 5

Table C-1 FWD testing data for 87th SG.

87th SG												
Test No.	**Eastbound**						**Westbound**					
	Station (ft)	D_1 (Mils)	D_1@ 9kips (Mils)	Air Temp. (◦F)	Surface Temp. (◦F)	AC Temp. (◦F)	Station (ft)	D_1 (Mils)	D_1@ 9kips (Mils)	Air Temp. (◦F)	Surface Temp. (◦F)	AC Temp. (◦F)
1	2+01	5.81	5.83	62	65	61.5	0+81	8.12	8.03	53	63	61.7
2	4+01	7.30	7.37	62	59	60.7	1+80	6.39	6.32	53	64	62.5
3	4+01	5.27	5.38	63	64	56.8	2+80	4.01	3.89	52	62	60.8
4	5+00	8.26	8.16	62	63	60.0	3+79	5.68	5.56	52	61	60.0
5	6+00	7.73	7.84	61	61	58.4	4+80	7.41	7.22	52	63	61.7
6	7+01	5.29	5.30	60	63	60.0	5+80	9.25	9.10	52	63	61.7
7	8+00	12.30	12.69	60	62	59.2	6+80	7.54	7.45	52	62	60.8
8	9+00	5.75	5.94	60	65	61.5	7+79	7.93	7.81	53	63	61.7
9	10+00	12.20	12.56	61	60	57.6	8+79	7.44	7.35	51	63	61.1
10	12+00	5.72	5.99	55	57	55.8	9+80	10.82	10.68	51	62	60.3
11	13+00	11.68	12.36	53	61	59.0	10+80	9.66	9.49	52	58	57.0
12	13+99	9.29	9.99	55	61	59.0	11+80	10.90	10.91	51	63	61.1
13	14+00	5.41	5.75	53	60	58.2	12+79	9.78	9.67	52	62	60.3
14	15+01	4.95	5.03	54	61	59.0	13+80	11.98	12.15	51	62	60.3
15	15+99	6.86	7.16	55	6	14.9	14+80	5.85	5.78	52	61	59.5
16	17+00	5.70	5.91	55	60	58.2	15+80	7.67	7.48	52	63	61.1
17	18+00	5.52	5.68	56	63	60.6	16+80	6.64	6.56	52	60	58.6
18	20+00	8.34	8.71	53	60	58.2	17+80	7.71	7.47	52	64	61.9
19	20+00	4.96	5.09	54	60	58.2	18+79	6.58	6.46	52	60	58.6
20	21+00	9.71	9.27	54	60	57.4	19+80	15.96	16.02	53	61	59.5
21	21+00	36.83	36.78	53	59	58.2	20+79	26.04	27.05	53	62	60.3
22	22+00	11.80	11.44	56	61	59.0	21+79	14.89	15.09	53	62	60.3
23	23+00	8.18	7.98	55	62	59.8	22+80	7.48	7.37	53	61	59.5
24	25+00	19.52	19.61	56	61	60.6	23+80	9.61	9.46	52	63	61.1
25	25+00	12.89	12.95	54	63	59.0	24+80	11.47	11.33	52	63	61.1
26	27+00	21.82	22.29	55	63	59.8	25+80	5.99	5.80	54	62	60.3
27	27+00	9.60	9.32	56	62	60.6	26+80	6.01	5.94	54	61	59.5
28	28+01	10.34	10.17	55	61	59.0	27+81	7.04	6.86	52	63	61.1
29	29+00	33.65	35.51	56	62	59.8	28+80	6.15	5.93	53	60	58.6
30	30+01	8.70	8.50	55	64	61.4	29+80	13.85	13.75	53	63	61.1
31	31+00	12.82	12.77	54	63	60.6	30+80	7.12	6.88	53	64	61.9
32	32+00	6.38	6.24	56	61	59.0	31+79	12.15	12.13	51	63	61.1
33	33+00	9.67	9.63	55	61	59.0	32+80	8.94	8.79	52	60	58.6

Table C-1 FWD testing data for 87th SG (Continued).

87th SG												
Test No.	**Eastbound**						**Westbound**					
	Station (ft)	D_1 (Mils)	D_1@ 9kips (Mils)	Air Temp. (◦F)	Surface Temp. (◦F)	AC Temp. (◦F)	Station (ft)	D_1 (Mils)	D_1@ 9kips (Mils)	Air Temp. (◦F)	Surface Temp. (◦F)	AC Temp. (◦F)
34	34+01	7.36	7.34	55	61	59.0	33+80	6.19	5.99	53	61	59.5
35	35+00	7.81	7.79	55	65	62.7	34+80	9.09	8.81	54	61	59.5
36	36+00	7.23	7.27	53	64	61.9	35+80	21.55	21.65	53	65	62.7
37	37+01	16.51	16.63	53	64	61.9	36+80	12.39	12.38	54	65	62.7
38	38+00	7.13	6.92	56	62	60.3	37+79	8.95	8.81	53	65	62.7
39	39+00	11.73	11.71	52	64	61.9	38+80	11.15	10.94	53	64	61.9
40	40+01	10.50	10.45	53	63	61.1	39+79	9.66	9.41	53	64	61.9
41	41+00	12.03	12.09	55	62	60.3	40+80	13.09	12.82	53	64	61.9
42	42+00	11.51	11.48	53	64	61.9	41+79	11.64	11.54	52	64	61.9
43	43+00	14.07	13.85	53	65	62.7	42+79	10.76	10.52	52	64	61.9
44	44+02	10.02	10.13	53	64	61.9	43+80	12.97	13.04	52	65	62.7
45	44+99	11.64	11.74	54	64	61.9	44+80	10.31	10.07	53	64	61.9
46	46+00	11.80	11.89	53	65	62.7	45+80	11.60	11.57	52	65	62.7
47	47+01	10.90	10.82	54	65	62.7	46+80	13.20	13.07	53	65	62.7
48	48+00	15.76	15.75	54	65	62.7	47+80	13.19	13.19	54	65	62.7
49	49+01	15.92	16.24	54	65	62.7	48+78	17.33	17.54	56	65	62.7
50	50+03	16.20	16.30	53	64	61.9	49+79	16.00	16.01	54	64	61.9
51	51+02	8.45	8.36	53	64	61.9	50+79	15.52	15.43	56	64	61.9
52							51+79	9.07	9.01	54	66	63.5
Average		10.9	11.0	55.5	61.2	59.2		10.3	10.3	52.7	62.8	61.0
St dev		6.3	6.41	2.9	8.1	6.6		4.1	4.3	1.1	1.7	1.4
COV		57.5	58.2	5.2	13.2	11.1		40.1	41.8	2.0	2.7	2.3

Table C-2 FWD testing data for 330th MN.

330th MN												
Test No.	EB						WB					
	Station (ft)	D_1 (Mils)	D_1@ 9kips (Mils)	Air Temp. (◦F)	Surface Temp. (◦F)	AC Temp. (◦F)	Station (ft)	D_1 (Mils)	D_1@ 9kips (Mils)	Air Temp. (◦F)	Surface Temp. (◦F)	AC Temp. (◦F)
1	1+01	5.98	6.09	38	50	50.2	0+80	3.25	3.35	39	54	54.0
2	2+00	3.02	3.07	39	49	49.5	1+80	2.97	2.97	39	54	54.0
3	3+00	3.76	3.83	40	50	50.2	2+81	2.85	2.85	40	53	53.3
4	4+01	2.47	2.50	40	51	50.9	3+80	3.86	3.84	39	52	52.5
5	5+00	3.53	3.58	41	50	50.2	4+80	5.13	5.07	40	54	54.0
6	6+00	6.06	6.07	48	50	50.3	5+79	6.13	6.10	40	54	54.0
7	7+00	3.77	3.82	47	53	52.5	6+80	5.40	5.40	38	54	54.0
8	8+00	5.13	5.16	42	51	51.1	7+79	5.01	5.01	38	53	53.3
9	9+00	5.23	5.29	39	50	50.3	8+80	4.67	4.69	38	53	53.3
10	10+00	5.39	5.37	38	49	49.6	9+80	6.25	6.24	38	43	45.9
11	11+00	5.49	5.45	40	50	50.3	10+80	5.02	4.98	38	54	54.0
12	12+00	5.28	5.30	40	50	50.3	11+80	5.82	5.76	38	53	53.3
13	13+00	4.91	4.94	39	50	50.3	12+80	6.53	6.53	39	53	53.3
14	14+00	6.94	6.92	40	51	51.1	13+80	6.91	6.91	38	52	52.5
15	15+01	5.75	5.73	39	50	50.3	14+80	6.43	6.42	39	53	53.3
16	16+00	5.60	5.62	38	50	50.3	15+79	4.94	4.89	39	54	54.0
17	17+00	4.28	4.26	40	50	50.3	16+80	4.88	4.83	38	54	54.0
18	18+03	5.64	5.74	39	50	50.3	17+80	4.81	4.76	38	53	53.3
19	19+00	5.18	5.48	37	50	50.3	18+79	7.20	7.20	38	54	54.0
20	20+00	5.32	5.35	39	51	51.1	19+80	7.01	6.98	39	54	53.5
21	21+00	5.16	5.18	39	51	51.1	20+80	5.05	4.91	38	54	53.5
22	22+00	5.51	5.58	39	51	51.1	21+79	5.10	5.05	38	54	53.5
23	23+00	6.76	6.90	40	52	51.8	22+80	7.05	6.97	39	54	53.5
24	24+00	6.61	6.74	42	50	50.3	23+80	4.63	4.59	38	54	53.5
25	25+00	5.58	5.72	42	52	51.8	24+80	5.74	5.63	38	55	54.2
26	26+00	5.08	5.27	39	51	51.1	25+80	4.90	4.86	39	55	54.2
27	27+00	6.17	6.42	40	50	50.3	26+80	6.60	6.55	39	54	53.5
28	28+00	6.45	6.70	40	49	49.6	27+80	5.10	5.06	39	54	53.5
29	29+00	5.28	5.51	38	49	49.6	28+80	8.10	8.11	37	53	52.8
30	30+00	5.85	6.00	40	49	49.6	29+80	7.27	7.27	39	53	52.8
31	31+00	5.63	5.88	38	48	48.9	30+81	5.52	5.53	38	53	52.8
32	32+00	7.19	7.52	40	49	49.6	31+80	6.98	7.07	39	54	53.5
33	33+00	5.32	5.51	40	50	50.6	32+80	6.09	6.04	39	53	52.8

Table C-2 FWD testing data for 330th MN (Continued).

330th MN												
Test No.	**EB**						**WB**					
	Station (ft)	D_1 (Mils)	Station (ft)	D_1 (Mils)	Station (ft)	D_1 (Mils)	Station (ft)	D_1 (Mils)	Station (ft)	D_1 (Mils)	Station (ft)	D_1 (Mils)
34	34+00	5.01	5.19	40	50	49.9	33+80	5.15	5.18	38	53	52.8
35	35+00	6.07	6.22	40	49	50.6	34+80	4.01	3.99	38	53	52.8
36	36+00	3.87	3.99	39	49	49.9	35+80	6.02	6.05	37	52	52.1
37	37+01	5.97	6.19	40	51	51.3	36+80	5.33	5.31	37	53	52.8
38	38+02	4.86	4.98	40	52	52.1	37+79	6.17	6.18	38	53	52.8
39	39+01	4.90	5.13	41	52	52.1	38+80	5.32	5.33	38	53	52.8
40	40+00	6.75	6.97	41	51	51.3	39+80	7.87	7.92	37	52	52.1
41	41+00	7.34	7.61	40	51	51.3	40+80	7.89	7.91	37	53	52.8
42	42+00	5.55	5.72	40	51	51.3	41+80	5.62	5.62	38	52	52.1
43	43+01	4.53	4.67	40	53	52.8	42+80	5.58	5.50	37	53	52.8
44	44+01	5.02	5.21	41	52	52.1	43+80	6.89	6.84	38	52	52.1
45	45+01	6.63	6.96	41	53	52.8	44+80	14.88	15.02	38	53	52.8
46	46+02	14.50	15.53	42	52	52.1	45+79	7.90	7.91	39	53	52.8
47	47+00	5.86	6.11	42	52	52.1	46+80	9.40	9.50	38	53	52.8
48	48+00	8.19	8.56	39	52	52.1	47+79	5.59	5.60	38	53	52.8
49	49+00	6.31	6.57	39	51	51.3	48+79	5.67	5.67	38	53	52.8
50	50+00	5.90	6.09	40	52	52.1	49+80	4.42	4.51	38	52	52.1
51	51+00	6.11	6.41	38	52	52.1	50+80	4.78	4.86	40	53	52.8
52	52+00	4.71	4.85	38	53	52.8	51+80	3.66	3.71	38	53	52.8
Average		5.6	5.8	40.0	50.6	50.9		5.9	5.9	38.3	53.1	53.0
St dev		1.6	1.8	1.9	1.2	1.0		1.8	1.9	0.8	1.6	1.2
COV		29.2	30.7	4.8	2.4	1.9		31.5	31.9	2.0	3.0	2.2

Table C-3 Back-calculated modulus versus station location at 87th SG EB lane.

87th SG (Eastbound)									
Station (ft)	AC Temp. (F)	Date/ Time	E_1 (ksi)	E_1 at 68◦F (ksi)	E_2 (ksi)	E_3 (ksi)	logE_1 at 68◦F	logE_2	logE_3
2+01	61.5	10/30/2018 9:55	707	560	261	47	2.75	2.42	1.67
4+01	60.7	10/30/2018 9:59	656	505	318	50	2.70	2.50	1.70
4+01	56.8	10/30/2018 10:00	930	622	297	26	2.79	2.47	1.41
5+00	60.0	10/30/2018 10:03	442	331	118	66	2.52	2.07	1.82
6+00	58.4	10/30/2018 10:04	641	454	150	46	2.66	2.18	1.66
7+01	60.0	10/30/2018 10:07	748	560	323	48	2.75	2.51	1.68
8+00	59.2	10/30/2018 10:08	505	367	57	47	2.57	1.75	1.67
9+00	61.5	10/30/2018 10:23	778	616	208	54	2.79	2.32	1.74
10+00	57.6	10/30/2018 10:24	565	389	67	37	2.59	1.82	1.57
12+00	55.8	10/30/2018 11:51	827	532	267	42	2.73	2.43	1.62
13+00	59.0	10/30/2018 11:52	665	480	92	24	2.68	1.96	1.38
13+99	59.0	10/30/2018 11:54	883	638	119	28	2.80	2.07	1.44
15+00	58.2	10/30/2018 11:54	798	560	245	50	2.75	2.39	1.70
15+01	59.0	10/30/2018 11:55	775	560	398	44	2.75	2.60	1.65
15+99	14.9	10/30/2018 11:58	1,837	272	214	30	2.43	2.33	1.48
17+00	58.2	10/30/2018 11:59	798	560	349	36	2.75	2.54	1.56
18+00	60.6	10/30/2018 12:01	813	622	509	30	2.79	2.71	1.47
19+00	58.2	10/30/2018 12:04	798	560	345	49	2.75	2.54	1.69
20+00	58.2	10/30/2018 12:05	798	560	121	41	2.75	2.08	1.61
21+00	57.4	10/30/2018 12:07	704	480	15	12	2.68	1.17	1.07
21+99	58.2	10/30/2018 12:10	798	560	116	37	2.75	2.06	1.57

Table C-3 Back-calculated modulus versus station location at 87th SG EB lane (Continued).

87th SG (Eastbound)									
Station (ft)	AC Temp. (F)	Date/ Time	E_1 (ksi)	E_1 at 68◦F (ksi)	E_2 (ksi)	E_3 (ksi)	logE_1 at 68◦F	logE_2	logE_3
22+00	59.0	10/30/2018 12:11	775	560	98	28	2.75	1.99	1.45
23+00	59.8	10/30/2018 12:13	753	560	240	27	2.75	2.38	1.43
24+00	60.6	10/30/2018 12:14	593	454	81	28	2.66	1.91	1.45
25+00	59.0	10/30/2018 12:15	485	350	35	27	2.54	1.55	1.43
26+00	59.8	10/30/2018 12:18	494	367	96	55	2.57	1.98	1.74
27+00	60.6	10/30/2018 12:18	224	171	27	42	2.23	1.42	1.62
28+01	59.0	10/30/2018 12:20	775	560	196	20	2.75	2.29	1.29
29+00	59.8	10/30/2018 12:21	247	184	22	13	2.26	1.33	1.13
30+01	61.4	10/30/2018 12:23	790	622	230	25	2.79	2.36	1.40
31+00	60.6	10/30/2018 12:24	695	532	78	27	2.73	1.89	1.44
32+00	59.0	10/30/2018 12:26	775	560	390	27	2.75	2.59	1.43
33+00	59.0	10/30/2018 12:28	775	560	131	30	2.75	2.12	1.47
34+01	59.0	10/30/2018 12:29	597	431	144	56	2.63	2.16	1.75
35+00	62.7	10/30/2018 12:32	677	560	138	48	2.75	2.14	1.68
36+00	61.9	10/30/2018 12:33	565	454	139	61	2.66	2.14	1.78
37+01	61.9	10/30/2018 12:35	567	455	39	35	2.66	1.59	1.55
38+00	60.3	10/30/2018 12:37	740	560	233	36	2.75	2.37	1.55
39+00	61.9	10/30/2018 12:38	663	532	96	27	2.73	1.98	1.43
40+01	61.1	10/30/2018 12:39	700	546	85	41	2.74	1.93	1.61
41+00	60.3	10/30/2018 12:41	487	368	64	45	2.57	1.81	1.66
42+00	61.9	10/30/2018 12:41	736	591	60	48	2.77	1.78	1.69
43+00	62.7	10/30/2018 12:42	552	456	51	42	2.66	1.70	1.62
44+02	61.9	10/30/2018 12:43	537	431	93	45	2.63	1.97	1.66

Table C-3 Back-calculated modulus versus station location at 87th SG EB lane (Continued).

87th SG (Eastbound)									
Station (ft)	AC Temp. (F)	Date/ Time	E_1 (ksi)	E_1 at 68◦F (ksi)	E_2 (ksi)	E_3 (ksi)	logE_1 at 68◦F	logE_2	logE_3
44+99	61.9	10/30/2018 12:44	565	454	73	39	2.66	1.87	1.59
46+00	62.7	10/30/2018 12:45	550	455	64	47	2.66	1.81	1.67
47+01	62.7	10/30/2018 12:46	644	532	102	31	2.73	2.01	1.49
48+00	62.7	10/30/2018 12:47	444	367	52	32	2.57	1.71	1.50
49+01	62.7	10/30/2018 12:48	677	560	54	23	2.75	1.73	1.36
50+03	61.9	10/30/2018 12:48	509	408	52	26	2.61	1.72	1.42
51+02	61.9	10/30/2018 12:50	698	560	157	34	2.75	2.20	1.54
Average	**59.2**		**681.4**	**480.5**	**155.0**	**37.4**	**3.4**	**2.1**	**1.5**
St dev	**6.6**		**220.9**	**126.0**	**115.3**	**12.0**	**5.0**	**0.3**	**0.1**
COV	**11.1**		**32.4**	**26.2**	**74.4**	**32.0**	**149.0**	**16.9**	**9.9**

Table C-4 Back-calculated modulus versus station location at 87th SG WB lane.

87th SG (Westbound)									
Station (ft)	AC Temp. (F)	Date/ Time	E_1 (ksi)	E_1 at 68◦F (ksi)	E_2 (ksi)	E_3 (ksi)	logE_1 at 68◦F	logE_2	logE_3
0+81	61.7	10/30/2018 13:37	601	479	152	42	2.68	2.18	1.63
1+80	62.5	10/30/2018 13:36	834	684	296	33	2.84	2.47	1.52
2+80	60.8	10/30/2018 13:35	717	554	1,356	27	2.74	3.13	1.43
3+79	60.0	10/30/2018 13:34	747	560	477	29	2.75	2.68	1.46
4+80	61.7	10/30/2018 13:34	703	560	202	38	2.75	2.31	1.58
5+80	61.7	10/30/2018 13:33	703	560	146	31	2.75	2.16	1.49
6+80	60.8	10/30/2018 13:32	652	504	194	37	2.70	2.29	1.56
7+79	61.7	10/30/2018 13:31	686	546	137	48	2.74	2.14	1.69
8+79	61.1	10/30/2018 13:30	727	567	183	38	2.75	2.26	1.58
9+80	60.3	10/30/2018 13:29	682	517	89	35	2.71	1.95	1.55
10+80	57.0	10/30/2018 13:29	790	532	106	38	2.73	2.03	1.57
11+80	61.1	10/30/2018 13:27	682	532	87	35	2.73	1.94	1.54
12+79	60.3	10/30/2018 13:25	740	560	94	42	2.75	1.97	1.62
13+80	60.3	10/30/2018 13:25	757	573	109	20	2.76	2.04	1.30
14+80	59.5	10/30/2018 13:24	762	560	199	62	2.75	2.30	1.79
15+80	61.1	10/30/2018 13:23	582	454	174	44	2.66	2.24	1.64
16+80	58.6	10/30/2018 13:22	706	504	218	47	2.70	2.34	1.67
17+80	61.9	10/30/2018 13:21	698	560	275	28	2.75	2.44	1.45
18+79	58.6	10/30/2018 13:20	1,172	837	348	27	2.92	2.54	1.44

Table C-4 Back-calculated modulus versus station location at 87th SG WB lane (Continued).

87th SG (Westbound)									
Station (ft)	AC Temp. (F)	Date/ Time	E_1 (ksi)	E_1 at 68◦F (ksi)	E_2 (ksi)	E_3 (ksi)	logE_1 at 68◦F	logE_2	logE_3
19+80	59.5	10/30/2018 13:20	364	268	49	34	2.43	1.69	1.53
20+79	60.3	10/30/2018 13:19	526	398	24	18	2.60	1.37	1.25
21+79	60.3	10/30/2018 13:18	668	505	58	26	2.70	1.77	1.41
22+80	59.5	10/30/2018 13:17	764	562	282	27	2.75	2.45	1.42
23+80	61.1	10/30/2018 13:16	647	504	128	33	2.70	2.11	1.51
24+80	61.1	10/30/2018 13:15	792	618	57	52	2.79	1.76	1.72
25+80	60.3	10/30/2018 13:15	740	560	302	43	2.75	2.48	1.63
26+80	59.5	10/30/2018 13:14	762	560	559	24	2.75	2.75	1.39
27+81	61.1	10/30/2018 13:13	798	622	371	26	2.79	2.57	1.42
28+80	58.6	10/30/2018 13:12	784	560	219	52	2.75	2.34	1.72
29+80	61.1	10/30/2018 13:11	647	504	86	22	2.70	1.93	1.34
30+80	61.9	10/30/2018 13:10	775	622	370	26	2.79	2.57	1.41
31+79	61.1	10/30/2018 13:10	798	622	88	24	2.79	1.94	1.39
32+80	58.6	10/30/2018 13:09	784	560	158	31	2.75	2.20	1.49
33+80	59.5	10/30/2018 13:08	762	560	206	53	2.75	2.31	1.72
34+80	59.5	10/30/2018 13:07	501	368	90	67	2.57	1.95	1.83
35+80	62.7	10/30/2018 13:06	309	255	36	24	2.41	1.55	1.39
36+80	62.7	10/30/2018 13:06	550	455	62	44	2.66	1.79	1.64
37+79	62.7	10/30/2018 13:05	644	532	122	40	2.73	2.09	1.60
38+80	61.9	10/30/2018 13:04	787	631	129	21	2.80	2.11	1.33

Table C-4 Back-calculated modulus versus station location at 87th SG WB lane (Continued).

87th SG (Westbound)									
Station (ft)	AC Temp. (F)	Date/ Time	E_1 (ksi)	E_1 at 68◦F (ksi)	E_2 (ksi)	E_3 (ksi)	logE_1 at 68◦F	logE_2	logE_3
39+79	61.9	10/30/2018 13:03	596	479	131	35	2.68	2.12	1.54
40+80	61.9	10/30/2018 13:02	326	262	57	53	2.42	1.76	1.73
41+79	61.9	10/30/2018 13:01	446	358	71	47	2.55	1.85	1.67
42+79	61.9	10/30/2018 13:00	552	443	67	60	2.65	1.83	1.78
43+80	62.7	10/30/2018 12:59	611	505	71	30	2.70	1.85	1.48
44+80	61.9	10/30/2018 12:59	509	408	91	45	2.61	1.96	1.65
45+80	62.7	10/30/2018 12:58	523	432	69	46	2.64	1.84	1.66
46+80	62.7	10/30/2018 12:57	381	315	63	42	2.50	1.80	1.62
47+80	62.7	10/30/2018 12:56	521	431	63	37	2.63	1.80	1.57
48+78	62.7	10/30/2018 12:55	360	298	43	32	2.47	1.64	1.51
49+79	61.9	10/30/2018 12:54	698	560	53	24	2.75	1.73	1.38
50+79	61.9	10/30/2018 12:53	565	454	59	26	2.66	1.77	1.42
51+79	63.5	10/30/2018 12:52	625	532	154	34	2.73	2.19	1.53
Average	**61.0**		**654.9**	**507.4**	**177.5**	**36.5**	**2.7**	**2.1**	**1.5**
St dev	**1.4**		**153.7**	**109.2**	**202.9**	**11.4**	**0.1**	**0.3**	**0.1**
COV	**2.3**		**23.5**	**21.5**	**114.3**	**31.3**	**3.9**	**16.1**	**8.7**

Table C-5 Back-calculated modulus versus station location at 330th MN EB lane.

330th MN (Eastbound)									
Station (ft)	AC Temp. (F)	Date/ Time	E_1 (ksi)	E_1 at 68◦F (ksi)	E_2 (ksi)	E_3 (ksi)	logE_1 at 68◦F	logE_2	logE_3
1+01	50.2	10/31/2018 10:25	1,062	560	240	25	2.75	2.38	1.39
2+00	49.5	10/31/2018 10:26	1,279	657	1,456	10	2.82	3.16	0.98
3+00	50.2	10/31/2018 10:27	1,286	678	706	22	2.83	2.85	1.35
4+01	50.9	10/31/2018 10:28	1,316	711	1,049	36	2.85	3.02	1.56
5+00	50.2	10/31/2018 10:30	1,286	678	784	17	2.83	2.89	1.24
6+00	50.3	10/31/2018 10:31	1,057	560	341	16	2.75	2.53	1.21
7+00	52.5	10/31/2018 10:32	1,035	592	1,086	7	2.77	3.04	0.87
8+00	51.1	10/31/2018 10:33	1,020	554	588	12	2.74	2.77	1.08
9+00	50.3	10/31/2018 10:34	1,564	828	410	16	2.92	2.61	1.21
10+00	49.6	10/31/2018 10:36	1,313	678	413	15	2.83	2.62	1.19
11+00	50.3	10/31/2018 10:37	1,280	678	485	13	2.83	2.69	1.11
12+00	50.3	10/31/2018 10:37	1,292	684	384	19	2.84	2.58	1.28
13+00	50.3	10/31/2018 10:38	952	504	675	11	2.70	2.83	1.03
14+00	51.1	10/31/2018 10:40	1,260	684	274	14	2.84	2.44	1.14
15+01	50.3	10/31/2018 10:41	1,175	622	303	21	2.79	2.48	1.32
16+00	50.3	10/31/2018 10:42	1,116	591	259	26	2.77	2.41	1.42
17+00	50.3	10/31/2018 10:43	1,152	610	784	13	2.79	2.89	1.11
18+03	50.3	10/31/2018 10:44	1,292	684	341	17	2.84	2.53	1.23
19+00	50.3	10/31/2018 10:46	1,478	783	470	10	2.89	2.67	1.01
20+00	51.1	10/31/2018 10:47	1,386	753	414	16	2.88	2.62	1.20

Table C-5 Back-calculated modulus versus station location at 330th MN EB lane (continued).

330th MN (Eastbound)									
Station (ft)	AC Temp. (F)	Date / Time	E_1 (ksi)	E_1 at 68◦F (ksi)	E_2 (ksi)	E_3 (ksi)	logE_1 at 68◦F	logE_2	logE_3
21+00	51.1	10/31/2018 10:49	1,134	616	484	16	2.79	2.69	1.21
22+00	51.1	10/31/2018 10:50	1,145	622	318	21	2.79	2.50	1.32
23+00	51.8	10/31/2018 10:50	1,116	622	208	20	2.79	2.32	1.30
24+00	50.3	10/31/2018 10:51	1,057	560	211	22	2.75	2.32	1.34
25+00	51.8	10/31/2018 11:24	1,105	616	365	18	2.79	2.56	1.24
26+00	51.1	10/31/2018 11:25	1,260	684	338	23	2.84	2.53	1.35
27+00	50.3	10/31/2018 11:26	1,280	678	364	11	2.83	2.56	1.04
28+00	49.6	10/31/2018 11:27	1,205	622	216	20	2.79	2.33	1.30
29+00	49.6	10/31/2018 11:27	1,313	678	415	15	2.83	2.62	1.18
30+00	49.6	10/31/2018 11:28	1,205	622	293	19	2.79	2.47	1.28
31+00	48.9	10/31/2018 11:29	1,496	753	400	12	2.88	2.60	1.08
32+00	49.6	10/31/2018 11:30	1,085	560	161	22	2.75	2.21	1.35
33+00	50.6	10/31/2018 11:31	1,549	828	386	16	2.92	2.59	1.19
35+00	49.9	10/31/2018 11:32	1,194	622	268	19	2.79	2.43	1.28
35+00	50.6	10/31/2018 11:34	1,152	616	519	14	2.79	2.72	1.13
36+00	49.9	10/31/2018 11:34	958	499	965	12	2.70	2.98	1.08
37+01	51.3	10/31/2018 11:35	1,020	560	352	15	2.75	2.55	1.19
38+02	52.1	10/31/2018 11:36	994	560	480	20	2.75	2.68	1.30

Table C-5 Back-calculated modulus versus station location at 330th MN EB lane (continued).

330th MN (Eastbound)									
Station (ft)	AC Temp. (F)	Date / Time	E_1 (ksi)	E_1 at 68◦F (ksi)	E_2 (ksi)	E_3 (ksi)	logE_1 at 68◦F	logE_2	logE_3
39+01	52.1	10/31/2018 11:37	833	469	813	7	2.67	2.91	0.83
40+00	51.3	10/31/2018 11:38	1,020	560	237	19	2.75	2.38	1.28
41+00	51.3	10/31/2018 11:39	1,509	828	244	11	2.92	2.39	1.05
42+00	51.3	10/31/2018 11:40	1,134	622	278	23	2.79	2.44	1.37
43+01	52.8	10/31/2018 11:41	863	499	810	10	2.70	2.91	1.01
44+01	52.1	10/31/2018 11:42	805	454	678	10	2.66	2.83	1.02
45+01	52.8	10/31/2018 11:44	1,433	828	294	12	2.92	2.47	1.07
46+02	52.1	10/31/2018 11:45	994	560	77	8	2.75	1.89	0.88
47+00	52.1	10/31/2018 11:46	1,203	678	427	12	2.83	2.63	1.07
48+00	52.1	10/31/2018 11:47	994	560	113	26	2.75	2.05	1.41
49+00	51.3	10/31/2018 11:48	1,134	622	208	22	2.79	2.32	1.34
50+00	52.1	10/31/2018 11:48	994	560	214	28	2.75	2.33	1.45
51+00	52.1	10/31/2018 11:50	1,094	616	267	18	2.79	2.43	1.27
52+00	52.8	10/31/2018 11:51	969	560	435	23	2.75	2.64	1.37
Average	**50.9**		**1,170.2**	**631.2**	**448.1**	**16.9**	**2.8**	**2.6**	**1.2**
St dev	**1.0**		**180.0**	**90.4**	**273.1**	**5.9**	**0.06**	**0.2**	**0.16**
COV	**1.9**		**15.4**	**14.3**	**60.9**	**34.9**	**2.2**	**9.6**	**13.0**

Table C-6 Back-calculated modulus versus station location at 330th MN WB lane.

330th MN (Westbound)									
Station (ft)	AC Temp. (F)	Date/ Time	E_1 (ksi)	E_1 at 68◦F (ksi)	E_2 (ksi)	E_3 (ksi)	logE_1 at 68◦F	logE_2	logE_3
0+80	54.0	10/31/2018 12:50	676	408	1,390	14	2.61	3.14	1.16
1+80	54.0	10/31/2018 12:50	882	533	1,549	8	2.73	3.19	0.93
2+81	53.3	10/31/2018 12:49	1,048	616	1,080	30	2.79	3.03	1.47
3+80	52.5	10/31/2018 12:47	1,249	715	701	22	2.85	2.85	1.34
4+80	54.0	10/31/2018 12:46	1,372	828	385	20	2.92	2.59	1.29
5+79	54.0	10/31/2018 12:45	1,247	753	303	16	2.88	2.48	1.21
6+80	54.0	10/31/2018 12:44	1,234	745	419	16	2.87	2.62	1.19
7+79	53.3	10/31/2018 12:43	1,152	678	585	12	2.83	2.77	1.09
8+80	53.3	10/31/2018 12:41	1,152	678	604	15	2.83	2.78	1.18
9+80	45.9	10/31/2018 12:41	1,652	745	309	13	2.87	2.49	1.12
10+80	54.0	10/31/2018 12:40	1,133	684	393	23	2.84	2.59	1.35
11+80	53.3	10/31/2018 12:39	943	554	562	9	2.74	2.75	0.96
12+80	53.3	10/31/2018 12:38	1,280	753	339	13	2.88	2.53	1.11
13+80	52.5	10/31/2018 12:36	1,315	753	332	10	2.88	2.52	1.02
14+80	53.3	10/31/2018 12:35	1,048	616	257	19	2.79	2.41	1.28
15+79	54.0	10/31/2018 12:35	1,372	828	413	20	2.92	2.62	1.30
16+80	54.0	10/31/2018 12:34	1,020	616	586	15	2.79	2.77	1.17
17+80	53.3	10/31/2018 12:33	943	554	720	11	2.74	2.86	1.05
18+79	54.0	10/31/2018 12:31	1,030	622	235	16	2.79	2.37	1.21

Table C-6 Back-calculated modulus versus station location at 330th MN WB lane (continued).

330th MN (Westbound)									
Station (ft)	AC Temp. (F)	Date/ Time	E_1 (ksi)	E_1 at 68◦F (ksi)	E_2 (ksi)	E_3 (ksi)	logE_1 at 68◦F	logE_2	logE_3
19+80	53.5	10/31/2018 12:30	1,142	678	309	12	2.83	2.49	1.09
20+80	53.5	10/31/2018 12:29	1,154	684	448	20	2.84	2.65	1.31
21+79	53.5	10/31/2018 12:28	1,142	678	545	14	2.83	2.74	1.15
22+80	53.5	10/31/2018 12:28	944	560	181	25	2.75	2.26	1.39
23+80	53.5	10/31/2018 12:26	1,142	678	605	16	2.83	2.78	1.20
24+80	54.2	10/31/2018 12:25	1,022	622	303	24	2.79	2.48	1.38
25+80	54.2	10/31/2018 12:24	745	454	799	10	2.66	2.90	0.99
26+80	53.5	10/31/2018 12:23	944	560	275	17	2.75	2.44	1.24
27+80	53.5	10/31/2018 12:23	1,142	678	588	12	2.83	2.77	1.08
28+80	52.8	10/31/2018 12:21	872	504	124	27	2.70	2.09	1.43
29+80	52.8	10/31/2018 12:20	1,433	828	262	12	2.92	2.42	1.07
30+81	52.8	10/31/2018 12:19	1,289	745	467	13	2.87	2.67	1.12
31+80	53.5	10/31/2018 12:18	1,049	622	233	17	2.79	2.37	1.23
32+80	52.8	10/31/2018 12:17	1,302	753	317	16	2.88	2.50	1.22
33+80	52.8	10/31/2018 12:16	1,055	610	632	10	2.79	2.80	1.02
34+80	52.8	10/31/2018 12:15	1,433	828	722	18	2.92	2.86	1.26
35+80	52.1	10/31/2018 12:14	1,094	616	426	12	2.79	2.63	1.07
36+80	52.8	10/31/2018 12:13	1,433	828	424	16	2.92	2.63	1.20

Table C-6 Back-calculated modulus versus station location at 330th MN WB lane (continued).

330th MN (Westbound)									
Station (ft)	**AC Temp. (F)**	**Date/ Time**	**E_1 (ksi)**	**E_1 at 68◦F (ksi)**	**E_2 (ksi)**	**E_3 (ksi)**	**logE_1 at 68◦F**	**logE_2**	**logE_3**
37+79	52.8	10/31/2018 12:12	1,066	616	421	11	2.79	2.62	1.06
38+80	52.8	10/31/2018 12:10	1,289	745	496	14	2.87	2.70	1.13
39+80	52.1	10/31/2018 12:09	1,094	616	268	10	2.79	2.43	1.02
40+80	52.8	10/31/2018 12:08	1,023	591	185	16	2.77	2.27	1.22
41+80	52.1	10/31/2018 12:07	984	554	579	9	2.74	2.76	0.97
42+80	52.8	10/31/2018 12:07	1,066	616	487	13	2.79	2.69	1.11
43+80	52.1	10/31/2018 12:05	1,470	828	243	14	2.92	2.38	1.16
44+80	52.8	10/31/2018 12:04	745	431	53	14	2.63	1.72	1.14
45+79	52.8	10/31/2018 12:03	1,433	828	232	11	2.92	2.37	1.04
46+80	52.8	10/31/2018 12:02	1,076	622	107	20	2.79	2.03	1.29
47+79	52.8	10/31/2018 12:01	1,172	678	437	12	2.83	2.64	1.10
48+79	52.8	10/31/2018 11:59	969	560	238	30	2.75	2.38	1.48
49+80	52.1	10/31/2018 11:59	1,094	616	539	18	2.79	2.73	1.26
50+80	52.8	10/31/2018 11:57	1,066	616	609	13	2.79	2.78	1.10
51+80	52.8	10/31/2018 11:56	1,044	604	1,058	11	2.78	3.02	1.04
Average	**53.0**		**1,128.4**	**656.3**	**476.4**	**15.6**	**2.8**	**2.6**	**1.2**
St dev	**1.18**		**196.3**	**105.1**	**293.5**	**5.1**	**0.07**	**0.27**	**0.1**
COV	**2.2**		**17.4**	**16.01**	**61.6**	**32.7**	**2.6**	**10.3**	**11.3**

Table C-7 Resilient Modulus of the Uncracked CMS Specimen No. 1 for the 87th SG Soil.

Parameter	**Chamber Confining Pressure**	**Actual Applied Cyclic Stress**	**Actual Applied Contact Stress**	**Resilient Modulus**
Designation	σ_3	σ_{cyclic}	$\sigma_{contact}$	M_r
Unit	psi	psi	psi	psi
Sequence 1	6	1.84	0.21	20684
Sequence 2	6	3.62	0.39	21139
Sequence 3	6	5.42	0.61	23735
Sequence 4	6	7.27	0.81	24831
Sequence 5	6	9.10	1.02	25375
Sequence 6	4	1.86	0.23	20014
Sequence 7	4	3.68	0.45	20705
Sequence 8	4	5.46	0.61	21577
Sequence 9	4	7.27	0.79	22563
Sequence 10	4	9.20	1.01	24102
Sequence 11	2	1.80	0.19	18011
Sequence 12	2	3.62	0.45	19517
Sequence 13	2	5.45	0.59	20894
Sequence 14	2	7.24	0.79	22217
Sequence 15	2	9.14	1.03	23614

Table C-8 Resilient Modulus of the Uncracked CMS Specimen No. 4 for the 87th SG Soil.

Parameter	**Chamber Confining Pressure**	**Actual Applied Cyclic Stress**	**Actual Applied Contact Stress**	**Resilient Modulus**
Designation	σ_3	σ_{cyclic}	$\sigma_{contact}$	M_r
Unit	psi	psi	psi	psi
Sequence 1	6	1.73	0.25	21118
Sequence 2	6	3.89	0.44	25945
Sequence 3	6	5.44	0.61	28696
Sequence 4	6	7.43	0.82	28487
Sequence 5	6	9.17	1.02	30551
Sequence 6	4	1.72	0.23	20756
Sequence 7	4	3.91	0.46	24329
Sequence 8	4	5.42	0.63	25952
Sequence 9	4	7.48	0.81	27832
Sequence 10	4	9.12	0.99	29612
Sequence 11	2	1.72	0.22	20025
Sequence 12	2	3.78	0.44	22712
Sequence 13	2	5.55	0.61	24682
Sequence 14	2	7.48	0.82	27571
Sequence 15	2	9.17	1.01	27907

Table C-9 Resilient Modulus of the Uncracked CMS Specimen No. 1 for the 330th MN Soil.

Parameter	Chamber Confining Pressure	Actual Applied Cyclic Stress	Actual Applied Contact Stress	Resilient Modulus
Designation	σ_3	σ_{cyclic}	$\sigma_{contact}$	M_r
Unit	psi	psi	psi	psi
Sequence 1	6	1.90	0.20	24647
Sequence 2	6	3.56	0.41	27068
Sequence 3	6	5.38	0.62	29988
Sequence 4	6	7.23	0.82	32558
Sequence 5	6	9.05	1.01	34438
Sequence 6	4	1.97	0.22	24422
Sequence 7	4	3.50	0.42	26608
Sequence 8	4	5.33	0.59	28877
Sequence 9	4	7.29	0.81	30712
Sequence 10	4	9.07	0.99	33268
Sequence 11	2	1.96	0.22	23927
Sequence 12	2	3.60	0.44	26161
Sequence 13	2	5.37	0.61	28762
Sequence 14	2	7.21	0.78	30449
Sequence 15	2	9.07	0.98	31961

Table C-10 Resilient Modulus of the Uncracked CMS Specimen No. 2 for the 330th MN Soil.

Parameter	Chamber Confining Pressure	Actual Applied Cyclic Stress	Actual Applied Contact Stress	Resilient Modulus
Designation	σ_3	σ_{cyclic}	$\sigma_{contact}$	M_r
Unit	psi	psi	psi	psi
Sequence 1	6	1.92	0.20	26906
Sequence 2	6	3.74	0.43	30863
Sequence 3	6	5.41	0.55	31913
Sequence 4	6	7.24	0.81	33197
Sequence 5	6	9.06	0.98	34460
Sequence 6	4	1.90	0.21	22279
Sequence 7	4	3.74	0.45	24378
Sequence 8	4	5.47	0.56	27861
Sequence 9	4	7.24	0.78	30671
Sequence 10	4	9.10	0.99	31203
Sequence 11	2	1.94	0.19	22241
Sequence 12	2	3.76	0.45	24299
Sequence 13	2	5.41	0.61	26102
Sequence 14	2	7.27	0.82	29429
Sequence 15	2	9.09	1.01	30103

Table C-11 Resilient Modulus of the Cracked CMS Specimen No. 2 for the 87th SG Soil.

Parameter	**Chamber Confining Pressure**	**Actual Applied Cyclic Stress**	**Actual Applied Contact Stress**	**Resilient Modulus**
Designation	σ_3	σ_{cyclic}	$\sigma_{contact}$	M_r
Unit	psi	psi	psi	psi
Sequence 1	6	1.78	0.24	25545
Sequence 2	6	3.71	0.44	28224
Sequence 3	6	5.41	0.61	30752
Sequence 4	6	7.25	0.80	32882
Sequence 5	6	9.15	1.02	34122
Sequence 6	4	1.79	0.23	23124
Sequence 7	4	3.67	0.44	27002
Sequence 8	4	5.46	0.62	28454
Sequence 9	4	7.28	0.81	32345
Sequence 10	4	9.14	0.99	33657
Sequence 11	2	1.80	0.22	22325
Sequence 12	2	3.69	0.44	23221
Sequence 13	2	5.53	0.61	24610
Sequence 14	2	7.28	0.78	26194
Sequence 15	2	9.19	0.98	28563

Table C-12 Resilient Modulus of the Cracked CMS Specimen No. 3 for the 87th SG Soil.

Parameter	**Chamber Confining Pressure**	**Actual Applied Cyclic Stress**	**Actual Applied Contact Stress**	**Resilient Modulus**
Designation	σ_3	σ_{cyclic}	$\sigma_{contact}$	M_r
Unit	psi	psi	psi	psi
Sequence 1	6	1.91	0.19	20714
Sequence 2	6	3.75	0.44	23146
Sequence 3	6	5.38	0.62	23290
Sequence 4	6	7.22	0.81	24347
Sequence 5	6	9.16	1.02	27875
Sequence 6	4	1.89	0.23	20223
Sequence 7	4	3.73	0.44	20295
Sequence 8	4	5.35	0.62	22790
Sequence 9	4	7.15	0.81	24278
Sequence 10	4	9.18	1.02	26141
Sequence 11	2	1.94	0.22	19460
Sequence 12	2	3.72	0.44	19901
Sequence 13	2	5.35	0.59	22063
Sequence 14	2	7.25	0.79	24141
Sequence 15	2	9.15	1.01	25306

Table C-13 Resilient Modulus of the Cracked CMS Specimen No. 3 for the 330th MN Soil.

Parameter	**Chamber Confining Pressure**	**Actual Applied Cyclic Stress**	**Actual Applied Contact Stress**	**Resilient Modulus**
Designation	σ_3	σ_{cyclic}	$\sigma_{contact}$	M_r
Unit	psi	psi	Psi	psi
Sequence 1	6	1.72	0.21	25614
Sequence 2	6	3.75	0.42	26478
Sequence 3	6	5.43	0.61	27400
Sequence 4	6	7.24	0.82	31923
Sequence 5	6	9.03	1.01	34702
Sequence 6	4	1.70	0.23	23290
Sequence 7	4	3.72	0.44	25778
Sequence 8	4	5.47	0.62	26587
Sequence 9	4	7.22	0.83	28061
Sequence 10	4	9.05	0.99	32583
Sequence 11	2	1.73	0.22	18376
Sequence 12	2	3.70	0.44	23872
Sequence 13	2	5.47	0.61	25373
Sequence 14	2	7.23	0.82	28159
Sequence 15	2	9.02	1.01	31239

Table C-14 Resilient Modulus of the Cracked CMS Specimen No. 4 for the 330th MN Soil.

Parameter	**Chamber Confining Pressure**	**Actual Applied Cyclic Stress**	**Actual Applied Contact Stress**	**Resilient Modulus**
Designation	σ_3	σ_{cyclic}	$\sigma_{contact}$	M_r
Unit	psi	psi	psi	psi
Sequence 1	6	1.86	0.24	28213
Sequence 2	6	3.75	0.43	32785
Sequence 3	6	5.65	0.65	34229
Sequence 4	6	7.26	0.83	33347
Sequence 5	6	9.11	1.02	40990
Sequence 6	4	1.84	0.25	27310
Sequence 7	4	3.76	0.45	31016
Sequence 8	4	5.66	0.64	33052
Sequence 9	4	7.26	0.79	32531
Sequence 10	4	9.11	1.03	35696
Sequence 11	2	1.80	0.22	25492
Sequence 12	2	3.74	0.45	28573
Sequence 13	2	5.68	0.63	29268
Sequence 14	2	7.27	0.81	32375
Sequence 15	2	9.12	1.01	34776

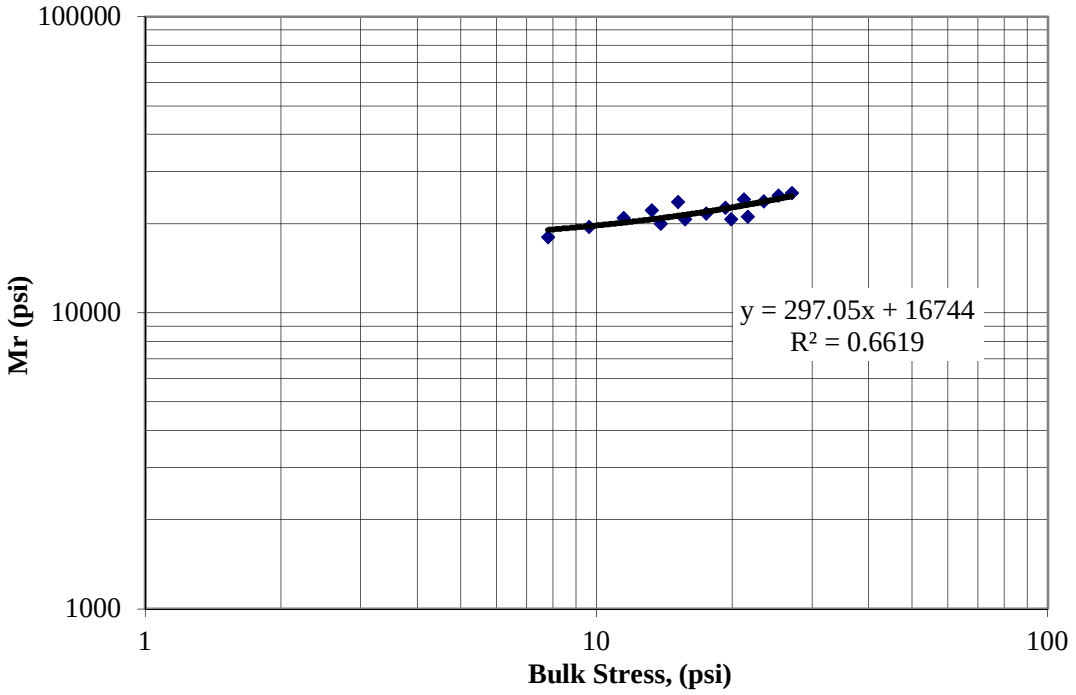

Figure C-1 M_r versus θ 87th SG Reconstituted Specimen 1 Uncracked.

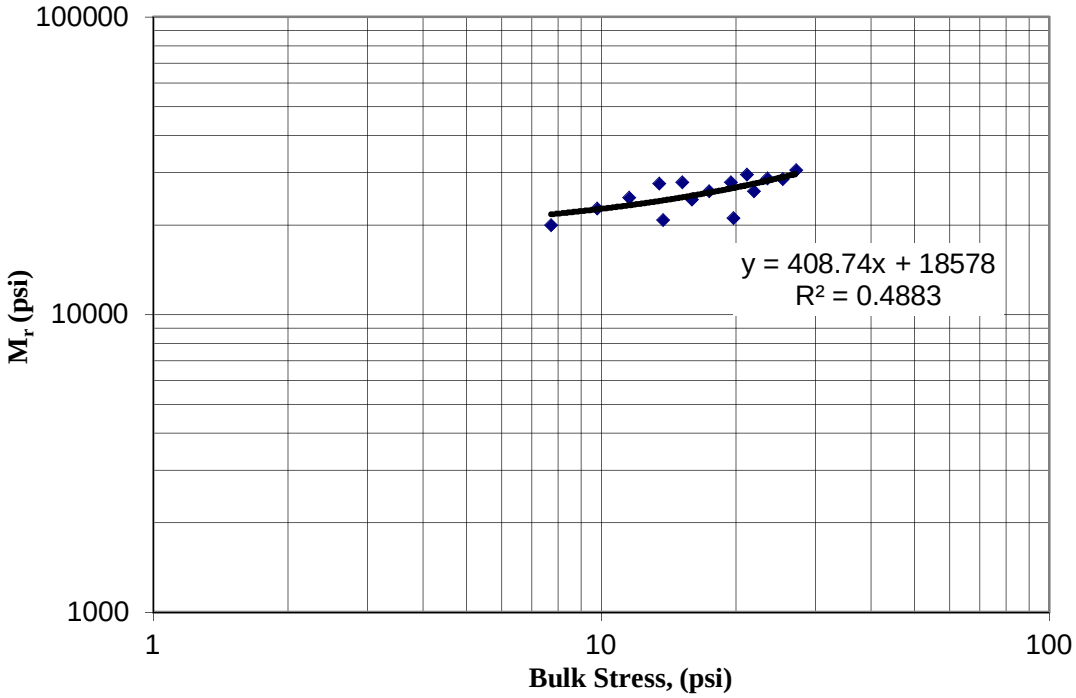

Figure C-2 M_r versus θ 87th SG Reconstituted Specimen 4 Uncracked.

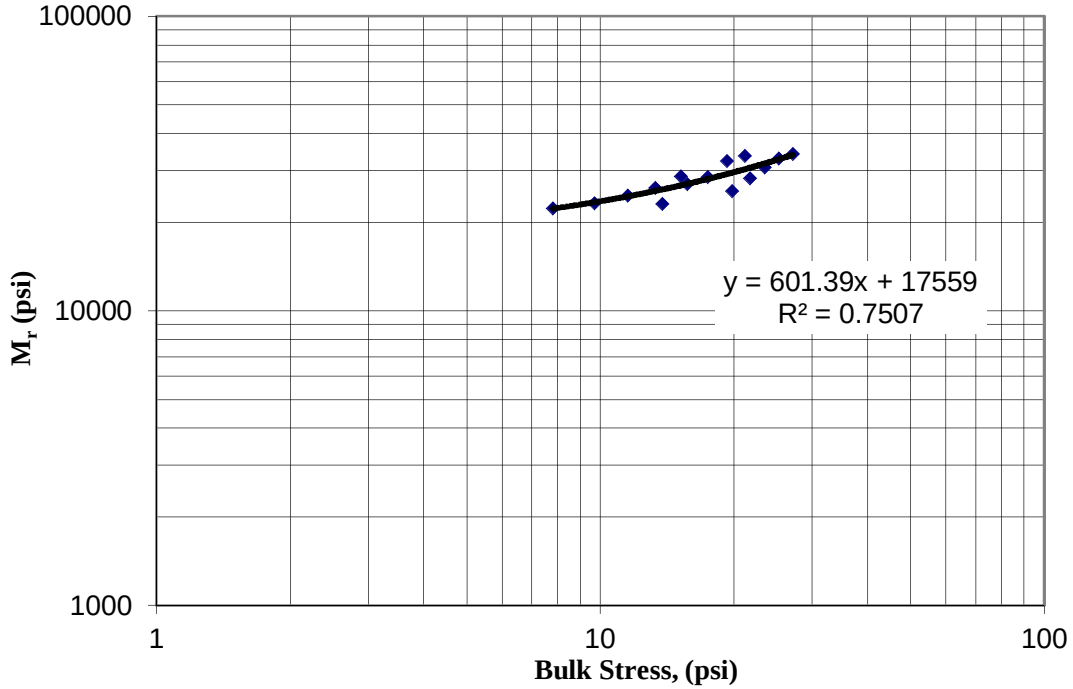

Figure C-3 M_r versus θ 87th SG Reconstituted Specimen 2 Cracked.

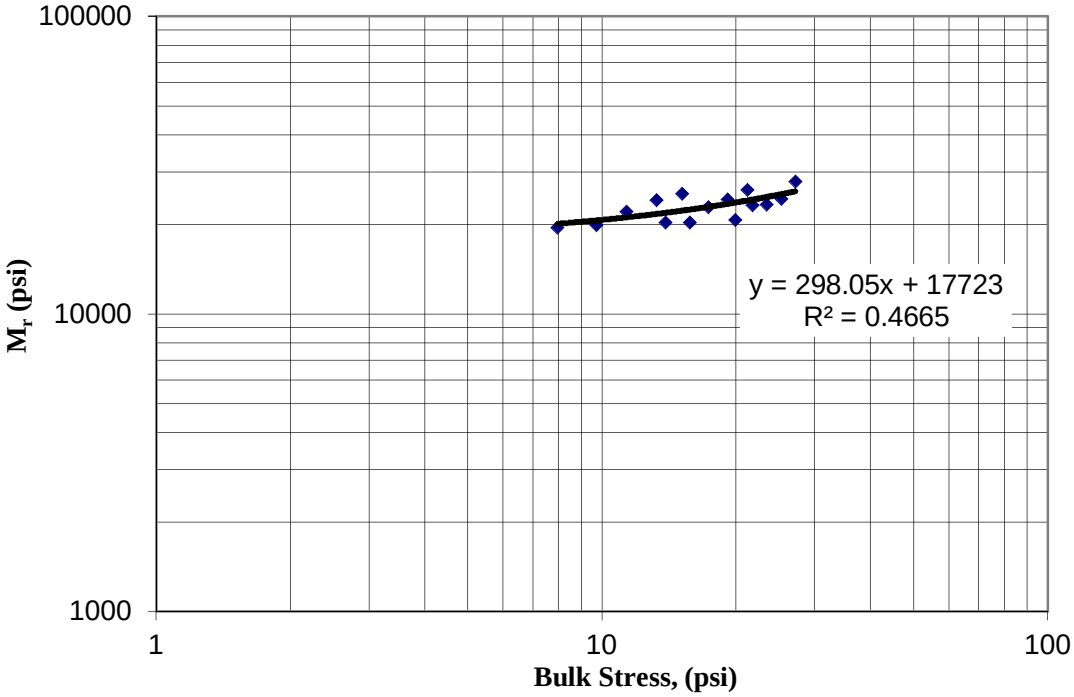

Figure C-4 M_r versus θ 87th SG Reconstituted Specimen 3 Cracked.

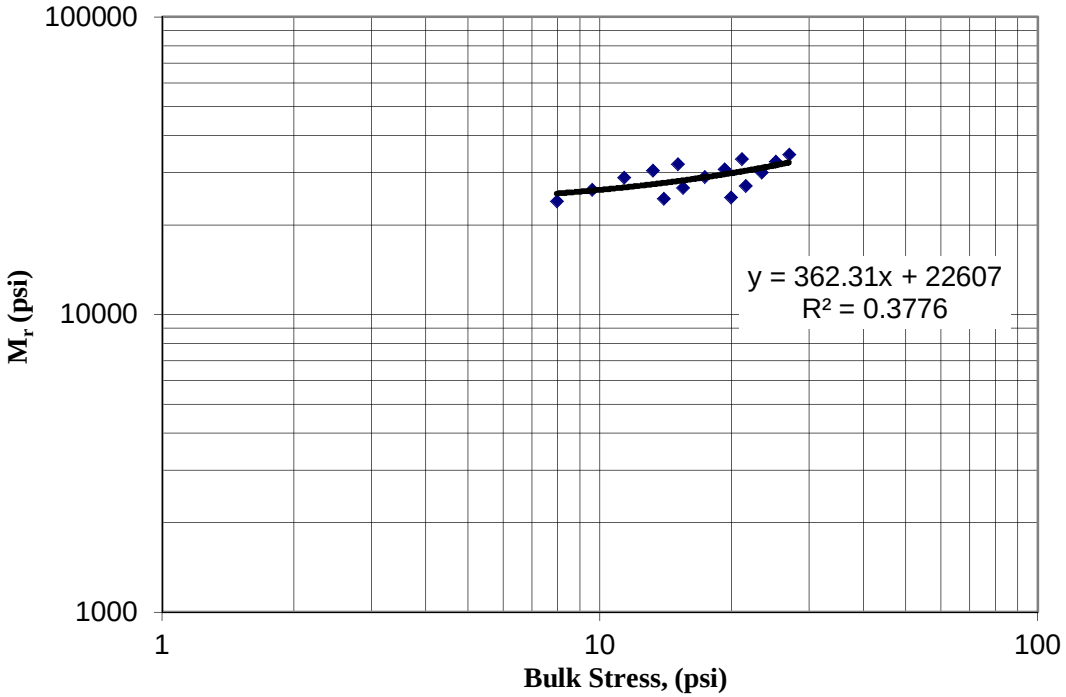

Figure C-5 M_r versus θ 330th MN Reconstituted Specimen 1 Uncracked.

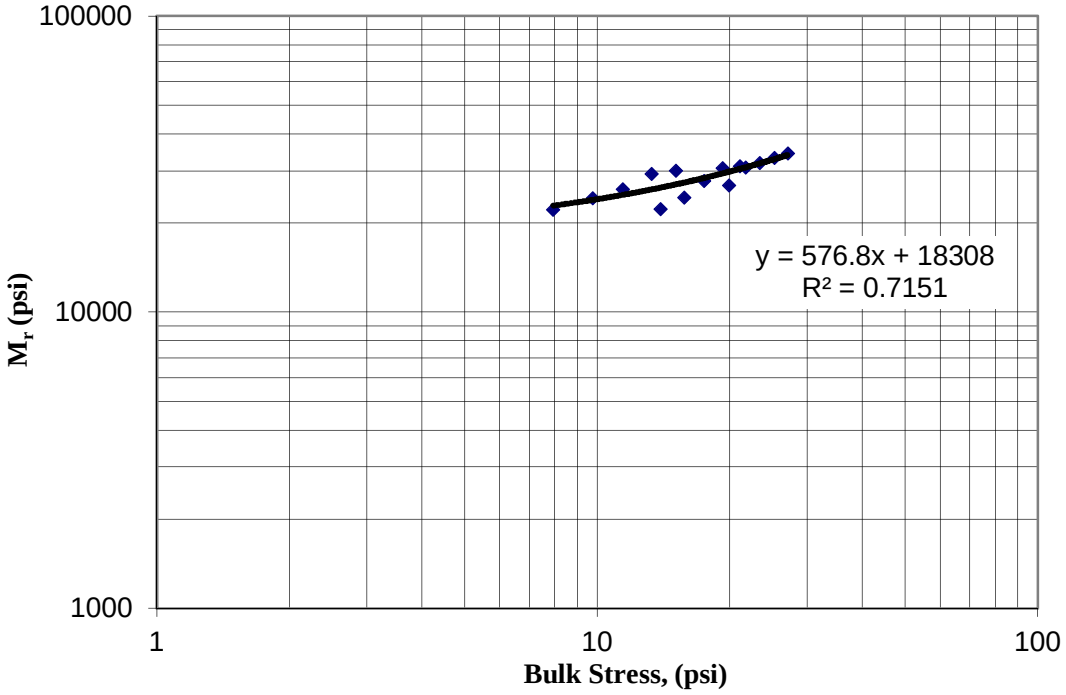

Figure C-6 M_r versus θ 330th MN Reconstituted Specimen 2 Uncracked.

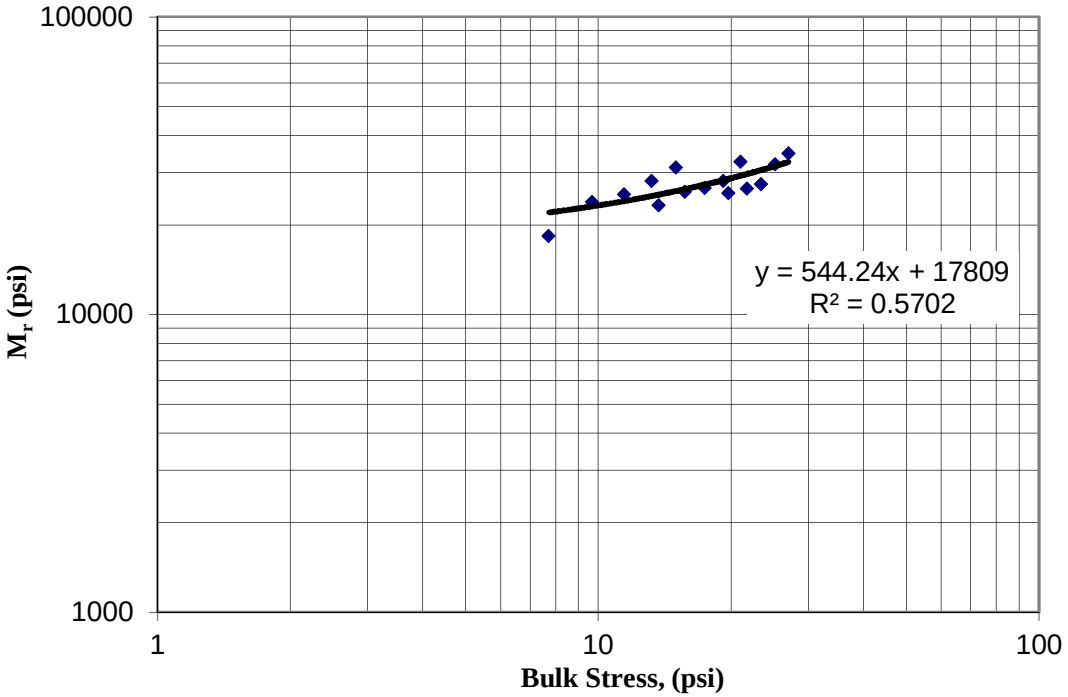

Figure C-7 M_r versus θ 330th MN Reconstituted Specimen 3 Cracked.

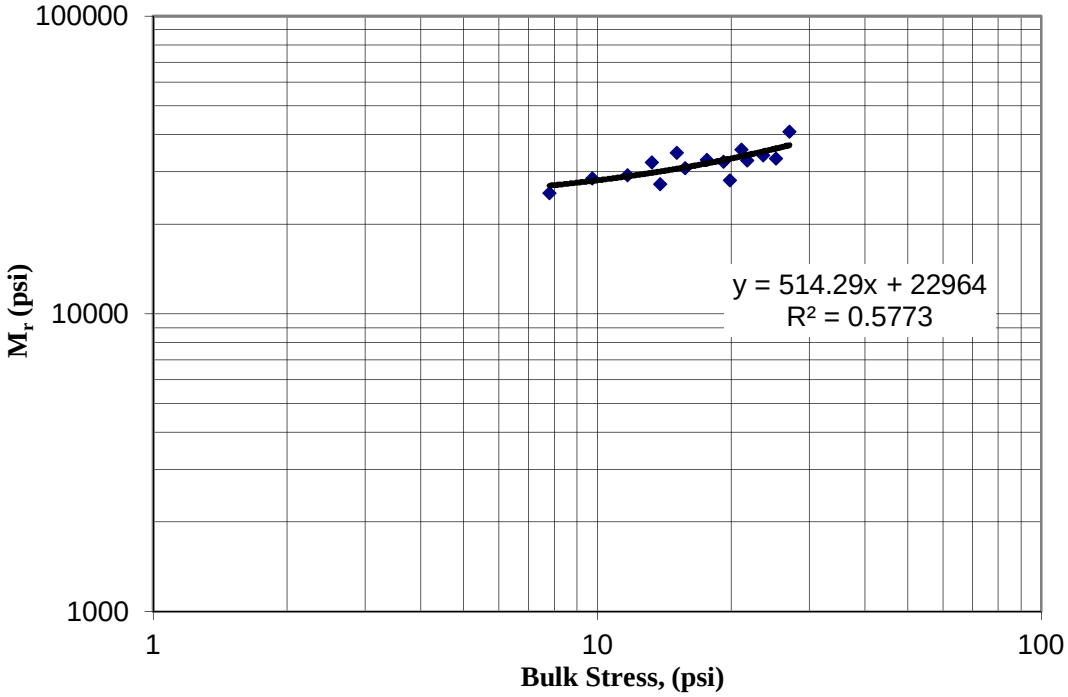

Figure C-8 M_r versus θ 330th MN Reconstituted Specimen 4 Cracked.

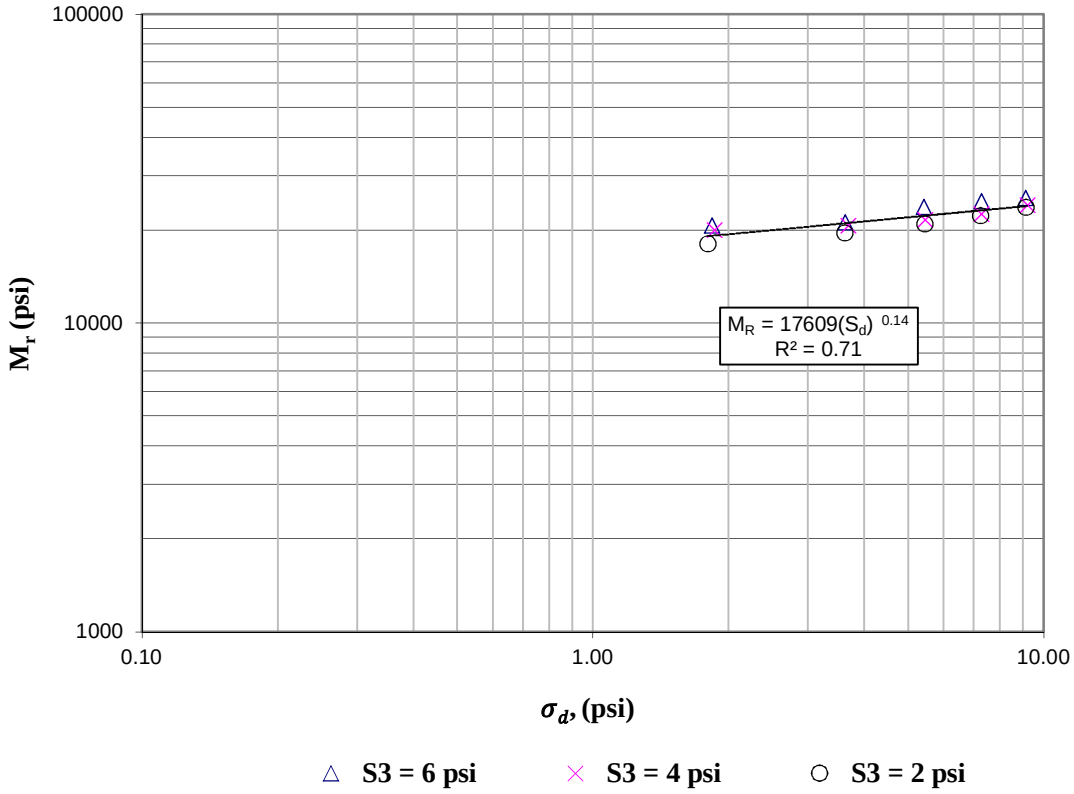

Figure C-9 M_r versus σ_d 87th SG Reconstituted Specimen 1 Uncracked.

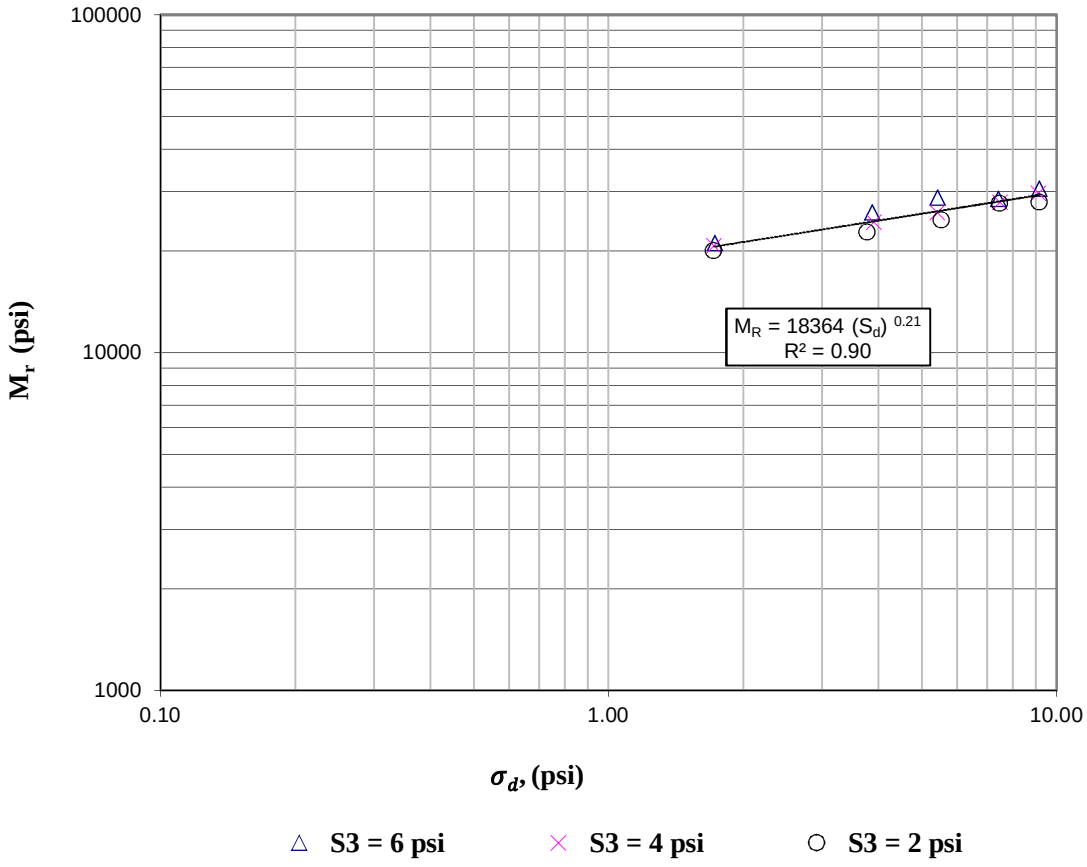

Figure C-10 M_r versus σ_d 87th SG Reconstituted Specimen 4 Uncracked.

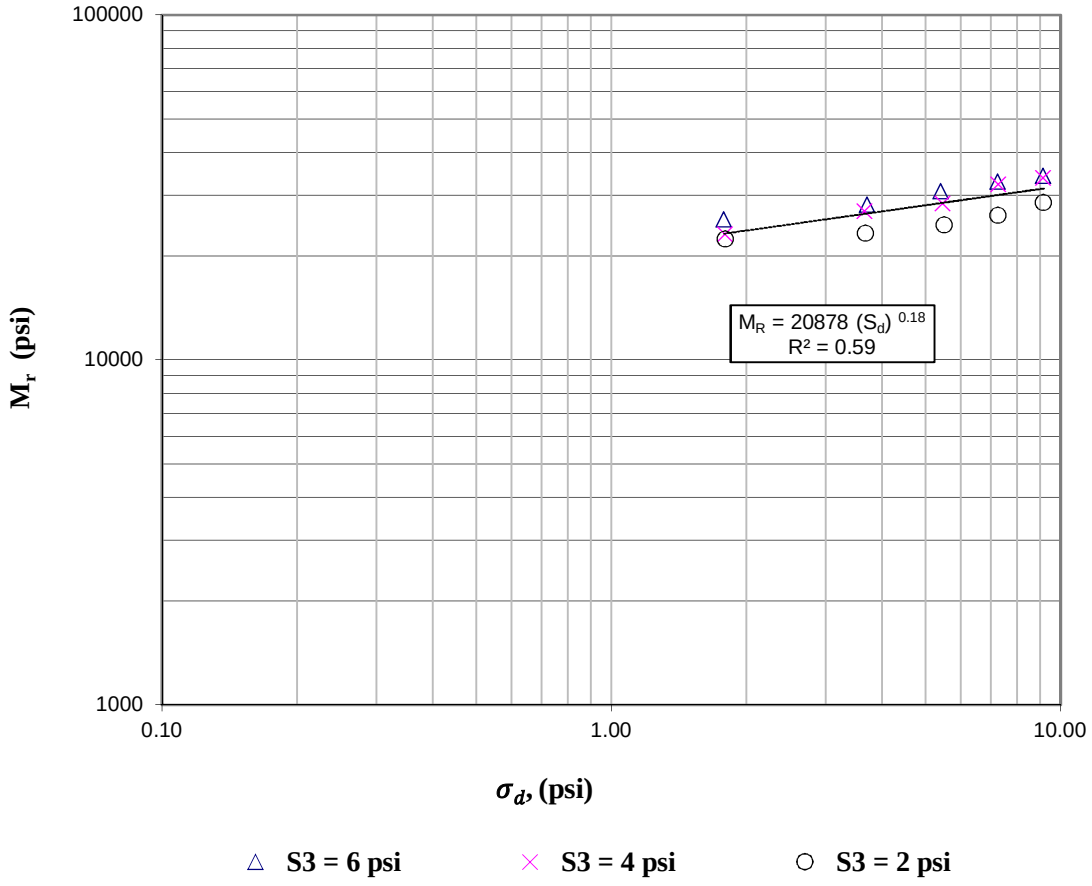

Figure C-11 M_r versus σ_d 87th SG Reconstituted Specimen 2 Cracked.

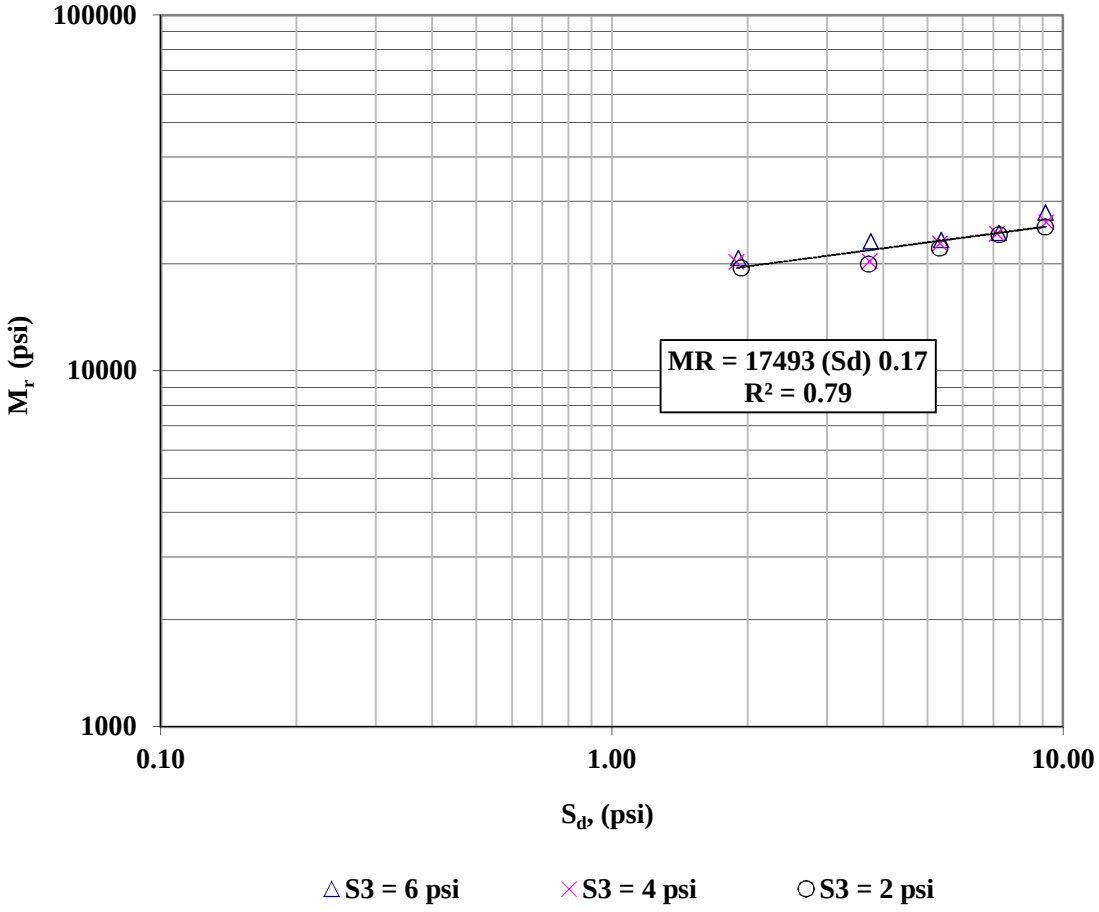

Figure C-12 M_r versus σ_d 87th SG Reconstituted Specimen 3 Cracked.

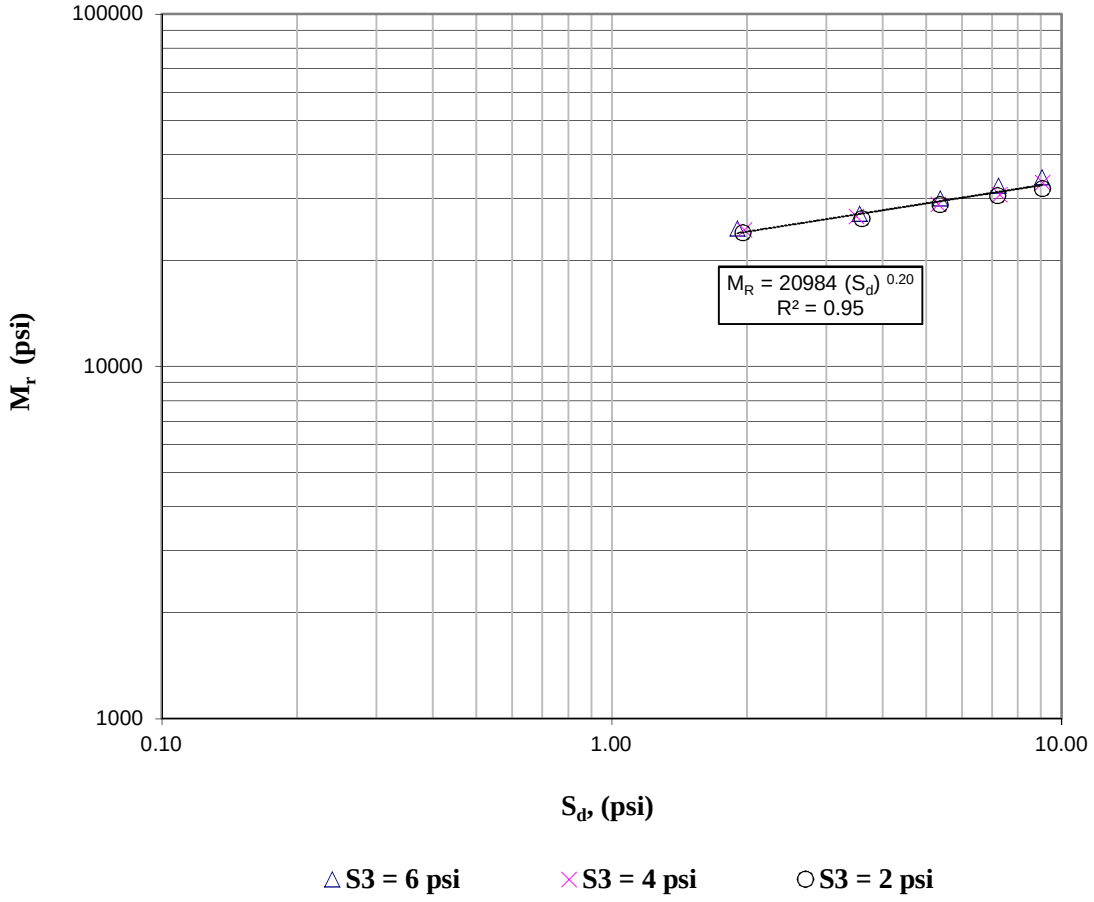

Figure C-13 M_r versus σ_d 330th MN Reconstituted Specimen 1 Uncracked.

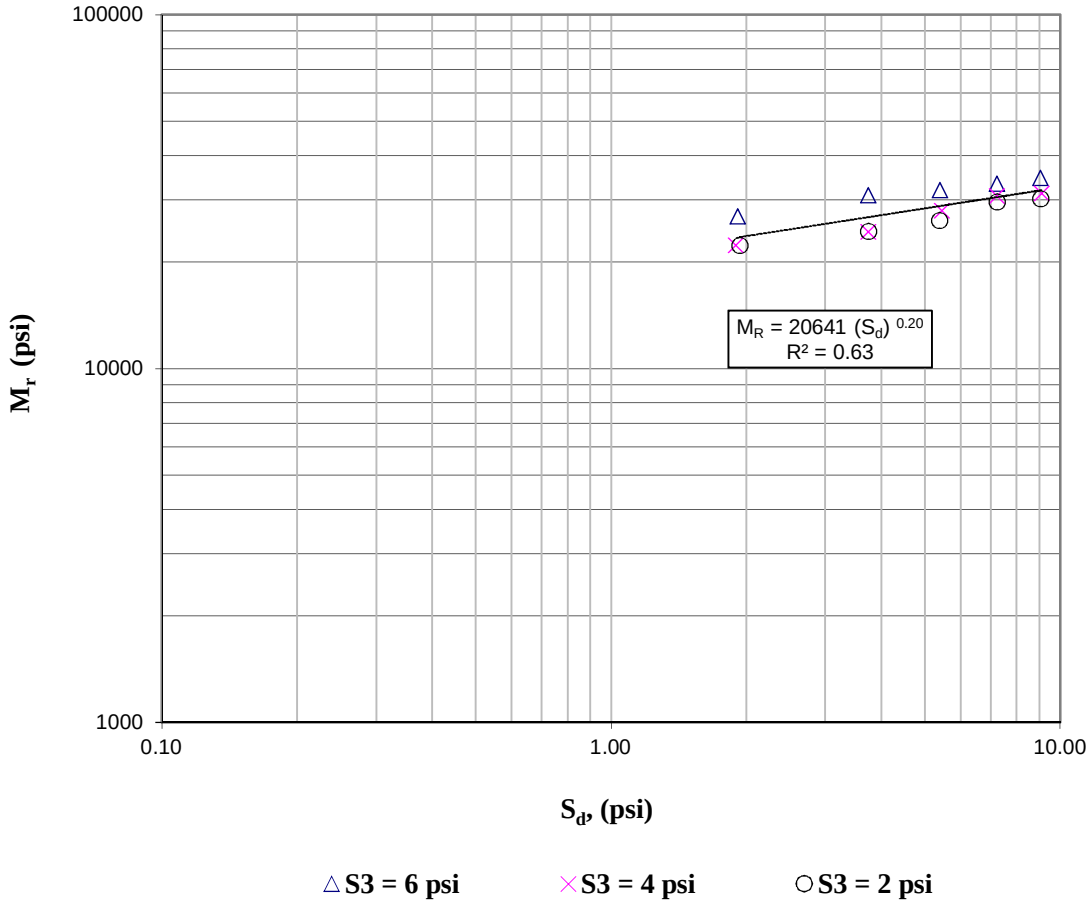

Figure C-14 M_r versus σ_d 330th MN Reconstituted Specimen 2 Uncracked.

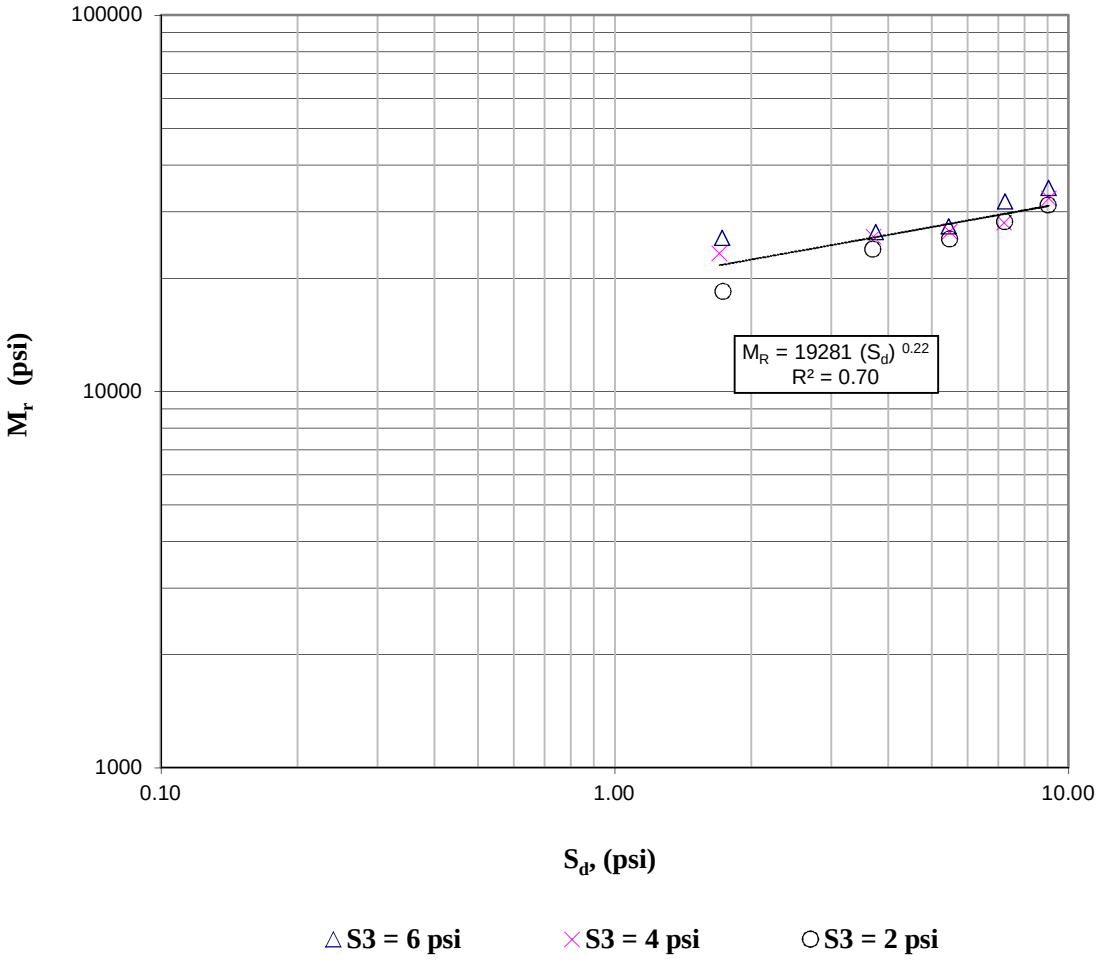

Figure C-15 M_r versus σ_d 330th MN Reconstituted Specimen 3 Cracked.

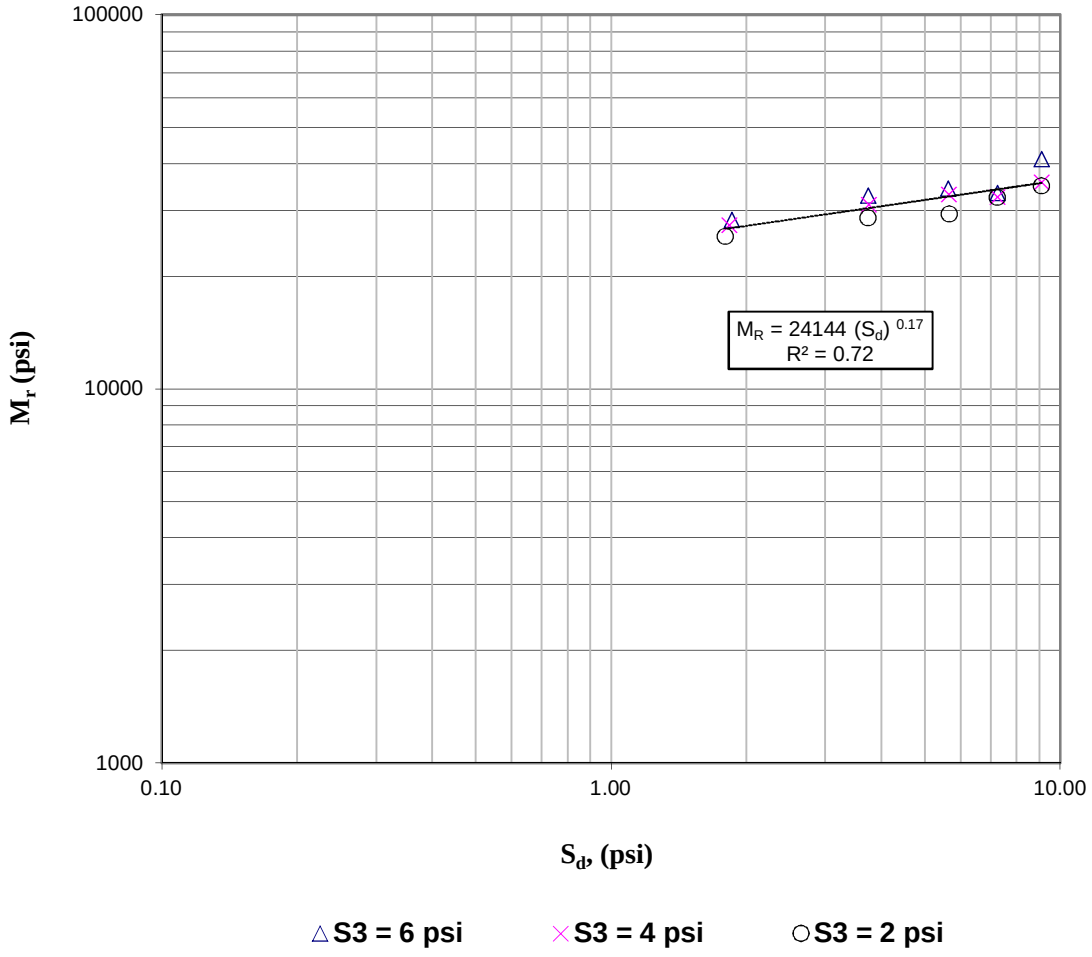

Figure C-16 M_r versus σ_d 330th MN Reconstituted Specimen 4 Cracked.